The PHILOSOPHICAL MAGAZINE

FIRST PUBLISHED IN 1798

VOL. 45 SEVENTH SERIES No. 365 June 1954

A Journal of Theoretical Experimental and Applied Physics

PRICE 15s. 0d.
Annual Subscription £8 0s. 0d. payable in advance

ED AND PUBLISHED BY TAYLOR & FRANCIS LTD., RED LION COURT, FLEET ST., LONDON, E.C.4

LXIV. *A Radio Astronomical Investigation of Drift Movements in the Upper Atmosphere*

By A. Maxwell and M. Dagg
Jodrell Bank Experimental Station, University of Manchester*

[Received March 1, 1954]

Summary

The metre wavelength emission from the radio stars is diffracted by irregularities in the electron density of the ionosphere, which occur mainly at night at a height of approximately 400 km. Fading records taken with three receiving equipments, triangularly sited, show systematic time displacements, and these are attributed to a steady translational movement of the diffracting screen. The motion is normally of the order of 50–300 m/sec, is generally transverse to the magnetic lines of force and often remains constant over periods of many hours. During the first half of the night the prevailing direction is towards the West, at approximately 01^h there is often a reversal, normally effected within a period of 30 minutes, and thereafter the motions are predominantly towards the East. The effective wavelength of the ionospheric irregularities remains appreciably constant over a velocity range of 20 : 1, so that the magnitude of the drift velocity may be estimated from a count of the fading rate. By observing the Cygnus source when it is low on the Northern horizon it is possible to determine the F region drift velocities in the auroral zone ; these are about 400 m/sec, that is, twice as fast as the F region motions at temperate latitudes.

Investigation of the drift motions at points separated by 800 km suggests that the drift speeds and directions are the same over wide areas, and experiments made in co-operation with members of the Cavendish Laboratory, Cambridge, over a 200 km base line support this. Observations of F region motions made elsewhere, with different techniques, are in good agreement with the present results.

§ 1. Introduction

During the past four years a number of observers have considered the information which may be deduced from the fading in the radio emission from the so-called radio stars or discrete sources. This fading, which occurs on metre wavelengths, is impressed on the incoming radiation as it passes through a diffracting screen of electron clouds in the F region of the ionosphere (Little and Maxwell 1951, Little 1951, Ryle and Hewish 1950, Hewish 1951, 1952). The height of the diffracting screen

* Communicated by Professor A. C. B. Lovell.

is not known precisely, but it is believed to lie between the maximum of ionization in the F region and the exosphere, possibly at a height of 400–500 km. This level is generally inaccessible to the normal pulse sounding techniques used in ionospheric investigations, so that the radio-astronomical observations provide useful additional information about the uppermost regions of the ionosphere.

Maxwell and Little (1952) have shown that with receiving equipments arranged triangularly over base lines of the order 2–3 km it is possible to detect small differences in the time of occurrence of the individual fluctuations recorded at the respective stations. The systematic nature of these time displacements shows that the diffraction pattern on the ground has a steady translational motion, and this is attributed to the drift of the electron clouds in the ionosphere. Provided that an appropriate correction is made to compensate for the steady angular motion of the ray track through the ionosphere, due to the apparent motion of the stars, it is therefore possible to estimate the drift speed and direction of the ionospheric irregularities.

Observations of this type have now been made at the Jodrell Bank Experimental Station since 1951, and the results of the investigation are described in the present paper. The equipment and observational techniques are outlined in §§ 2 and 3. The results of 400 observations of the movements of the ionospheric diffracting screen are described in § 4 and an investigation of ionospheric motions in the auroral zone in § 5. The similarity of the drift motions over an 800 km base line is discussed in § 6, and in § 7 the present results are compared with observations of F region movements made elsewhere with different techniques.

The present paper is concerned only with the ionospheric movements ; their relation to various geomagnetic phenomena, and the nature and origin of the diffracting screen will be discussed elsewhere.

§ 2. Equipment

The apparatus used in these experiments comprised three receiving equipments operating at a wavelength of 3·7 metres, each consisting of a steerable aerial, a receiver of low noise factor and high gain (similar to that described by Little and Maxwell 1951) and a pen recording meter. One equipment was sited permanently at Jodrell Bank, and was used in conjunction with a 30 ft. aperture focal-plane paraboloid, the beamwidth of which to half power was $\pm 15°$ in the E plane and $\pm 13°$ in the H plane. The two remote equipments were mobile. One was used in conjunction with an array of two Yagi aerials (each consisting of 4 directors, folded dipole and reflector) whose beamwidth was $\pm 11°$, $\pm 22°$; the other was connected to a single steerable Yagi of slightly different design (6 directors, folded dipole and reflector), beamwidth $\pm 18°$, $\pm 20°$. All three aerials were constructed to receive radiation in the one plane of polarization, viz. vertical polarization when at zero elevation, and they were mounted with their electrical centres at heights

of 20 ft. so that the Cygnus source could be observed when at lower culmination (i.e. at angle of elevation of 4°). The time constants of the pen recorders were approximately 0·5 seconds, and this placed an upper limit of approximately 60 maxima per minute on the fading rate which could be observed. The fading rates recorded were all less than 30 per minute.

With adequately stabilized power supplies, observations of the fading of the signal strength of the radio stars are limited only by the statistical fluctuations, or noise ripple, in the receiver output. Ryle and Vonberg (1948) have shown that the noise ripple is given by $\Delta P/P=\sqrt{(1/\Delta f \,.\, T)}$ where ΔP=noise ripple for an input signal of power P, Δf=receiver bandwidth, T=output time constant. With the present equipment Δf=0·5 Mc/s, T=0·5 seconds (the receiver output time constants of 0·2 seconds being overweighted by the time constant of the pen recorders), hence the noise ripple was 1/500 of the receiver noise output. In practice only fading records with amplitudes greater than 1/200 receiver noise were used for analysis. During periods of deep fading, peak values showed intensities up to 40 times the minimum detectable signal.*

§ 3. Observational Techniques

(i) *Geographical Location of the Ionospheric Regions under Observation*

The radio stars used for these experiments were the two most intense sources, in the constellations of Cassiopeia, declination 58° 32′ and right ascension $23^h\ 21^m$, and Cygnus, declination 40° 35′ and right ascension $19^h\ 57^m$ (Smith 1951). The intensity of the radiation from these sources at a wavelength of 3·7 metres is of the order of 2×10^{-22} watts m^{-2} c.p.s.$^{-1}$.

Since the Jodrell Bank Experimental Station is situated at latitude 53° 14′ North and longitude 2° 18′ West both the Cassiopeia and Cygnus radio stars are circumpolar ; their elevations at transit are respectively 85° and 77° and at lower culmination 22° and 4°. As the elevation of a radio star changes, its line of sight cuts a given level of the ionosphere at a range R given by

$$R=\frac{r_0+h}{\cos E}\sin\chi,$$

where

$$\chi=\cos^{-1}\left[\frac{r_0\cos E}{r_0+h}\right]-E,$$

and E=the angle of elevation of the radio star, r_0=radius of the earth, h=height of the given ionospheric level. These expressions have been evaluated for h=400 km ; and the loci of the intersection of the lines of sight to the radio stars with the 400 km level, as their azimuths and elevations vary throughout the sidereal day, have been plotted in fig. 1.

* With apparatus of very great sensitivity, however, there is no doubt that fading of small amplitudes would always be observed, because the ionospheric layers are never entirely homogeneous.

(ii) *Times of Observation*

When the Cassiopeia and Cygnus sources are at angles of elevation greater than 15°, observations of fading phenomena are mainly confined to the hours of darkness (except during gross geophysical disturbances such as aurorae), because at temperate latitudes the F region diffracting screen occurs only during the night (Little and Maxwell 1951, 1952). The observations were further restricted by the fact that fading only occurred on one night in three throughout the year. When the Cygnus source is low on the Northern horizon, however, and its sight line passes through the highly disturbed ionospheric regions of the auroral zone, fading is invariably observed, both by day and night ; this occurs when the source is within ± 3 hours of lower culmination.

Fig. 1

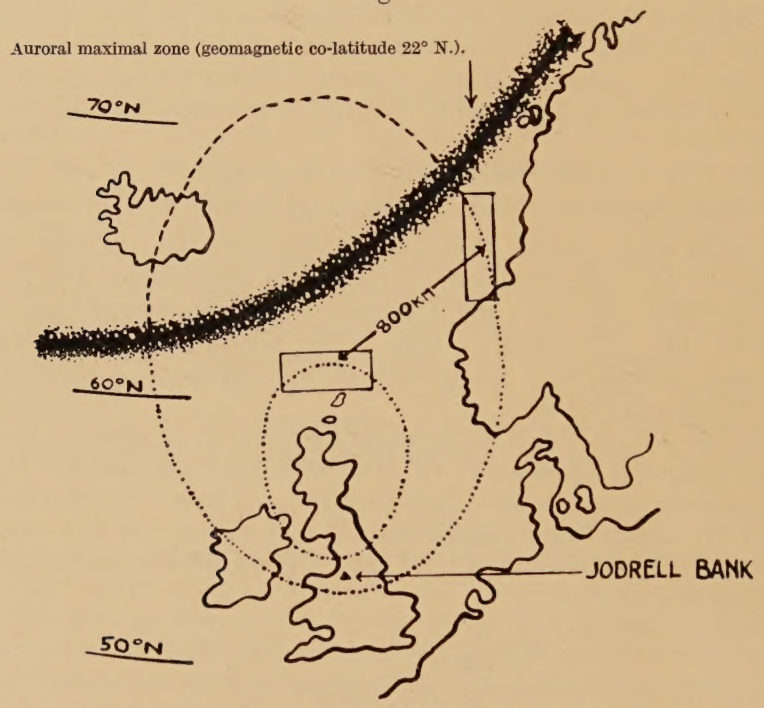

Paths traced out by the intersection of the Cassiopeia and Cygnus lines of sight with the 400 km level of the ionosphere.

(iii) *Correction for Earth Rotation*

The diffraction pattern of the ionospheric screen irradiated by a radio star will acquire a component of motion due to the steady angular motion of the star, and a correction must be made for this if the true motion of the screen relative to the ground is to be determined. The correction will be a function of the range of the disturbing region in the ionosphere as well as of the apparent angular motion of the star. At transit the

range of the disturbing region along the line of sight to each of the sources is 400 km, and their steady angular motions introduce components of motion towards the East—of the order of 16 m/sec for the Cassiopeia source (angular motion 8° per hour) and 24 m/sec for the Cygnus source (angular motion 12° per hour). At lower culmination the ranges are respectively 850 and 1950 km, and the components of motion are towards the West—approximately 35 m/sec for Cassiopeia and 115 m/sec for Cygnus. At times between transit and lower culmination the correction varies in a complex manner, and for the present experiments it has been deduced graphically from fig. 1, the magnitude of the correction vectors being given by the horizontal rate of change of position of the intersection of the line of sight with the ionosphere, and its direction by the tangent to this point on the locus. In most cases these corrections were about 20% of the true ionospheric velocities.

(iv) *Siting of Equipment*

Three different sets of triangular base lines were used for the experiments, as listed in table 1.

Table 1. Siting of Spaced Receivers

(Home receiver A ; remote receivers B, C)

Period of observation	*Receiver B* Distance and bearing from home site	*Receiver C* Distance and bearing from home site	Radio star observed	Geographical location of ionosphere under observation
1951 May–June	3·88 km 176° E. of N.	4·48 km 243° E. of N.	Cassiopeia at lower culmination	Region 500–900 km North of Jodrell Bank
1951 Sept.–Oct.	3·88 km 176° E. of N.	2·93 km 135° E. of N.	Cassiopeia and Cygnus at transit	Overhead
1952 April–1953 April	368 metres 177° E. of N.	315 metres 87° E. of N.	Cassiopeia and Cygnus mainly near lower culmination	Observations mainly (i) 500–900 km N. (ii) 1000–2000 km N. and (iii) a few observations overhead

The first two series of experiments have been briefly reported elsewhere (Maxwell and Little 1952). In these, each equipment was provided with its own pen recorder, running at chart speeds of 12 inches per hour, and a small transmitter operating on the receiver wavelengths was used to transmit calibration time pulses to the three stations. The subsequent

change to close spacing in the third series enabled an observer to alter the settings of all three steerable aerials from one radio star to the other within fifteen minutes ; in this way it was possible to study ionospheric conditions at widely separated areas almost simultaneously. In these latter experiments a duplex pen recorder was used with chart speeds of 1 to 12 inches per minute, and the receiver outputs were connected to it

Fig. 2

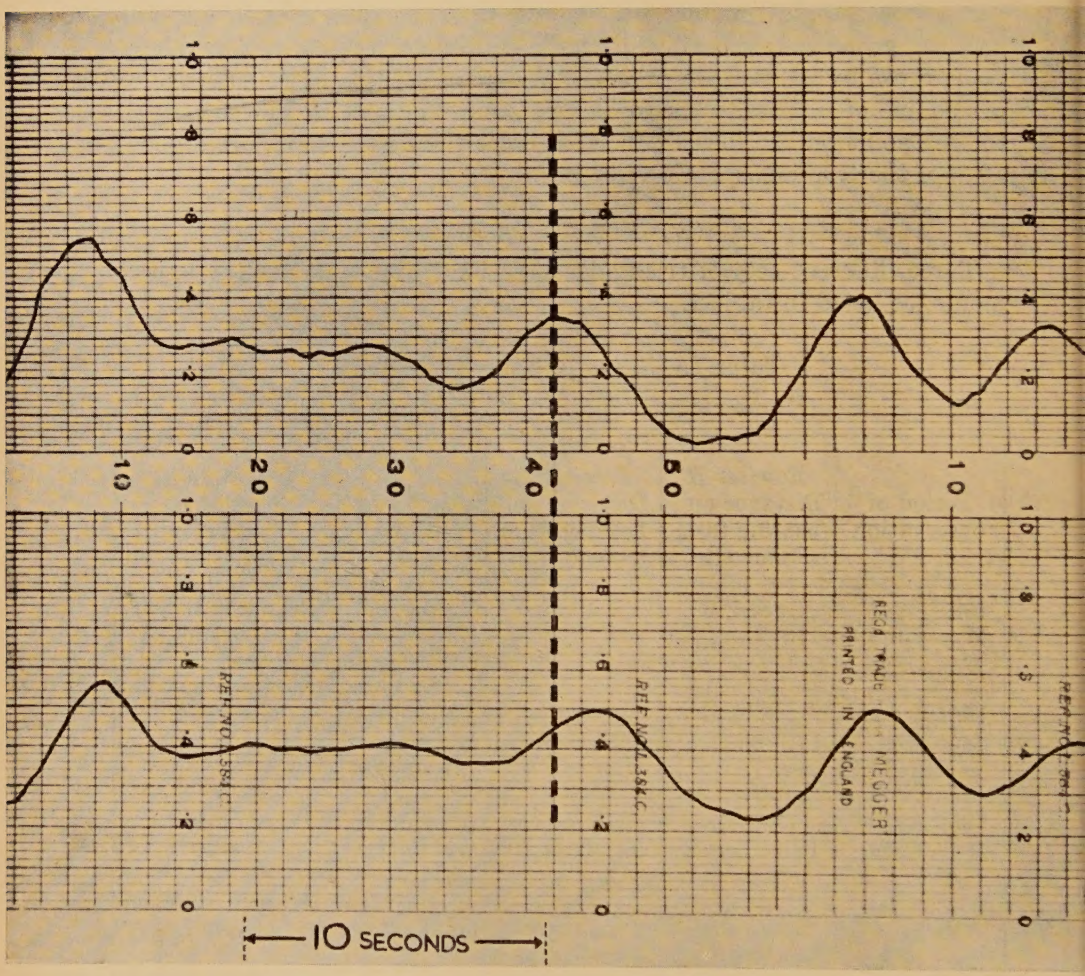

Radio star fading records taken simultaneously with two receiving equipments spaced 300 metres apart on an East–West base line. (1952 May 28, $23^h\ 50^m$; Cassiopeia source.)

in pairs, approximately three to five minutes of record being taken with each pair. Experience gained from the earlier experiments, where continuous records were taken over periods of many hours, indicated that the drift motions were normally fairly constant over 15 minutes, and that such a procedure was justified.

(v) *Analysis of Records*

(*a*) *Time Differences*

The time differences occurring between records taken at two stations are most accurately determined from their cross-correlogram in time, but in the present experiments the equipments were so arranged that the records were always closely correlated, and under these circumstances any time differences could be read off directly. Typical pairs of records, such as those shown in fig. 2, normally contained some half dozen fading maxima. For each pair of records six estimates of time displacements were obtained by two independent observers; in most cases the deviations of the 12 individual estimates from the mean value were small, but on some few occasions they were considerable, i.e. there appeared to be large random motions.

(*b*) *Fading Rate*

The fading, or fluctuation rate will be defined as the number of individual maxima occurring per minute. It will be seen from fig. 2 that the fluctuations themselves are irregular in shape, duration and amplitude, and it is inevitable that, to some extent, a visual count of the fading rate will be subjective. In order to establish consistency between estimates of the fading rate for small and large amplitudes, deviations of less than 10% of the average fluctuation amplitude were disregarded.

§ 4. Drift Movements in the Upper F Region

(i) *Observational Data*

The results discussed in this section are derived from 400 observations of the drift of the sporadic irregularities in the F region, made at intervals of not less than $\frac{1}{2}$ hour on 62 separate nights. They were taken when the Cassiopeia source was within ± 5 hours of lower culmination, and therefore refer to ionospheric conditions 500–900 km North of Jodrell Bank. Previous work (Maxwell and Little 1952) has shown that there is a marked similarity between the speed and direction of the drift motions which occur overhead and those that exist 500–900 km North. It is therefore probable that the results summarized here apply to the region extending from England to the zone of high auroral activity. Longitudinal effects are assumed to be small, because over the area of the observations the maximum difference in solar time is only 50 minutes. In this region the radio star fading occurs only at night, hence the observations were limited to the hours 18–05. Most of the results for the period 01^h–05^h were obtained during the months December–March, since fading of the radio star emission during these hours is rare in the summer months. The observations extended from 1951 April to 1953 April, but for the purpose of this analysis they have been considered in terms of their diurnal variations.

Following the ionospheric convention now generally adopted, the direction (or azimuth, or bearing) will be taken as the vector direction, that is the direction *towards* which the diffracting screen is moving.

(ii) *Magnitude and Direction of Drift Motions*

The analysis of the above data showed that the drift speeds of ionospheric irregularities varied from 30 m/sec to 1200 m/sec,* with a mean value of 200 m/sec. A histogram of their distribution is shown in fig. 3 ; the most frequently occurring drift speed was 100 m/sec.† The speeds varied considerably from night to night and showed a close correlation

Fig. 3

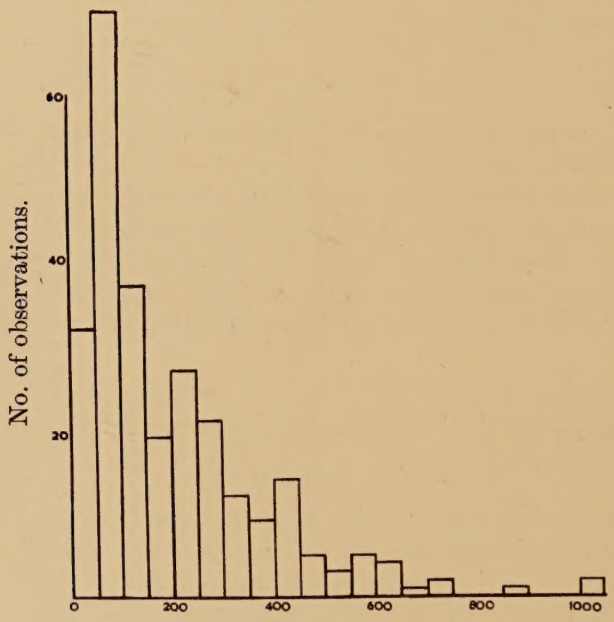

Drift speed in metres per second.

Histogram of F region drift speeds.

with the disturbance variations in the geomagnetic field. Subject to stable geomagnetic conditions the speeds during any given night remained constant. The change in the *average* speed from hour to hour is given in

* In this connection it is interesting to notice that the velocity of sound in the F region is also of the order of 1000 m/sec., and hence at the upper limit of drift speeds the gas must be compressible.

† Similar observations taken at Cambridge by Hewish (1952) with two receivers spaced over a 1 km East–West base line are in good agreement with the Jodrell Bank results. On the assumption that the drift movements were predominantly East and West, Hewish found the most probable drift speed to lie between 100 m/sec and 300 m/sec.

table 2, and the relation of these average speeds to the average geomagnetic K-indices will be considered elsewhere.

The direction of the motion of the diffracting screen was nearly always along an East–West line, North–South components normally being less than 30 m/sec. This may be seen from the polar histograms of fig. 4, which show the number of occasions on which the drift directions lay in each 15° sector. During the first half of the night, from 19^h to 00^h, the prevailing direction was towards the West, between 00^h and 01^h the direction changed by 180°, and from 01^h to 05^h the prevailing direction was towards the East. The interpretation of these results in terms of a regular reversal at 00^h–01^h must at present be regarded with caution, as only 60 observations were taken after 01^h; these were made on 19 nights during the winter months, often during magnetically disturbed conditions.

Table 2. F Region Average Drift Speeds

Hour	Average speed in m/sec	Hour	Average speed in m/sec
$19^h\,30$	159	$00^h\,30$	161
$20^h\,30$	187	$01^h\,30$	286
$21^h\,30$	181	$02^h\,30$	288
$22^h\,30$	231	$03^h\,30$	268
$23^h\,30$	183	$04^h\,30$	172

On 16 separate occasions observations were taken throughout the periods when the drift direction changed by more than 120°. Normally such reversals were completed within 30–60 minutes, and on 10 occasions they occurred within the hours $23^h\,30$–$01^h\,30$. On four occasions the drift direction reversed for only one or two hours and then reverted to the original direction. Apart from the tendency to reverse at midnight the direction was usually remarkably constant, often remaining within a sector of 20° even when the drift speed changed by as much as a factor of five.

(iii) *Relation of Drift Speed to Fading Rate*

The earliest observations of radio star fading showed that the average value of the fading rate was 2 maxima per minute, but that this could vary within the range 0·2 to 10 or 20 maxima per minute on exceptional nights. It was suspected that these changes might be caused by varying wind speeds in the upper ionosphere, in much the same way as varying wind speeds in the troposphere change the rate of twinkling of ordinary visual stars. For example, Little and Maxwell (1951) pointed out that wind velocities of the order of 120 metres per second, such as those observed in the lower F region by Munro (1948) with ionospheric sounding equipment, would lead to fading with a period of 30 seconds, and that in

Fig. 4

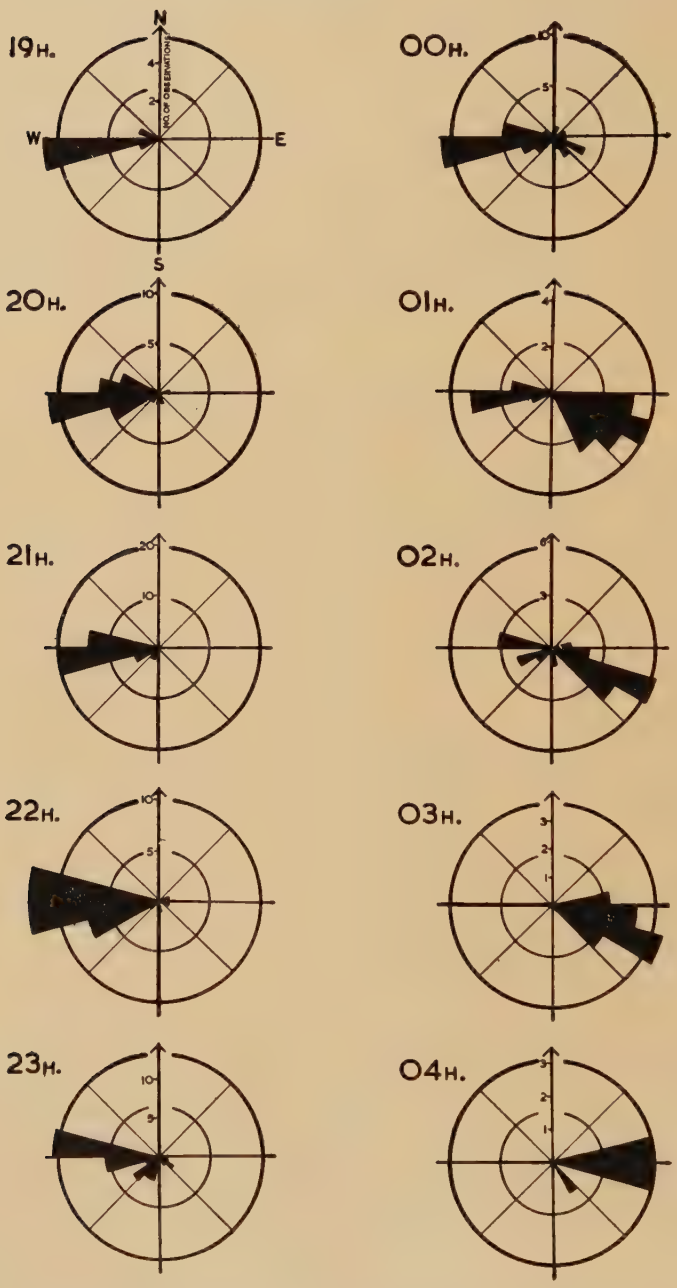

Hourly polar histograms of F region drift directions.

the absence of winds the apparent motion of the radio star would lead to fading with a period of approximately 3 minutes. These estimates were made on the assumption that the ionospheric irregularities had dimensions of the order of 4 km. It was not certain, however, whether varying wind speeds were the sole cause of the differing fluctuation rates, or whether associated changes in the size of the ionospheric irregularities also contributed to the observed variations.

Fig. 5

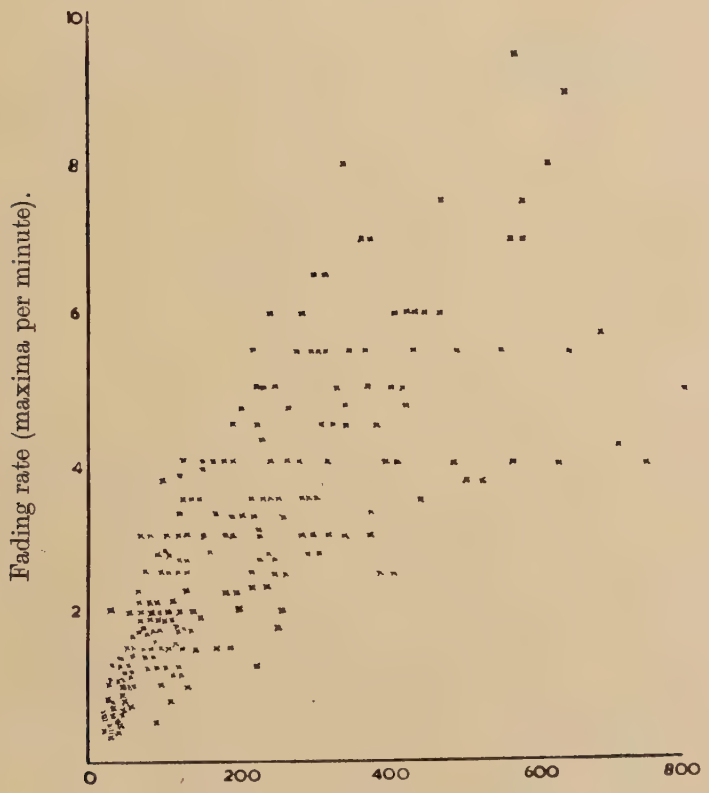

F region drift speed *v*. fading rate.

With accurate determinations of velocity made by three receiver techniques it has been possible to resolve this ambiguity. Figure 5 shows the relation between the ionospheric velocities and the corresponding fading rates. For the range of velocity magnitudes 30–1000 m/sec the fading rate and velocity are nearly linearly related, and the scatter of points is within 20%. (Correlation of the fading rate with the velocity of the diffraction pattern across the ground shows slightly less scatter, as it is the drift of this paternt through an aerial system, i.e. the vector

resultant of the true ionospheric motion and the apparent motion of the star, which determines the fading rate.) It would appear then that the wavelength of the irregularities in the ionospheric screen remains effectively constant for all velocities of the screen. It is therefore possible to make an estimate of the drift speed from a count of the fading rate ; for the Jodrell Bank observations the average values of the F region drift speeds for increasing fading rates may be tabulated as follows :

Table 3

Fading rate (maxima per min)	Magnitude of drift velocity (metres per second)
1	50
2	120
3	190
4	270
5	330
6	390
7	440
8	480
9	530

§ 5. Drift Movements in the F Region of the Auroral Zone

As mentioned in § 3, it is possible to investigate ionospheric conditions in the auroral regions by observing the Cygnus source at lower culmination. At these low angles of elevation, however, it is difficult to determine the extent to which the Cygnus radiation is affected by irregularities in the troposphere and E region. Little and Maxwell (1951) have suggested that for angles of elevation above 4° tropospheric effects will be small, as the variations in refractive index for the troposphere are approximately 1000 times less than in the F region, and the slant thickness only 1/10 that of the F region. It is also unlikely that sporadic E has any appreciable effect on the present low-angle observations, even though this type of ionospheric irregularity is much more intense in the auroral regions than at lower latitudes.* For, in the extreme case, when the Cygnus source is at lower culmination, the intersection of the sightline with the E region is 800 km North of Jodrell Bank, which is well outside the auroral zone, and the relative thicknesses of the F and E regions are still of the order of 6 : 1. The 200 observations described in this section are therefore believed to refer to the F region movements in the auroral zone. They were made when the Cygnus source was within ± 3 hours of lower culmination during the year 1952 April–1953 April.

* In the auroral zone, sporadic E sometimes returns pulse transmissions up to frequencies of 16 Mc/s at vertical incidence ; cf. *Researches of the Department of Terrestrial Magnetism*, Washington (1947), **12,** 9.

A histogram showing the distribution of the observed drift speeds is given in fig. 6. The speeds varied from approximately 50 m/sec to 1000 m/sec, and their average was 360 m/sec.* During stable geomagnetic conditions the velocities remained constant (cf. §4 (ii)). The *average* drift speeds over the four 6-hour periods commencing at noon are given in table 4, from which it will be seen that the average drift speeds were much the same throughout the 24 hours of the day.

Table 4. F Region Average Drift Speeds (Auroral Zone)

Period U.T.	Average drift speed m/sec	Number of observations
12^h00–17^h30	365	36
18^h00–23^h30	313	92
00^h00–05^h30	410	60
06^h00–11^h30	487	9 (No observations between 06^h00 and 08^h30)

Fig. 6

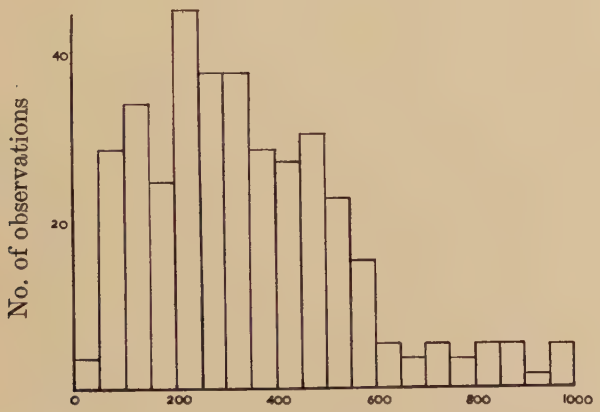

Histogram of F region drift speeds in the Auroral Zone.

Between 09^h and 21^h the preferred drift direction was towards the West, and from 21^h to 06^h towards the South-East or South-West (fig. 7). It must be remarked, however, that apparent North–South components could be due entirely to drifts which were vertically upwards, so that the interpretation of the motions in terms of horizontal components must be regarded with caution.

* Only 6 of these observations were taken when the geomagnetic K-indices were higher than 6.

The magnitude of the drift velocity was again found to be nearly linearly related to the fading rate, so that a rough estimate of the drift speed of the F region irregularities in the auroral zone can be obtained from a count of the fading rate (table 5). These estimates are, however, less accurate than the data given for the region overhead (table 3) because the correction for the steady angular motion of the star is much larger.

Fig. 7

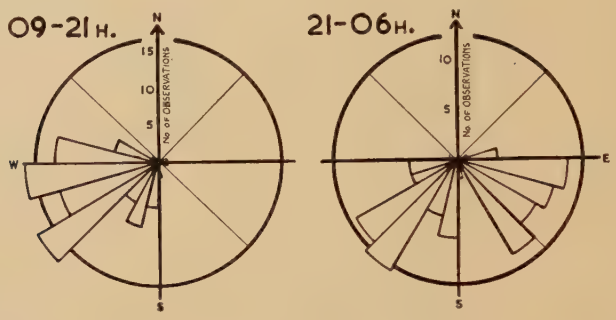

Polar histograms of F region drift directions in the Auroral Zone.

Table 5

Fading rate (maxima per min)	Magnitude of drift velocity (metres per second)
1	100
2	170
3	240
4	300
5	375
6	450
7	520
8	570

§ 6. Comparison of F Region Drift Motions over Extended Base Lines

By making simultaneous observations of the fading of radio stars at different celestial coordinates it is possible, from the one set of observing sites, to compare ionospheric drift movements over widely separated areas. In the present experiments the F region motions over the Shetland Islands have been compared with those occurring almost simultaneously over Western Norway ; these areas are at approximately the same geomagnetic latitude, and the distance between them is 800 km along a line to the North East. The observations were made entirely from Jodrell Bank, the directions of the aerial beams being changed from the Cygnus source at 3–4 hours past lower culmination to the Cassiopeia source at lower culmination (see the map in fig. 1 ; the radio sources

differ in right ascension by $3^h\ 24^m$). The investigation was made on 18 different nights during 1952 April, May, June and 1953 February, March, and the observations of the F region motions in the two areas were normally made within 1–1½ hours of one another.

Analysis of the results showed that in general the velocities in the two areas were in excellent agreement. The drift directions were identical to within a standard deviation of 10° and the differences in drift speed were, on the average, less than 30%. This accordance held for both Westerly and Easterly drift directions, and it may be concluded, therefore, that over the 800 km base line the drift velocities were substantially the same.

A series of observations of F region movements made simultaneously over a 200 km base line between Cambridge and Jodrell Bank in May and June 1952 provide further evidence in favour of this conclusion. The Cambridge observations were made at 6·7 m, the Jodrell Bank observations at 3·7 m, and both stations used the Cassiopeia source near lower culmination. At Cambridge, two receivers were used, and these were situated on an East–West base line of 1 km. For comparison purposes therefore, the East–West component was taken from the Jodrell Bank results and the appropriate time delays over an East–West base line were scaled to correspond to a base line of 1 km. Over the 30 observing nights 80 observations were made at Cambridge and 100 at Jodrell Bank, but only 30 of these were taken simultaneously at the two stations or within half an hour of each other. The results of this comparison may be summarized as follows :

(i) The directions of the movements (i.e. East–West component either towards W. or towards E.) agreed on 90% of occasions. (ii) The correlation between the actual time displacements over a 1 km base line, as recorded at Cambridge and estimated at Jodrell Bank, was 0·5, which for 30 results is significant, the probability of a random coincidence being much less than 1 in 100. (iii) The correlation between the fluctuation rate, which has been shown to be linearly related to the wind velocity, at the two sites was approximately 0·6.

These results indicate that over a distance of 200 km the F region movements are similar—as would be expected from the observations covering a 800 km base line described above. However, there remain certain definite and significant discrepancies between the directions and time differences recorded at Cambridge and Jodrell Bank, and it is obvious that many further observations made with three receiver techniques at two such stations are required to determine the exact degree of correlation between the speed and direction of the F region irregularities at large distances.

§ 7. Comparison with Results Obtained by Other Methods

Apart from the radio-astronomical observations there are at present two other methods of investigating F region movements : ionospheric sounding measurements, in which a pulsed transmission is examined after

Table 6. Comparison of Existing Experimental Evidence about F Region Motions

Observer	Country	Method	Time of year	Local time of day	Direction	Average speed in m/sec
Hewish[1]	England	Radio Star Fading; 2 receivers on E.–W. base line	1951 Jan.–April	1800 (6 observations) 0000–0500	West Predominantly East	100–300
Maxwell & Little[2] Maxwell & Dagg[3]	England	Radio Star Fading; 3 receivers triangularly sited	1951 April–1953 April	1800–0030 0030–0500	West Predominantly East	50–300
		Auroral Zone observations	1952 April–1953 April	1100–2100 2100–1100	West South (?)	200–500
Meek[4]	N. Canada	*Auroral Zone* observations; h'–f records (1 equipt. only)	1949 March			200–350
Munro[5]	E. Australia	Reflection from large scale irregularities	1948 Winter 1948–9 Summer 1950–1–2 June 1952	0900–1700 0900–1700 0900–1700 Night	20° East of North 110° East of North Change from 50° E. of N. to 15° E. of N. during day Predominantly West	80–130
Price[6]	W. Australia.	ditto	1950–2 Winter 1950–2 Summer	0900–1700 0900–1700	0–60° East of N. 90–180° East of N.	90–330
Bramley & Ross[7]	England	ditto				35–350
Beynon[8]	England	ditto	1942–3 Winter	Sunrise	West	120
Phillips, Briggs & Spencer[9]	England	Reflection from small scale irregularities	1949 Feb.–1951 June 1952 Jan. onwards	1900–0500 1900–0500 0500–1900	Predominantly West West East	100
Salzberg & Greenstone[10]	U.S.A.	ditto	1949 Feb.–1951 June	1900–0500	West	100
Chapman[11]	Canada	ditto	1950 June–1951 June			100
Krautkramer[12]	Germany	ditto	1941–2 Winter			90
Roach, Williams & Petit[13]	U.S.A.	*Photometric*: 5577 Å line in night glow	1951 Jan. 6 and 1952 Nov. 19 (2 nights only).	Night {until 0000 after 0000	West South-East	150
Hutuhata[14]	Japan	*Photometric*: 8000–11500 Å emission in night glow	1949 Jan.–1950 Dec.	Night	North-North East or South-South West.	100

[1] Hewish, *Proc. Roy. Soc.* A (1952), **214,** 494 ; [2] Maxwell & Little, *Nature* (1952), **169,** 746 ; [3] Maxwell & Dagg (present paper) ; [4] Meek, *J. Geophys. Res.* (1949), **54,** 339 ; [5] Munro, *Nature* (1948), **162,** 886 ; *Nature* (1953), **171,** 693 ; *Proc. Roy. Soc.* A (1950), **202,** 208 ; [6] Price, *Nature* (1953), **172,** 115 ; [7] Bramley & Ross. *Proc. Roy. Soc.* A (1951), **207,** 251 ; *Nature* (1951), **167,** 626 ; [8] Beynon, *Nature* (1948), **162,** 887 ; [9] Phillips, Briggs & Spencer, *J. Atmos. Terr. Phys.* (1952), **2,** 141 ; *Rep. Phys. Soc. Progr. Phys.* (1954), **17** ; [10] Salzberg & Greenstone, *J. Geophys. Res.* (1951), **56,** 521 ; [11] Chapman, *Can. J. Phys.* (1953), **31,** 120 ; [12] Krautkramer, *Archiv. der Eleck. Uber.* (1950), **4,** 133 ; [13] Roach, Williams & Petit, *Astrophys. J.* (1953), **117,** 456 ; [14] Hutuhata, *Nature* (1953), **171,** 419 ; Report of Ionosphere Research in Japan (1952), **6,** 31.

reflection from the F region (information from such experiments has been collated by Briggs and Spencer 1954), and photometric observations of the drift of the intensity contours of certain emission lines in the night sky glow. The photometric observations are at present not very numerous, and there is some uncertainty about the height at which the emission clouds actually occur (Bates and Dalgarno 1953). Observers in the United States of America consider that the results which they have recently obtained from measurements of (OI) 5577 Å line refer to a height of 250–300 km. Infra-red emissions in the band 8500–11000 Å, which are believed to be associated with (OH) ion-clouds, and whose motions have been studied by Japanese observers, are also believed to be at a height of 300 km.

The existing information about F region motions is summarized in table 6, which shows that the results obtained from the various techniques are in good agreement. The drift speeds lie within the range 50–300 m/sec, and most observers find that the movements are predominantly due East or due West. The radio-sounding observations suggest that the motion is towards the East during the day and towards the West at night, but this is in conflict with the radio-astronomical results which indicate that Easterly movements may often predominate after midnight. It is very probable, however, that the ionospheric transmission screen which causes the radio star fading is quite distinct from the screens which reflect the pulse transmissions from the ground; for example, the radio astronomical screen appears only at night and is believed to be above the level of maximum ionization, whereas the reflecting screens used by the sounding methods are always present and occur below the maximum of ionization. This would suggest that the circulation in the upper levels of the F region may be distinct from that of the lower levels.

The relation of the F region movements to those of the E region has been considered by Briggs and Spencer (1954). They find that the drift velocities in the E region are distinguished from those of the F region by strong diurnal and semi-diurnal rotating components, and that the magnitude of their total velocity is somewhat lower, approximately 50–100 m/sec.

§ 8. Discussion

The results described in this paper show that in the uppermost levels of the ionosphere there are systematic translational movements of the electrons, and that these are similar over wide geographical areas. In the auroral zone, however, the circulation appears to be quite different from that at latitudes 10° or 20° further South; the drift movements there are much faster, 360 m/sec average compared with 210 m/sec, and they do not show the tendency to reverse from West to East at 01^h (the direction changes that do occur seem to take place at 21^h). The continuity and extent of the observations were limited by the sporadic nature of the high level diffracting screen which gives rise to the fading,

but there is no reason to assume that the drift velocities were zero on nights when fading was not observed, as no one to one correlation has been established between the amplitude of the fading and the drift velocity. In the auroral zone, at least, the drift velocities are much the same both by day and night (§ 5), and at temperate latitudes pulse sounding measurements give a similar result for the lower levels of the ionosphere.

The results have not been analysed for rotational vectors superimposed on the prevailing directions. The main vector shows no obvious rotation, but it is not impossible that a rotating component of 1/10 magnitude of the main vector might be present. The correction for the steady angular velocity of the ray track through the ionosphere is, however, of this order, and its direction changes steadily. If this correction, which is known only to a first approximation, were slightly over-emphasized it would give rise to a small but spurious rotating component. The uncertainty in individual velocity measurements, determined from sets of time differences such as those described in § 3 (v) is of the order of 10% in drift speed and $\pm 5^\circ$ in direction. Calculation of the inaccuracies in the actual measurement of the time differences indicates that approximately half of this may be attributed to the experimental limitations, and that the remainder is probably due to true variations in the velocity over the 10 minute period required for an observation, and also to the fact that the electron clouds which successively drift across the receiving equipments may have lines of maximum density that are slightly skew.*

No attempt has been made to discuss the relation of the motion of the localized irregularities in electron density to the motion of the neutral particles at the 400–500 km level. It is to be expected that the motion of the unionized matter, for instance, will be under thermal and gravity control, and that the direction and magnitude of the electrodynamic forces which govern the movements of the localized irregularities will depend on the relative motion of the neutral particles with respect to the earth's magnetic field. Vestine (1954) has derived qualitative wind systems for geomagnetic storm-time and disturbance daily variations. At temperate latitudes the diurnally varying part requires high-level zonal wind systems which are towards the West from 12^h to 00^h and towards the East thereafter. This prediction is in interesting agreement with the experimental observations described in § 4.

Acknowledgments

The authors wish to thank Professor A. C. B. Lovell, Director of the Jodrell Bank Experimental Station for his helpful advice and criticism, and their colleague Dr. C. G. Little for assistance in taking the observations. They are also indebted to Dr. A. Hewish and Mr. R. L. Adgie of

* The authors are indebted to Mr. J. A. Ratcliffe for drawing their attention to this latter point.

the Cavendish Laboratory, Cambridge, for their co-operation in making simultaneous observations during May and June 1952. The work described in this paper forms part of a research programme made possible by financial assistance from the Department of Scientific and Industrial Research. One of the authors (M. D.) is individually indebted to the Department for the award of a maintenance grant.

References

Bates, D. R., and Dalgarno, A., 1953, *J. Atmos. Terr. Phys.*, **4,** 112.
Briggs, B. H., and Spencer, M., 1954, *Rep. Phys. Soc. Prog. Phys.*, **17** (in publication).
Hewish, A., 1951, *Proc. Roy. Soc.* A, **209,** 81 ; 1952, *Ibid.*, **214,** 494.
Little, C. G., 1951, *Mon. Not. Roy. Astr. Soc.*, **111,** 289.
Little, C. G., and Maxwell, A., 1951, *Phil. Mag.*, **42,** 267 ; 1952, *J. Atmos. Terr. Phys.*, **2,** 356.
Maxwell, A., and Little, C. G., 1952, *Nature, Lond.*, **169,** 746.
Munro, G. H., 1948, *Nature, Lond.*, **162,** 886.
Ryle, M., and Hewish, A., 1950, *Mon. Not. Roy. Astr. Soc.*, **110,** 381.
Ryle, M., and Vonberg, D. D., 1948, *Proc. Roy. Soc.* A, **193,** 98.
Smith, F. G., 1951, *Nature, Lond.*, **168,** 555.
Vestine, E. H., 1954, *J. Geophys. Res.* (in publication).

LXV. *The Classification and Mean Lifetimes of θ^0- and Λ^0-Particles*

By D. B. GaythER *
The Physical Laboratories, The University, Manchester†

[Received March 17, 1954]

Abstract

A study is made of the properties of the decays of about 50 V^0-particles in a medium-sized cloud chamber equipped with either one or two lead plates but without a magnetic field. The decays are classified into those due to θ^0- and to Λ^0-particles using methods suggested by Podolanski and Armenteros (1954). The mean lives of the θ^0- and Λ^0-particles are found to be $(1{\cdot}2^{+0{\cdot}8}_{-0{\cdot}3}) \times 10^{-10}$ sec and $(4{\cdot}0^{+3{\cdot}7}_{-1{\cdot}2}) \times 10^{-10}$ sec respectively.

§ 1. Introduction

The Wilson cloud chamber has been used for the study of V^0-particles by many workers. If a magnetic field is employed then it is unusual to have more than one lead plate inside the chamber, the majority of magnet chambers being used without a lead plate. If no magnetic field is available, however, it is usual to have a considerable number of thin lead plates inside the chamber. In the present experiment, a medium-sized cloud chamber without a magnetic field, but with only one or two lead plates, is used for a study of the properties of V^0-particles, particularly their mean lifetimes.

The various groups using magnet cloud chambers, and to a lesser degree those using multiplate chambers, have shown that the majority of V^0-events are produced by two types of V^0-particle which probably decay spontaneously according to the decay schemes

$$\Lambda^0 \rightarrow p^+ + \pi^- + 37 \text{ mev}, \quad . \quad . \quad . \quad . \quad . \quad . \quad (1.1)$$

$$\theta^0 \rightarrow \pi^+ + \pi^- + 210 \text{ mev}. \quad . \quad . \quad . \quad . \quad . \quad . \quad (1.2)$$

The results of the numerous experiments made before the beginning of 1953 have been summarized by Rochester and Butler (1953); the more recent work is summarized in the report of the Bagneres de Bigorre conference on cosmic rays (1953). Various groups, notably Leighton *et al.* (1953), Ballam *et al.* (1953) and Barker (1954) have described a few V^0-events which cannot be interpreted by schemes (1.1) and (1.2). It is generally agreed, however, that not more than about 10% of the V^0-events are of the anomalous type.

* Communicated by Professor P. M. S. Blackett, F.R.S.
† Now at A.E.R.E., Harwell.

In the present paper, a detailed discussion is given of the decays of 44 V^0-particles produced inside the cloud chamber. The analytical methods of Podolanski and Armenteros (1954) are used to classify many of these events into θ^0- and Λ^0-particles.

§ 2. The Apparatus

2.1. *The Cloud Chamber*

The cloud chamber is of the solid piston type and has an illuminated volume of approximately $40 \times 30 \times 20$ cm^3. The illumination is provided by two cylindrical quartz discharge lamps, each dissipating 650 joules per flash. The tracks are photographed stereoscopically on 35 mm Ilford 5G91 film at a lens aperture of $f/9$ and a mean magnification of 1/12.

The chamber is situated at the Observatoire du Pic-du-Midi at an altitude of 2867 m.

Fig. 1

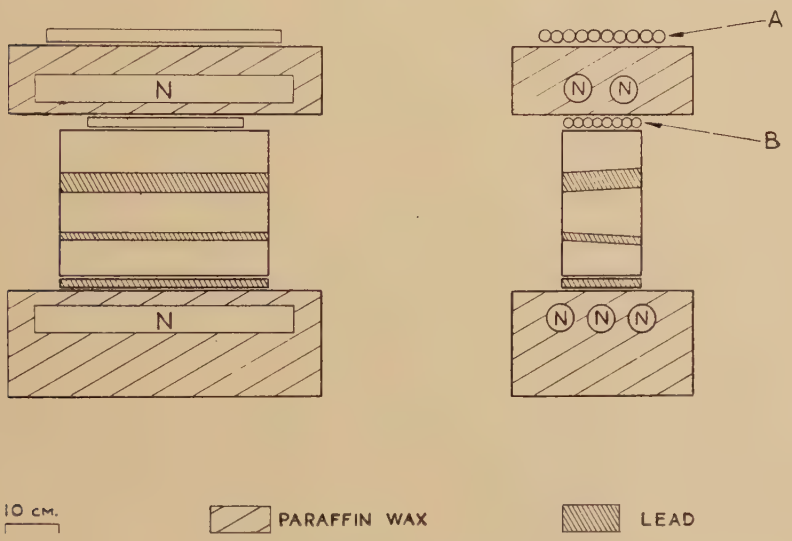

The counter control system

The first counter arrangement was a four-fold Geiger system under a producing layer of 7·5 cm of lead. A two-fold tray was placed immediately on top and a two-fold tray, screened by 10 cm of lead, immediately below the chamber. Later, in order to study the types of interactions producing V^0-particles, a selection system using both Geiger and neutron counters was used. This arrangement is sensitive to low energy interactions in the lead plates produced by protons since no ionizing particles are required below the chamber. The arrangement is shown in fig. 1 and closely resembles that described by Barker *et al.* (1953). The chamber is triggered if at least two slow neutrons from nuclear interactions are

detected in a 400 μsec gate opened 5 μsec after the pulse from the Geiger counter telescope AB. The five neutron counters N are connected in parallel. The efficiency of detecting neutrons produced in the 4 cm lead plate was measured using a calibrated Ra–α–Be source. The value is 1% after correction for the loss of neutrons captured after the termination of the neutron coincidence gate (cf. Barker *et al.* 1953).

Three slightly different lead arrangements, namely B, C and D, have been used with the neutron detecting system. A preliminary analysis of the photographs is given in table 1.

Table 1. Analysis of Photographs

Selection system	A	B	C	D
Counter arrangements	Geiger	Neutron	Neutron	Neutron
Lead producing layer above chamber (cm)	7·5	4	2	—
Lead plate(s) inside chamber (cm)	1·8	1·8	4·0 1·5	4·0 1·5
Total no. of photographs	2007	4377	1490	8691
No. of interactions in 1·8 cm or 4·0 cm plate	~97	~280	215	1470
No. of V^0-tracks produced in 1·8 cm or 4·0 cm plate	5	9	3	27

The second lead plate used in systems C and D was introduced in order to facilitate the identification of nuclear interactions in the upper plate since at least one penetrating particle is required to identify a shower as a nuclear interaction.

A detailed study is being made of the types of interaction in which the V^0-particles were produced.

§ 3. The Classification of the V^0-Events

3.1. *Classification Procedure*

It was mentioned in § 1 that the majority of the V^0-events are produced by the decay of θ^0- and Λ^0-particles according to the decay schemes (1.1) and (1.2). If these two schemes are assumed, many of the decays photographed in the chamber described in § 2 can be identified. A brief discussion of a useful method, which is applicable to low-energy events, will now be described.

The secondary particles of a two-body decay scheme have equal and opposite momenta, p^*, in the rest system. The value of p^* for each

decay process can be calculated from the known mass of the unstable particle and the masses of the two secondary particles. Furthermore, it is usual to assume that in each two-body decay process the secondary particles are emitted isotropically in the rest system. The angle between the trajectory of a V^0-particle and the direction of the secondary particles in the rest system is called θ^*.

In order to classify a V^0-event, the angles ϕ_1 and ϕ_2 between the line of flight of the V^0-particle and the two charged secondary particles must be measured. In addition, estimates of the ionizations of the secondary particles, which have unknown momenta p_1 and p_2, are required.

If, for a particular decay, a transformation is made from the rest frame of reference to the laboratory frame, the components of the momenta of the secondary particles transverse to the trajectory of the V^0-particle are unaltered. Thus the transverse momentum, p_t, is given by

$$p_t = p^* \sin\theta^* = p_1 \sin\phi_1 = p_2 \sin\phi_2. \quad . \; . \; . \quad (3.1.1)$$

Since each decay scheme has a unique value of p^* then, if θ^* can be found from the values of ϕ_1 and ϕ_2 for each scheme in turn, two sets of values of p_1 and p_2 can be found. Now the masses of the secondary particles are known so that the expected ionizations of the secondaries can be calculated from the two sets of p_1 and p_2 and compared directly with the observed values. In general, provided that the basic assumptions of the analysis are correct, only one set of calculated ionizations will agree with the experimental values for each event. In a small percentage of the examples it may not be possible to make an identification.

For the determination of θ^* and, when the decay has been classified, the momentum, P, of the V^0-particle, the elegant methods of Podolanski and Armenteros (1954) are used. A particular decay is described by two non-dimensional parameters α and ϵ.

α is defined by the relation

$$\alpha = \frac{p_1^2 - p_2^2}{P^2} = \alpha^* + 2p^* \cos\theta^* \left\{\frac{1}{M^2} + \frac{1}{P^2}\right\}^{1/2}, \quad . \quad (3.1.2)$$

where $\alpha^* = (m_1^2 - m_2^2)/M^2$ and M, m_1, m_2 are the masses (in Rossi units) of the V^0-particle and the two secondary particles respectively. α^* is a constant for a particular decay scheme. The α-value for an event is derived from the measured quantities ϕ_1 and ϕ_2 by using the expression

$$\alpha = \sin(\phi_2 - \phi_1)/\sin\phi \quad . \; . \; . \; . \; . \quad (3.1.3)$$

where $\phi = \phi_1 + \phi_2$.

The second parameter, ϵ, is defined by

$$\epsilon = 2p_t/P = 2 \sin\phi_1 \sin\phi_2/\sin\phi. \quad . \; . \; . \; . \quad (3.1.4)$$

α and ϵ may conveniently be used as coordinates in a diagram on which all the events are plotted. For a given decay scheme, it can be shown that lines of constant V^0-particle momentum, P, are confocal ellipses,

with foci F_1 and F_2 on the α axis at $(\alpha^*-\epsilon^*)$ and $(\alpha^*+\epsilon^*)$ respectively. ϵ^* is also a constant for the decay scheme, and is given by $\epsilon^*=2p^*/M$. Lines of constant θ^* are confocal hyperbolae with the same foci as the ellipses.

The (α, ϵ) diagram for Λ^0-particles is shown in fig. 2. The diagram for θ^0-particles has a similar shape but is symmetrical about the line $\alpha=0$.

Fig. 2

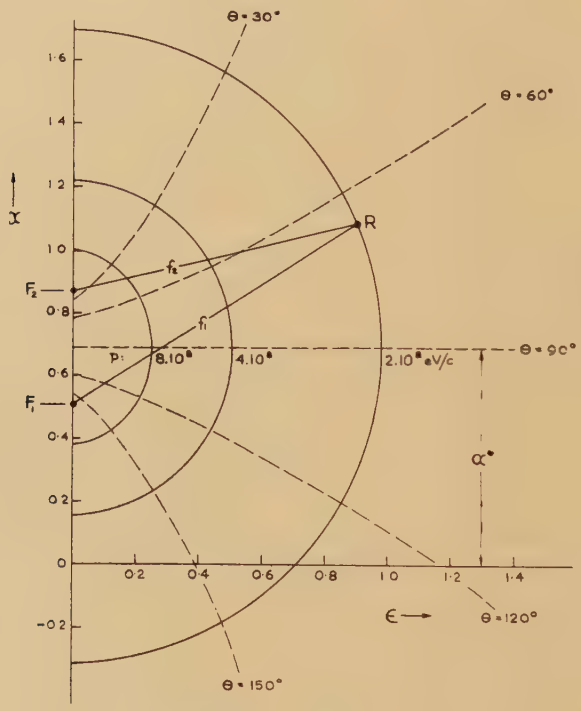

The (α, ϵ) diagram.

The point R in fig. 2 represents the decay of a V^0-particle. To find θ^* for the decay, the distances f_1 and f_2 from the two foci to this point are measured and it can be shown that θ^* is given by

$$\cos\theta^*=(f_1-f_2)/2\epsilon^*. \quad . \quad . \quad . \quad . \quad . \quad . \quad . \quad (3.1.5)$$

When an event has been classified, the velocity, β, of the V^0-particle can be found from the relation

$$\beta=2\epsilon^*/(f_1+f_2) \quad . \quad . \quad . \quad . \quad . \quad . \quad . \quad . \quad (3.1.6)$$

whence P may be obtained. θ^* and P may also be determined analytically from α and ϵ, but the simple graphical method devised by Podolanski and Armenteros is far quicker and sufficiently accurate for most purposes.

The values of the basic constants for the two decay schemes (1.1) and (1.2) are given in table 2.

Table 2

	Λ^0-particle	θ^0-particle
p^*	100 Mev/c	204 Mev/c
α^*	0·69	0
ϵ^*	0·18	0·41

3.2. *The Experimental Data*

In the present series of experiments, 44 V^0-tracks have been observed which are clearly associated with a nuclear interaction in the top lead plate inside the cloud chamber. In addition, one event has been included in the analysis which was produced in the top wall of the chamber. For 30 of these events, the origin of the interaction could be determined in order to find ϕ_1 and ϕ_2 sufficiently accurately for the classification to be attempted. Each origin is found by tracing back the tracks of shower particles (usually identified by their penetration of the lower lead plate) in the x–y and y–z projections of the event. In this manner the x- and y-coordinates of the interaction are generally found to within about $\pm 1{\cdot}5$ mm and the z-coordinate (depth in chamber) to within about ± 2 mm.

In the remaining 15 cases, classification is impossible since the origins, and hence the angles ϕ_1 and ϕ_2, cannot be found sufficiently accurately. Five of these decays are associated with large showers with a considerable electronic component making it difficult to trace back the penetrating particles to their origin. The apexes of two of the events are only about 3 mm from the lower face of the 4 cm lead plate and their origins are not well defined. The remaining eight are associated with showers of various sizes containing up to eight shower particles, and in two of these cases the opening angle of the V-track is very small.

The data for the 30 events with accurately determined origins are given in table 3. The estimated errors for the angles ϕ are all within the range (1–3) deg. The errors of the derived quantities α and ϵ vary considerably, but the estimated errors in both are generally about $\pm(10\text{–}15)\%$. The estimated ionizations of the secondary particles are given in columns (5) and (6) of table 3, and are compared with the calculated ionizations assuming in turn that the unstable particle is a θ^0- or a Λ^0-particle. The calculated ionizations which agree best with the estimates are given in columns (7) and (8) and the classifications are given in column (9). In only one case, D 319, is it impossible to decide which is the correct classification. Eight of the decays can be interpreted by the decay of θ^0-particles and the remaining 21 by the decay of Λ^0-particles.

In addition to the use of the (α, ϵ) diagram, a simpler method can often be applied for the classification of low energy V^0-particles. Event D 6379, reproduced in Plate 17, is such an example. The essential measurements are given in table 3. Suppose the V-track represents the decay of a θ^0-particle. By substituting the values of ϕ_1 and ϕ_2 in eqn. (3.1.1), the ratio of the secondary momenta is found to be $p_1/p_2 = 9{\cdot}5$. Now track (1) has an estimated ionization of greater than twice the minimum value and since both tracks are assumed to be π-mesons, p_1 must be less than 120 Mev/c. Therefore the momentum of track (2)

Table 3. The Classification of 30 V^0-Tracks

Event	(1) ϕ_1 (deg.) $\phi_1 < \phi_2$	(2) ϕ_2 (deg.)	(3) α	(4) ϵ	(5) $I_1/I_{\min}$ est.	(6) $I_2/I_{\min}$ est.	(7) $I_1/I_{\min}$ calc.	(8) $I_2/I_{\min}$ calc.	(9) Type of V^0-particle	(10) δ (deg.)
A 419	14	46	+0·61	0·4	4–8	2–4	4·4	1·6	Λ^0	0·8±1·5
A 1208	11	126	±1·33	0·45	<2	3–8	1	3	θ^0	0·8±1·5
B 596	11	68	+0·85	0·36	3–6	1·5–3	3·4	2·3	Λ^0	1·0±1·5
B 1843	29·5	39·5	±0·19	0·67	<2	<2	1	1	θ^0	0·0±2
B 1990	20·5	58·5	±0·63	0·61	<2	<2	1	1·4	θ^0	3·0±2
B 2166	4·5	37·5	+0·83	0·15	<2	2–4	1·4	1·6	Λ^0	0·8±1·5
B 4312	8·5	48·5	+0·77	0·26	2–4	1·5–3	2·3	1·6	Λ^0	3·9±3·5
C 389	18	53	+0·61	0·52	3–6	$<I_1$	6·3	1·8	Λ^0	1·8±2
C 718	5·7	32·8	+0·73	0·17	<2	<2	1·6	1·4	Λ^0	0·2±1·5
C 1060	16	76	+0·87	0·54	3–7	<3	5·5	2·3	Λ^0	3·0±3
D 319	5·5	33·5	±0·75	0·17	<2	3–6	—	—	?	4·5±3
D 532	10·5	22·5	+0·38	0·26	6–12	<3	5	1·4	Λ^0	5·2±3·5
D 721	6	25·7	+0·64	0·17	2–4	<2·5	1·6	1	Λ^0	1·5±2
D 1060	15	80	+0·91	0·51	4–8	1·5–3	6	2·7	Λ^0	6·3±4
D 1967	19·7	48·3	±0·52	0·54	<2	2–4	1	1·2	θ^0	7·5±4
D 2050	9	23	+0·46	0·23	1·5–3	<2	3·6	1·3	Λ^0	0·2±1·5
D 2941	30·2	57·3	+0·46	0·85	>10	<2	14·5	1·9	Λ^0	5·4±2·5
D 3587	5	6·5	±0·13	0·1	<2·5	<2·5	1	1	θ^0	3·0±3
D 3754	33·5	66·5	±0·55	1·0	<3	<3	1	1·3	θ^0	1·3±1·5
D 5123	7·4	74·8	±0·93	0·25	<2	4–8	1	4·8	θ^0	3·4±3
D 5155	11	26	±0·43	0·28	<2	<2	1	1·2	θ^0	3·5±3·5
D 5255	9·5	32·5	+0·58	0·27	2–4	<2	2·8	1·4	Λ^0	4·1±1·5
D 6193	15	71	+0·83	0·49	4–8	<3	5	2·2	Λ^0	0·9±2·5
D 6379	5·6	67·1	+0·92	0·19	2–3	3–7	2·1	3·3	Λ^0	2·0±1·5
D 6384	23·3	37·2	+0·28	0·55	6–12	1·5–3	13	1·6	Λ^0	4·0±3·5
D 6501	23	80	+0·86	0·79	6–12	<3	9·4	2·3	Λ^0	12·0±7
D 7230	28	71·5	+0·7	0·9	>10	<3	12·7	2·2	Λ^0	3·3±3·5
D 7561	11	114	+1·19	0·42	3–6	4–8	3·7	5·7	Λ^0	0·0±1
D 8364	11·4	46·6	+0·68	0·34	2–5	2–4	3·2	1·6	Λ^0	0·8±1·5
D 8570	6·2	18	+0·5	0·16	<3	<2	2·2	1	Λ^0	2·0±1·5

must be less than 13 Mev/c and its ionization greater than 30 times minimum, in disagreement with the estimated value of (3–7) minimum. Thus the decay cannot be due to a θ^0-particle and must be assumed to be due to a Λ^0-particle ; the same conclusion is reached using the (α, ϵ) diagram. To find which secondary particle is the proton, the fact that the maximum value of p_t for the Λ^0-type of decay is 100 Mev/c is used. Consider track (2) : I_2 is estimated to be less than seven times minimum, therefore if track (2) is the proton, p_2 must be greater than 300 Mev/c

and p_t greater than 270 Mev/c. Hence it is concluded that track (1) must be the proton. This method has been used for finding the signs of the parameter α given in column (3) of table 3.

3.3. *The Isotropy of Emission of the Secondary Particles in the Rest System of the Λ^0-Particles*

The angle θ^* is the angle between the direction of the proton in the rest system of each Λ^0-particle and the direction of the Λ^0-particle. For isotropic emission in the rest system half of the decays should have $\theta^* > 90°$ and half $\theta^* < 90°$. The corresponding values of α are $\alpha < \alpha^*$ and $\alpha > \alpha^*$. In fact, for 11 of the 21 Λ^0-particles, the proton is emitted forwards in the rest system (i.e. $\theta^* < 90°$) and, for the remaining 10, the proton is emitted backwards. Since the only criterion for selection of the events has been that the origin of the nuclear interaction should be well-defined, and since all except one of the V^0-tracks have been classified, there is no apparent experimental bias for observing events with preferred values of θ^*.

3.4. *The Coplanarity of the V^0-Tracks*

Both of the assumed decay schemes involve only two secondary particles so that, if all the observed events are to be interpreted by these schemes, the planes of the V-tracks should intersect the origins of the V^0-particles. The experimental angles, δ, between the trajectories of the V^0-particles and the planes of the V-tracks are given in column (10) of table 3. Brueckner and Thompson (1952) have shown that, even if a light neutral particle occurs in the decay scheme of the Λ^0-particle, the coplanarity should not be unduly disturbed. They obtained an approximate theoretical expression for the distribution of δ assuming either a neutrino or π^0-meson as neutral particle. The present data have been examined using this relationship and, in common with the data of Bridge *et al.* (1953), they support the two-body hypothesis.

The decays of the θ^0-particles are all coplanar with their origins within the accuracy of the measurements. Detailed considerations, following the method of Leighton *et al.* (1953), show that, if a neutral secondary is assumed to exist, then its component of momentum transverse to the path of the θ^0-particle is less than 40% of that of one of the charged secondaries. The evidence thus excludes the possibility that a π^0-meson is a secondary of the θ^0-particle, since the π^0-meson would be expected to take, on the average, the same transverse momentum as one of the charged secondaries. Hence it is concluded that if a neutral particle does occur in the decay of the θ^0-particle, it is probably a neutrino or a photon. Barker (1954) has reached a similar conclusion from measurements on seven θ^0-particles. Fretter *et al.* (1953) and Bridge *et al.* (1953) have also found a small number of θ^0-particles to be coplanar with their origins.

§ 4. The Mean Lifetimes of θ^0- and Λ^0-Particles

Wilson and Butler (1952) were the first to describe the type of measurement that must be made in order to determine the mean lifetime of a particular type of V^0-particle. It is necessary to measure the path length, l, of the V^0-particle in the chamber and also its path, L, assuming that it failed to decay inside the chamber. The second quantity is sometimes known as the potential path length. In addition, the momentum of the V^0-particle must be known in order that l and L may be converted into the corresponding times of flight, t and T. Wilson and Butler (1952) also pointed out that considerable care must be taken in the measurement of the lengths l and L if serious bias effects are to be avoided. They suggested that the measurements should be made from suitably chosen fiducial surfaces drawn inside the illuminated volume of the chamber. Recently Newth (1954) and Page and Newth (1954) have described a simpler procedure. They measure l from a point on the trajectory of the V^0-particle nearest the edge of the illuminated volume where the apex of the V^0-track can be identified with certainty. The measurement of L starts from the same point but finishes before the potential path leaves the illuminated volume since it is necessary to subtract from the potential path a chosen length which is sufficient for the V^0-track to be measured and classified. Bias effects are eliminated if every event could have been selected by the classification procedure adopted, even if its apex occurred at any point on the potential path.

4.1. *The Mean Life of the θ^0-Particle*

In § 3 it was shown that eight of the V^0-decays could be interpreted by the decay scheme of the θ^0-particle, but the analysis ignored the possibility that perhaps 10% of the decays may differ from those of the θ^0- and Λ^0-particles. Most of the anomalous examples are probably placed in the θ^0 category. Without more data on the nature of the anomalous decays it is impossible to assess their influence on the lifetime measurements described below in which it is assumed that all eight cases are really due to θ^0-particles with the decay scheme (1,2).

The values of l and L and the reduced momenta are given in table 4.

In the determination of l and L, each decay has to be considered separately, and the observer must decide on the amount of correction to be applied. For the majority of the events, the trajectory of the V^0-particle after emerging from the plate was unobscured by shower particles, but both lengths were measured from a fiducial surface 3 mm below the plate. In a few events one of the tracks of the V^0-particle moved back towards the plate, and in these cases the fiducial surface was chosen to give a length for this track of 1·5 cm supposing the particle decayed at the fiducial surface. In the remaining cases the lengths were measured from the point nearest the plate where it was considered that each decay could have been recognized among the shower particles. The ends of the potential path

lengths were determined by requiring a minimum length for measurement of 1·5 cm on the shortest track of the decay. For the few narrow angle decays this length was increased to 2 cm.

The values of the reduced momenta ($\gamma\beta$) for the eight assumed θ^0-particles are given in column (3) of table 4 and the times t and T in columns (4) and (5). In four cases, the potential path traverses the lower plate and enters the illuminated region below this plate, thus there is an unobservable region in the potential path. To allow for this region, two additional times T_1 and T_2 must be measured. T_1 is the time, from the beginning of the time scale of t, at which the potential path of the particle crosses a surface drawn above the lower plate. This fiducial surface is chosen exactly as described for the determination of T, and is the surface at which the decay would have still been recognized and measured before entering the plate. T_2 is measured to the point below the lower plate where the decay would still have been recognized (i.e. T_2 is generally measured to a point 3 mm below the underside of the lower plate). The values of T_1 and T_2 are given in columns (6) and (7) of table 4.

Table 4. Lifetime Data for Eight θ^0-Particles

Event	(1) l (cm)	(2) L (cm)	(3) $P/M=\gamma\beta$	(4) t	(5) T	(6) T_1	(7) T_2
				(10^{-10} sec)			
A 1208	1·2	8·3	0·30	1·3	9·2	—	—
B 1843	0·2	11·0	0·60	0·1	6·1	—	—
B 1990	1·7	14·0	0·49	1·1	9·5	—	—
D 1967	4·0	16·7	0·58	2·3	9·6	5·1	7·2
D 3587	2·2	10·0	3·70	0·2	0·9	—	—
D 3754	1·3	15·0	0·35	1·2	14·3	7·7	10·0
D 5123	2·6	14·4	0·46	1·9	10·4	5·7	8·0
D 5155	1·2	14·1	1·00	0·4	4·7	2·5	3·8

Bartlett (1953 a and b) has described a maximum likelihood statistical procedure for the evaluation of lifetime of the unstable particles from the values of t, T, T_1 and T_2. The standard error is symmetrical about the reciprocal of the lifetime. Bartlett's method has been discussed and used for Λ^0-particles by Page and Newth (1954).

The value of the mean life, τ, for the θ^0-particle, found from the measurements on the eight cases is given by

$$1/\tau=(0{\cdot}82\pm0{\cdot}33)\times10^{10}\ \text{sec}^{-1},$$

i.e.

$$\tau=(1{\cdot}2\,{}^{+0{\cdot}8}_{-0{\cdot}3})\times10^{-10}\ \text{sec}.$$

4.2. *The Mean Life of the Λ^0-Particle*

Data similar to that described in § 4.1 have been obtained for the 21 decays attributed to Λ^0-particles; the details are given in table 5.

Again it is possible that a very small percentage of the decays listed in table 5 may have been produced by the anomalous V^0-particles. Unfortunately, it is impossible to separate any of the cases and it must be

Table 5. Lifetime Data for 21 Λ^0-Particles

Event	(1) l (cm)	(2) L (cm)	(3) $P/M=\gamma\beta$	(4) t	(5) T	(6) T_1	(7) T_2
				(10^{-10} sec)			
A 419	1·2	8·2	0·44	0·9	6·2	—	—
B 596	2·3	13·9	0·46	1·7	10·1	—	—
B 2166	2·1	3·9	1·00	0·7	1·3	—	—
B 4312	0·1	4·5	0·65	0·05	2·3	—	—
C 389	4·4	6·0	0·34	4·3	5·9	—	—
C 718	0·2	8·7	1·00	0·05	2·9	—	—
C 1060	2·9	15·0	0·32	3·0	15·6	8·9	12·9
D 532	2·0	5·5	0·47	1·4	3·9	—	—
D 721	6·0	12·6	1·00	2·0	4·2	—	—
D 1060	2·4	4·4	0·32	2·5	4·6	—	—
D 2050	2·3	7·6	0·60	1·3	4·2	—	—
D 2941	2·4	8·3	0·20	4·0	13·9	—	—
D 5255	5·0	9·7	0·62	2·7	5·2	—	—
D 6193	3·1	14·6	0·65	1·6	7·5	4·2	5·2
D 6379	3·8	15·1	0·66	1·9	7·6	4·2	5·8
D 6384	1·1	4·8	0·26	1·4	6·2	—	—
D 6501	1·6	7·3	0·22	2·4	11·0	—	—
D 7230	3·4	4·5	0·20	5·6	7·5	—	—
D 7561	4·4	15·5	0·28	5·3	18·5	9·2	14·6
D 8364	2·7	8·3	0·53	1·7	5·2	—	—
D 8570	4·9	9·4	0·82	2·0	3·8	—	—

assumed that the 21 decays are all of one type. Using Bartlett's method of analysis, the value of the decay constant is found to be

$$1/\tau=(0{\cdot}25\pm0{\cdot}12)\times10^{10}\ \text{sec}^{-1},$$

whence

$$\tau=(4{\cdot}0\ {}^{+3{\cdot}7}_{-1{\cdot}2})\times10^{-10}\ \text{sec}.$$

4.3. *Discussion*

If the assumptions underlying the classification procedure of § 3 are correct, the momenta of the particles are accurately known and consequently do not make an appreciable contribution to the errors in the values of the lifetimes. Likewise, once the fiducial criteria have been chosen, the errors in the path length measurements are insignificant. There remains, however, the possibility that some bias remains due to the observer's choice of fiducial criteria. In the present analysis it is considered that bias effects have mainly been eliminated. The large errors in the values of τ are entirely due to statistical fluctuations arising from the small samples of decays available. Considerably more data are required in order to reduce the purely statistical errors.

Several groups of workers have made measurements of the lifetime of θ^0-particles, notably Fretter *et al.* (1953), Astbury (1953), Deutschmann (1953) and Bridge *et al.* (1953). The various methods of selecting the data vary considerably. For example, Astbury selects mainly high momentum θ^0-decays with negative values of the parameter α. Λ^0-decays with the same momentum all have positive values of α. The decays analysed by Deutschmann and Bridge *et al.* are mostly of fairly low energy and are comparable with the present data. The results of the different groups are summarized in table 6. The remarkably high accuracy of the present data is due to the fact that the decays of low energy θ^0-particles have been selected.

Table 6. Estimates of the Mean Lifetime of θ^0-Particles

Group	Number of decays	Mean lifetime (10^{-10} sec)
Fretter *et al.* (1953)	11	4 ± 3
Astbury (1953)	11	$1{\cdot}6\ ^{+2{\cdot}2}_{-0{\cdot}6}$
Deutschmann (1953)	9	$2{\cdot}3\ ^{+2{\cdot}1}_{-0{\cdot}7}$
Bridge (1953)	6	$0{\cdot}9\ ^{+1{\cdot}6}_{-0{\cdot}3}$
Gaynther (1954)	8	$1{\cdot}2\ ^{+0{\cdot}8}_{-0{\cdot}3}$

It has been shown by Page and Newth (1954) that since Fretter *et al.* do not make any corrections for particles decaying in the lead plates of their chamber, a bias is introduced into their result tending to increase its value. The remaining results in table 6 are now combined to give a weighted mean value of

$$(1{\cdot}7\ ^{+0{\cdot}6}_{-0{\cdot}35}) \times 10^{-10} \text{ sec.}$$

Since this result is based on measurements on only 34 events, the error is still largely the statistical error.

Page and Newth (1954) have reviewed all the available evidence on the lifetime of the Λ^0-particle including the present data. The weighted mean value of τ is

$$(3{\cdot}7\ ^{+0{\cdot}8}_{-0{\cdot}6}) \times 10^{-10} \text{ sec}$$

based on 127 decays. Recently Page (1954) has analysed 23 decays of slow Λ^0-particles. He finds a mean lifetime of

$$(3{\cdot}6\ ^{+1{\cdot}1}_{-0{\cdot}7}) \times 10^{-10} \text{ sec};$$

including this result, the weighted mean value of all the published results is

$$(3{\cdot}7\ ^{+0{\cdot}6}_{-0{\cdot}5}) \times 10^{-10} \text{ sec.}$$

The data described in §§ 4.2 and 4.3 are in excellent agreement with the weighted mean values.

Acknowledgments

I wish to thank Dr. C. C. Butler for his guidance and the considerable help he has given me in all aspects of this work. Dr. K. H. Barker and Mr. R. Armenteros have frequently given me the benefit of their advice. I would also like to thank Mr. J. A. Newth for many helpful discussions on the problem of the measurement of lifetimes. Mr. M. S. Coates helped to run the equipment during the early stages of the experiment. I am indebted to Dr. Rosch for permission to work at the Observatoire du Pic-du-Midi, and to the Department of Scientific and Industrial Research for a maintenance grant.

References

Astbury, P. J., 1953, private communication.
Ballam, J., Harris, D. R., Hodson, A. L., Rau, R. R., Reynolds, G. T., Treiman, S. B., and Vidale, M., 1953, *Phys. Rev.*, **91,** 1019.
Barker, K. H., 1954, *Proc. Roy. Soc.* A, **221,** 328.
Barker, K. H., Sard, R. D., and Sowerby, M. G., 1953, *Phil. Mag.*, **44,** 46.
Bartlett, M. S., 1953 a, *Phil. Mag.*, **44,** 249 ; 1953 b, *Ibid.*, **44,** 1407.
Bridge, H. S., Peyrou, C., Rossi, B., and Safford, R., 1953, *Phys. Rev.*, **91,** 362.
Bridge, H. S., 1953, private communication.
Brueckner, K. A., and Thompson, R. W., 1952, *Phys. Rev.*, **87,** 390.
Deutschmann, M., 1953, private communication.
Fretter, W. B., May, M. M., and Nakada, M. P., 1953, *Phys. Rev.*, **89,** 168.
Leighton, R. B., Wanlass, S. D., and Anderson, C. D., 1953, *Phys. Rev.*, **89,** 148.
Newth, J. A., 1954, *Proc. Roy. Soc.* A, **221,** 406.
Page, I., 1954, private communication.
Page, I., and Newth, J. A., 1954, *Phil. Mag.*, **45,** 38.
Podolanski, J., and Armenteros, R., 1954, *Phil. Mag.*, **45,** 13.
Rochester, G. D., and Butler, C. C., 1953, *Prog. Rep. Phys.*, **16,** 364 (London: Physical Society).
Wilson, J. G., and Butler, C. C., 1952, *Phil. Mag.*, **43,** 993.

LXVI. *The Remanent Magnetism of Some Sedimentary Rocks in Britain*

By J. A. Clegg, Mary Almond and P. H. S. Stubbs
Department of Physics, Imperial College of Science and Technology*

[Received March 17, 1954]

Abstract

This paper describes a survey which was carried out to measure the natural remanent magnetism of Triassic sediments in England. Rocks from nine separate sites distributed over a wide area were found to have consistent polarizations, being magnetized in an approximately North East–South Westerly direction with dips significantly less than that of the present earth's field. Similar results were obtained for sediments of the Carboniferous and Old Red Sandstone periods taken from two other sites. Approximately half of the specimens showed reverse polarization. Tests were also made to measure the magnetic stability of the rocks. The possible implications of the results are discussed.

§ 1. Introduction

The remanent magnetism of sedimentary rocks has been studied during the past two decades and has yielded important information concerning the prehistory of the earth's magnetic field.† The most reliable data obtained in this way to date have come from the investigation of the natural magnetization of varved clays. Johnson, Murphy, and Torreson (1948) in particular made a very complete set of measurements on a continuous vertical sequence of New England clays, extending back in age to 15 000 B.C., and found that the directions of polarization show regular variations about geographic North ; while Nagata (1951), Kawai (1951) and others observed similar directions of magnetization in certain Japanese clays dating back to the early Miocene period.

The information concerning earlier sediments is more scanty, but the data published to date indicate that the majority have magnetic polarizations lying reasonably close to the axial dipole field, and that while a number show oblique magnetization, the distribution is not such as to indicate a significant deviation towards any other preferential direction.

In October, 1952, we undertook a study of the remanent magnetism of certain sediments of the Triassic system. The first set of samples from North West Cheshire showed a consistent direction of magnetization which differed appreciably from that of the present earth's field. A more comprehensive investigation extending first to other parts of

* Communicated by Professor P. M. S. Blackett, F.R.S.

† For a general review of magnetic measurements made on igneous and sedimentary rocks, see Nagata (1953).

Cheshire, and later over a wider area, showed that the majority of English rocks of the same geological system had similar polarizations. This survey has since been extended to rocks of earlier ages, and the detailed results are set out below.

§ 2. Method of Collection and Measurement

The rocks were taken from exposures in road cuttings, quarries, the beds and banks of rivers, and sea cliffs. A photograph of a typical exposure is shown in Plate 18. Each sample* consisted of a slab a few inches in thickness, and was oriented *in situ* before removal. Whenever possible at least two samples were taken from positions a few feet apart at each site. These slabs were cored in the laboratory with a diamond trepanning tool, and the cylindrical cores were cut with a diamond wheel into disc-shaped specimens $1\frac{3}{8}$ in. diameter and $\frac{3}{16}$ in. in thickness. The plane faces of the discs were cut parallel to the original bedding surfaces of the rock and the upper surface of each was marked with an arrow drawn perpendicular to the strike, to indicate the downward direction of tilt† of the strata.

The direction and intensity of magnetization of the specimens were measured by means of a magnetometer of the type designed initially by Blackett (1952). This instrument consists essentially of a pair of carefully astaticized magnets suspended on a torsion fibre, the earth's magnetic field at the magnet system being annulled by three pairs of mutually perpendicular Helmholtz coils. Its sensitivity was such that a vertical field gradient of 10^{-7} oersteds per cm produced a scale deflection of 1 mm. The specimen was mounted with its axis vertical on a horizontal turntable which could be raised and lowered beneath the magnetometer. The method of using this magnetometer to measure the horizontal direction and intensity of magnetization by bringing the turntable up to the magnet system in four successive positions, and the 'off centre' method of measuring the dip have been described in detail elsewhere (Blackett 1952).

The rocks had intensities of magnetization ranging from 6×10^{-7} to 150×10^{-7} c.g.s. units. The standard error of a single determination of declination was 3°, and of dip 4°.

All directional measurements were made relative to the tilt arrow marked on the upper face of the specimen. No attempt was made to correct for the tilt of the strata, and the declinations and dips quoted below are referred to the bedding planes, the zero of declination being the intersection of the bedding surface of the parent rock with the plane of the earth's magnetic meridian.

---

* Throughout this paper the slabs initially taken from the parent rock will be referred to as 'samples' and the term 'specimen' will be used for the individual cylindrical discs, a number of which were cut from each sample.

† See footnote at bottom of table 1.

§ 3. Results

(i) *The Remanent Magnetism of Triassic Sediments in England*

We undertook these investigations on the supposition that the remanent magnetic moment of certain sedimentary rocks was acquired during

Fig. 1

Map showing positions of sites from which specimens were taken.

deposition by alignment of the ferromagnetic particles along the earth's magnetic field, the direction of polarization having been preserved unchanged throughout subsequent geological ages up to the present time.

This implies that the sediments were laid down under tranquil conditions and did not subsequently undergo undue deformation, and that the original magnetic constituents were sufficiently stable to resist any demagnetizing effects to which they may have been exposed since deposition. Among the Triassic rocks which we examined, and for which it appeared likely that these conditions might have been fulfilled, were certain fine red sandstones occurring at Frodsham, Cheshire (site (1), fig. 1). These deposits, which had well defined uniform bedding planes with a tilt of only 5°, were exposed in a newly made road-cutting, and samples were taken from the same horizon at 20 yard intervals over a horizontal distance of 100 yards. Measurements made on a number of specimens cut from each sample showed a consistent direction of magnetization, approximately 40° East of the present magnetic North, with a dip somewhat lower than that of the present earth's field. A second set of samples taken from other horizons at the same site, over a vertical range of 12 ft., yielded similar results, and the mean direction for all specimens was found to be 41° East of magnetic North in declination, and 52° downward in inclination.

These sandstones occur close to the base of the Keuper Marl series, and have an age of the order of 180 million years. We decided to examine other red sandstones of the same period taken from sites several miles apart in Cheshire, at Congleton (2), Holmes Chapel (3), and Wilmslow (4). The measured directions and intensities of magnetization are shown in table 1 and the directions of polarization are plotted on the projection in fig. 2. The results for site (3) correspond closely with those for site (1), but the polarization of the rocks of site (4) was in almost exactly the reverse direction. The samples from site (2), on the other hand, were reversed in declination but had almost zero dip. It appears, therefore, that the Triassic rocks throughout Cheshire are magnetized in an approximately North–East to South–West line, the dips being somewhat variable but on the whole considerably less than that of the present earth's field, and that in some cases the direction of magnetization is reversed. This consistency in the direction of the axis of magnetization appears more striking when we consider the probable difference between the ages of the rocks from the four sites. Thus, Wilmslow and Holmes Chapel are considerably nearer to the centre of the Cheshire Basin than the other two sites, and the horizons from which the samples were taken may well differ by 1500 feet.

In view of this uniformity of magnetization, it appeared expedient to extend our investigations to other parts of the Trias outside the Cheshire Basin, and we examined samples of similar red sandstones of the same geological series from the Wirral Peninsula (5), Beaumont, Cumberland (6), Carlisle (7), Nottingham (8), the River Leven at Rudby, North Yorkshire (9), and Sidmouth, Devon (10). The results shown in table 1 and fig. 2 for sites (5) to (9) are in general agreement with those obtained for the previous locations. The rocks from Sidmouth (site (10)), however,

Table 1. Results Obtained for Rocks of Keuper Marl Series

Site no.	Locality	Nat. grid reference	Mean direction of downward tilt*	Mean angle of tilt	Total no. of samples taken	Total no. of specimens measured	Intensity of magnetization $\times 10^{-7}$ e.g.s.	Mean declination E. of M.N.†	Mean dip*	Radius of 50% circle of confidence‡
1	Frodsham, Cheshire	352·7 E ; 378·2 N	69½°	5½°	12	191	7·2	41°	+52° down	2·5°
2	River Dane, Cheshire	388·7 E ; 368·9 N	26°	8½°	6	33	9·2	236°	+9° down	1·5°
3	Holmes Chapel, Cheshire	377·8 E ; 367·6 N	186½°	7°	2	38	12·0	45°	+39° down	1·5°
4	River Bollin, Cheshire	381·3 E ; 382·8 N	260°	4°	2	37	35·2	208°	−28° up	1·5°
5	Wirral Peninsula	325·3 E ; 387·3 N	318½°	4½°	6	39	34·4	34°	+27° down	2·0°
6	Beaumont, Cumberland	335·1 E ; 560·0 N	172½°	36½°	2	37	12·8	246°	−27° up	1·5°
7	Carlisle, Cumberland	337·8 E ; 556·6 N	236°	5°	3	37	11·2	44°	+28° down	3·0°
8	River Trent, Notts.	464·8 E ; 340·0 N	84°	4°	8	119	6·3	225°	−16° up	1·5°
9	River Leven, N. Yorks.	446·1 E ; 507·1 N	107°	15°	2	9	140·5	26°	+22° down	1·5°

Table 2. Results Obtained for Rocks of Old Red Sandstone and Upper Coal Measure Series

Site no.	Locality	Nat. grid reference	Mean direction of downward tilt*	Mean angle of tilt	Total no. of samples taken	Total no. of specimens measured	Intensity of magnetization $\times 10^{-7}$ e.g.s.	Mean declination E. of M.N.†	Mean dip*	Radius of 50% circle of confidence‡
11	Frampton Cotterill, Gloucester	366·8 E ; 183·2 N	73°	19°	1	14	4·7	44°	+35° down	5·0°
12	Mitcheldean, Gloucester	367·2 E ; 218·5 N	277°	42°	3	39	6·7	244°	−22° up	5·5°

* Throughout this paper the term ' tilt ' refers to the inclination of the bedding planes. The term ' dip ' is used to indicate the inclination of the remanent magnetization and is measured relative to the plane of the strata.

† All azimuthal directions are measured in degrees East of Magnetic North, in the plane of the strata.

‡ This has been computed by the method devised by Fisher (1953).

showed random polarizations, and were found to be unstable in the earth's field. The possible implication of this instability will be discussed in § 5.

(ii) *The Remanent Magnetism of Carboniferous and Devonian Rocks*

Following the measurements on Triassic rocks we embarked on a preliminary survey of the remanent magnetism of sediments of other geological periods. This is still continuing, but measurements have been made to date on two sets of samples. The first of these were of Pennant

Fig. 2

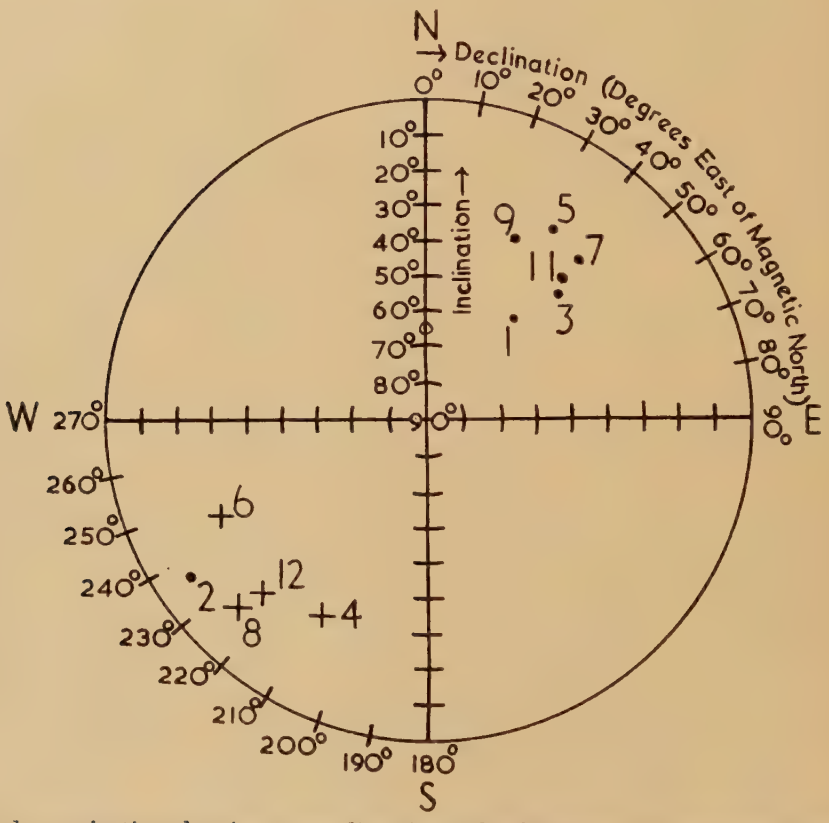

Polar projection showing mean directions of polorization of specimens from various sites.

● Downward dip
+ Upward dip
○ Present magnetic North

Sandstone of the Upper Coal Measures occurring at Frampton Cotterill, Gloucestershire (site (11)). The second from Mitcheldean in Gloucestershire (site (12)), were of Lower Old Red Sandstone (Brownstone series) approximately 300 million years old. The results, which are included in fig. 2 and table 2, indicate that these rocks have the same general axis of magnetization, the first showing a North Westerly declination with a downward dip and the second being polarized in the reverse direction.

The most notable feature of the foregoing results is the consistency in the declination measurements. This becomes particularly evident when a combined histogram is drawn, as in fig. 3(*a*),* showing the frequency distribution of the declinations of the individual specimens from all the sites listed in tables 1 and 2. It can be seen that they fall into two approximately numerically equal groups, corresponding to azimuthal directions of magnetization of 37° and 226° East of present magnetic North. The inclinations are proportionately more scattered, but the distribution in fig. 3(*b*) shows two well defined maxima at +33° and −27°. The fact that the mean upward dip was greater than the downward is mainly due to the specimens from sites (2) and (8), where the inclinations were scattered and were distributed about zero.

Fig. 3(*a*)

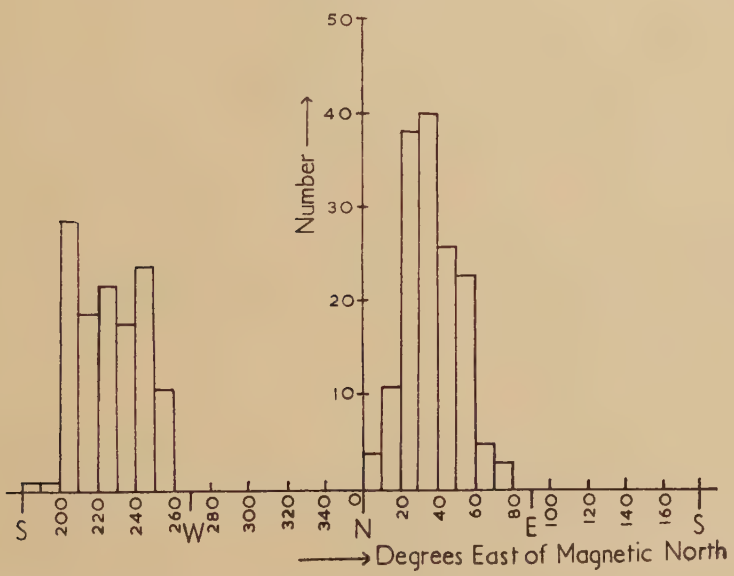

Frequency distribution of declinations.

§ 4. Stability of Magnetization

The fact that all the rocks with the exception of those from site (10) show such marked uniformity in direction of magnetization, and that this direction differs significantly from that of the present earth's field, evidently indicates some degree of magnetic stability over a considerable period of time. Particularly good evidence of this is afforded by the measurements made on samples from Beaumont, Cumberland (site (6)).

* Since different numbers of specimens were taken from the different sites, the following procedure was adopted to obtain the histograms shown in fig. 3. Separate distributions were first found for each of the 11 individual sites. These were normalized to correspond to a total of 25 specimens from each site, and were then added.

These rocks, which were found in the bed of the River Eden, were tilted downwards towards the South at an angle of 35°, the strike being almost perpendicular to the magnetic meridian. The figures in table 1 show that

Fig. 3 (*b*)

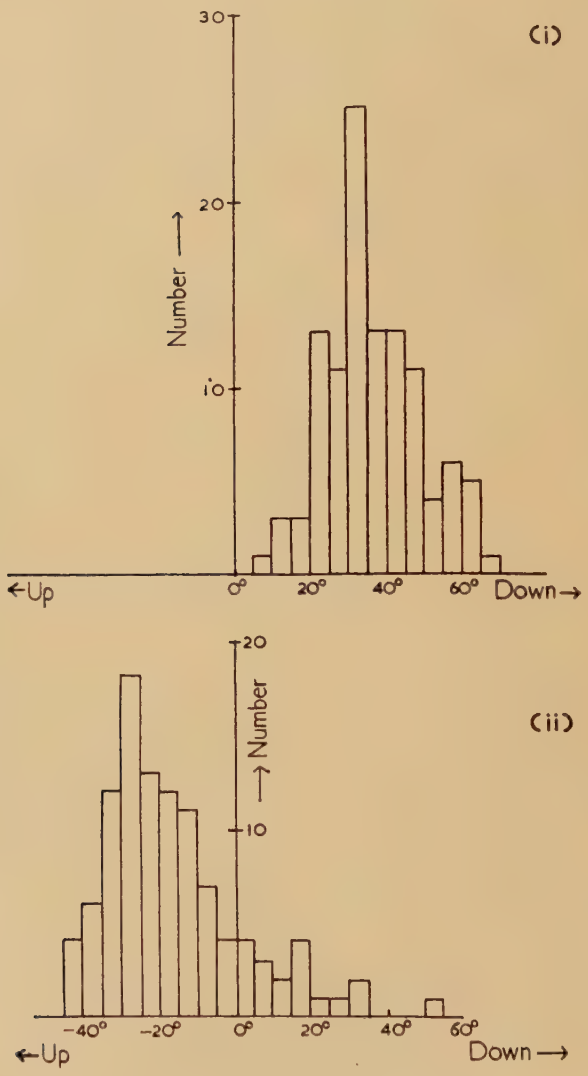

Frequency distribution of dips.
(i) Dips of specimens showing N.E. declinations.
(ii) Dips of specimens showing S.W. declinations.

the direction of magnetization, referred to the bedding planes, corresponds reasonably well with the directions found for other reversed specimens taken from sites where the bedding was nearly horizontal. This suggests

that the magnetization was acquired before tilting, and that the direction of polarization, which is almost perpendicular to that of the present earth's field, has since been preserved. It is not possible to obtain an accurate estimate of the time which has elapsed since the tilting occurred, nor has the mechanism by which it was effected been ascertained, but the extent of the erosion required to reduce the beds to their present topography indicates that it must have taken place at least some thousands of years ago. It therefore appears highly probable that the remanent magnetization of at least some of these Triassic Sandstones can remain substantially unchanged in the earth's field over periods of this order. That it remains stable over short periods was confirmed in the laboratory, where specimens were stored with their magnetic axes oriented in random directions. With the single exception of the rocks from site (10), measurements made on numerous specimens at intervals of several weeks gave values for the directions and intensities of magnetization which agreed within the probable error of measurement. However, all specimens from site (10) were markedly unstable in the laboratory, and the direction of magnetization could be substantially changed by changing the orientation relative to the earth's field for a period of a few hours. Measurements on these samples have therefore not been included in the results quoted in this paper.

In view of the fact that the rocks may have been subjected in the past to fields somewhat greater than the present earth's field, and may, furthermore, have been heated by burial, we carried out a series of magnetic stability tests on specimens from all sites excluding site (10) in the laboratory. A brief résumé of our results is given below.

(i) *The Effect of Steady Magnetic Fields at Room Temperature*

Although the magnetization of the specimens remained stable in the earth's magnetic field, it could readily be changed by applying steady fields of the order of a few oersteds. A notable feature of the changes produced by d.c. fields was that they were found to depend not only on the field strength, but also on the length of time during which it was applied. They were moreover reversible, and on removing the applied field, provided this was not too big, the magnetic moment of the specimen returned slowly towards its initial value. A typical example of this time dependence is depicted in fig. 4. A particular specimen was first placed in a field of 5 oersteds for one hour, with its axis of remanent magnetism directed along the field. Measurements made at intervals of several minutes showed that the intensity of magnetization $J(t)$ increased during the whole of this period, and the curve OA shows the ratio of $J(t)$ to the initial intensity $J(o)$ plotted as a function of time. After one hour the magnetizing field was removed, and during the following two hours the ratio $J(t)/J(o)$ reverted to unity, in the way shown by the curve AB. The curve OA′B′ shows the results obtained for the same specimen when a magnetizing field of 16 oersteds was applied for the

same length of time. In this case $J(t)/J(o)$ did not return to unity after the removal of the field but to a final value $J(\infty)/J(o)=1{\cdot}26$, which subsequently remained substantially constant over a period of months.

Tests similar to these were made to find the effects of steady magnetic fields on numerous samples, and the results can be summarized briefly as follows :

(*a*) The magnetization remains unchanged provided that the applied field strength is less than a certain critical value H_c. This critical value differs from sample to sample but never exceeds 5 oersteds and in some cases is as low as 0·5 oersteds. The instability of the samples from site (10) appears to be due to the fact that the critical value is less than the earth's field in this case.

Fig. 4

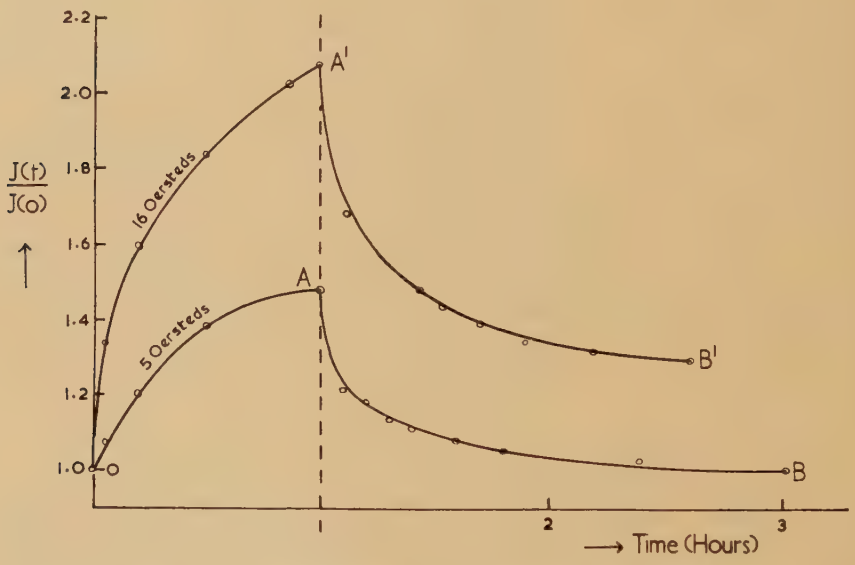

Isothermal magnetization and decay in steady fields.

(*b*) When the applied field H is greater than H_c, the intensity of magnetization changes rapidly at first, and then more slowly, finally attaining a constant value after a period of the order of a few hours. When the field H is removed, the induced magnetism decays in a similar period. For small values of $(H-H_c)$ the intensity $J(t)$ finally reverts to the initial value $J(o)$, but for sufficiently large values of $(H-H_c)$ it approaches a constant value $J(\infty)$ not equal to $J(o)$. In the latter case, therefore, there is a permanent induced magnetization $J(H)=J(\infty)-J(o)$ which is a function of the applied field strength H.

(ii) *The Effect of Alternating Magnetic Fields*

In contrast to their magnetic instability when exposed to d.c. fields, the rocks show a high degree of stability when exposed to alternating fields. In a series of a.c. demagnetizing tests made on a number of specimens taken from different sites, using a frequency of 50 c/s, the

magnetic moment was found to remain unchanged even when the strength of the demagnetizing field exceeded 300 oersteds.

Moreover, when a specimen had acquired a permanent induced magnetization $J(H)$ by the application of a sufficiently large d.c. field in the way described in (i) above, this could be removed, and the rock reduced to its original magnetic condition, by the application of relatively low a.c. fields.

(iii) *Temperature Effects*

It was found that the effects of steady magnetic fields described in (i) were sensitive to relatively small changes in the ambient temperature, the critical field strength H_c required to change the magnetization being reduced in many cases by a half when the temperature was increased from 16°c to 45°c. At temperatures greater than 80°c H_c invariably became so small that the magnetization was unstable in the earth's magnetic field. The rate of rise and decay of the induced magnetism could also be accelerated, and the amplitude of the decay curve could be increased, by increasing the temperature.

The ease with which the magnetization of these rocks can be changed by small d.c. fields and subsequently reduced again to its original value, combined with the high stability of the initial remanent magnetism in a.c. fields, can best be explained on the assumption that they contain at least two magnetic components with very different properties. We suppose that the first or soft component accounts for the effects described in (i) and (iii) above. It is not affected by the earth's field at room temperature and is normally unmagnetized in the native rock (the exception to this being the rocks from site (10), for which the critical field H_c required to change the magnetization is evidently less than that of the earth). Under normal conditions it is unstable in steady fields of the order of a few oersteds, and the stability can be decreased by increasing the temperature. It can, moreover, be demagnetized easily in a.c. fields.

The second, or hard, component, which is less easily changed, is responsible for the remanent magnetism found in the native rocks.

§ 5. Laboratory Deposition Tests

It has already been pointed out that the first Frodsham sandstones found at site (1) had all the characteristic features of quiet sedimentation. In order to obtain some indication of the magnetization that they might have acquired on deposition, a number of rocks from this site were powdered and redeposited in the laboratory. Although we do not propose to give a complete description of these experiments in the present paper, certain unpublished results due to Mr. J. L. Lloyd are germane to the discussion in the following section and may be quoted.

The powdered rock was redeposited in still water in the earth's magnetic field. The water was then decanted and the sediment was allowed to dry. Specimens taken from this deposit were found to have a magnetic polarization which coincided in declination with the earth's field, but which had a dip some 8° lower than the magnetic inclination. The

intensity of magnetization was about three times as great as that of the original rock before powdering. On the basis of these results, the assumption that the rocks took up their magnetization on deposition appears feasible. The lower magnetic intensity of the natural specimens could be accounted for by a rise in the strength of the earth's field since Triassic times, or by turbulence during deposition. Alternatively it may be due to the decay of the remanent magnetism with time, and in this connection it may be worth noting that Königsberger (1932) and Nagata (1943) have found decay times comparable to this in the remanent magnetism of igneous rocks.

Many of the Triassic rocks collected later did not show such regular banding as those originally found at Frodsham. Certain samples had obviously been deposited under excessively turbulent conditions, while others showed sun cracks and breccias. That the magnetic polarization of rocks such as these should have been taken up on deposition appears improbable. In this connection, however, certain other laboratory tests are of interest. A quantity of the powdered rock was deposited in water in zero magnetic field, and the water was then decanted. The sludge remaining in the bottom of the tank still contained about 75% by weight of water, which dried out in the course of a few days. By applying a magnetic field at different stages of the drying process it was found that a magnetization of comparable intensity to that of the parent rock could be induced so long as the water content of the deposit was greater than 50% by weight.

§ 6. Discussion of Results

The measurements described in § 3 appear to show conclusively that Triassic sediments throughout England have a preferential direction of remanent magnetization, differing significantly from that of the present earth's field, and that this direction is shared by at least some of the Carboniferous and Devonian sediments. They also show that the magnetic polarization is reversed in approximately 50% of the rocks examined. This consistency evidently has some physical significance, and while it is not possible, on the basis of such a limited survey, to draw any definite conclusions as to its cause, sufficient data is now available to justify a tentative consideration of the more obvious explanations.

Since our interpretation of the results will be influenced by our view as to the way in which the rocks acquired their magnetization, this question will first be considered in somewhat greater detail. The uniformity in the direction of the magnetic axis and the problem of the magnetic reversals will then be discussed separately.

(i) *The Origin of the Remanent Magnetism*

(*a*) *Magnetization Before Cementation*

The information gleaned from the deposition tests described in § 5 indicates that the rocks may well have become magnetized before cementation. This could have occurred in some cases on deposition, or,

in view of the magnetic mobility of the saturated sediments, at some time later, even perhaps during the resaturation of the unconsolidated deposits.

(*b*) *Magnetization by Heating*

In considering the origin of the remanent magnetism of these rocks, it is impossible, on the basis of the data at present available, to rule out the alternative possibility of its having been acquired by heating due to burial deposition. The total thickness of the sediments later than the Trias in England may amount to some 10 000 feet (O. T. Jones, private communication). Taking this as the maximum depth to which the New Red Sandstones could have been buried, we obtain an upper temperature limit of the order of 100°C. While the soft magnetic component present in the rocks would be magnetized in the earth's field at this temperature, it seems unlikely, in view of the laboratory tests made so far that the hard component would be affected. However, conclusive evidence on this point can only be obtained by a more extensive study of the composition and physical properties of the magnetic minerals present.

(ii) *The Direction of the Magnetic Axis*

In the following discussion we will assume that the mean direction of the earth's dipole axis has corresponded in the past with the axis of rotation. Modern theories of the earth's field (Bullard 1949, Runcorn 1954) support this view, and as we have already pointed out, there is some weight of experimental evidence which suggests that the general direction of the earth's field has coincided reasonably closely with that of an axial dipole during the past 17 000 years (Johnson, Murphy and Torreson 1948) and probably for the past 20 million years (Nagata 1951, Kawai 1951).

The mean direction of polarization of the rocks examined differs by 34° from geographical North. It appears unlikely that a deviation as large as this and of such wide-spread consistency, could be caused by a difference between the local magnetic declination and true North at the time of magnetization. It is true that the apparent North Easterly declination may have been enhanced by other causes. Thus if the earth's field had a sufficiently steep dip at the time when the rocks were magnetized, a small departure of its direction from the plane of the geographic meridian could give rise to a large Easterly declination. A similar result might be produced if the rocks had been tilted about an East–West axis since the time when they took up their magnetization. It might be argued that the present North–East to South–Westerly direction of the remanent magnetism could be due to either of these effects, or to the two working in conjunction, but a numerical consideration of the possible combinations of magnetic inclination and the tilt of the strata shows this to be improbable. The geological evidence indicates that the tilting of the rocks could not have amounted to more than a few degrees, and the dip of the earth's field required to change the apparent declination by an appreciable factor would in consequence be considerably

greater than that found experimentally in the rocks. A still more cogent objection to any explanation based on the foregoing arguments is presented by consideration of the relative time scales involved. The time period of the secular changes in the earth's field are of the order of hundreds of years, and it appears inconceivable, however the remanent magnetism was acquired, that rocks distributed over such a wide area and having ages ranging from the Devonian to the Triassic should all have acquired their polarization at times when the field had the same general direction.

It is possible to envisage ways in which the direction of the magnetization of the rocks might have been influenced by mechanical forces acting during deposition. For example, if the deposits were laid down as Aeolian sands and if the magnetic particles were needle or disk shaped, they might be expected to orient themselves in some preferred direction relative to the prevailing wind. A similar result could be produced by current bedding in water. It seems impossible, however, that the magnetism of the rocks from all eleven sites could have been influenced by effects such as these. The probability of uniform current conditions of any kind having prevailed over the whole area for the required length of time is evidently negligible.

Another conceivable way in which the preferential direction of magnetization may have been acquired is by the action of shearing strains on the rock after consolidation. Such distortion might be expected to lead to the orientation of the magnetic mineral grains in a preferential direction. There is, however, no geological evidence of such a distortion having occurred in any of the rocks examined.

Finally, it seems therefore that the most likely explanation of the observed horizontal direction of magnetization of the sediments studied is that the whole of the land mass which now constitutes England has rotated clockwise through 34° relative to the earth's geographical axis. This movement must have occurred since the rocks acquired their magnetization, which was probably at or soon after the time of deposition (150 to 200 million years in the case of the Triassic sediments), but conceivably much later.

If such a rotation of England has occurred, it could have been a local movement of part only of the earth's crust, or alternatively the earth's mantle could have moved as a rigid whole relative to the geographical poles. The first hypothesis would consider the rotation either as a purely local movement or as part of a drift of large continental land masses. The second would adduce pole wandering as the operative mechanism. By measuring the direction of the remanent magnetism of rocks of different geological ages in different parts of the world, it should be possible to distinguish between these hypotheses.

It has been shown that the rocks also have a mean magnetic dip markedly less than that of the axial dipole field in the latitude of England (68°). Some part of this difference may be accounted for by deformation

or compaction subsequent to deposition, but when due allowance has been made for these effects it still seems probable that the magnetic dip at the time of magnetization was appreciably less than today. If this is true, it would imply an increase in magnetic latitude, since magnetization and consequently, on the assumption of an average coincidence between the magnetic and rotational axes, an increase in geographical latitude.

(iii) *Magnetic Reversals*

Of the rocks from the eleven sites studied, those from six are magnetized in a roughly North-Easterly direction with a mean downward dip and those from the other five in a South-Westerly direction with a mean upward dip. As seen from tables 1 and 2 and fig. 3, the angle between the average magnetic polarizations of the two sets is quite close to 180°, and no specimens are magnetized in directions nearly perpendicular to this. We have been unable to find any significant difference between the magnetic and other physical properties of the directly and reversely polarized specimens.

Although this appears to be the first time that this effect has been demonstrated so definitely in sedimentary rocks, an exactly similar phenomenon has been observed with igneous rocks by Bruckshaw and Robertson (1949), Roche (1950), Hospers (1951, 1953). In particular, Bruckshaw and Robertson measured the remanent magnetism of a number of tholeiite dykes of the Tertiary Epoch occurring in Northern Britain, and found many examples of reverse remanent magnetization, while Hospers in a series of measurements on recent Icelandic lava flows found approximately equal numbers of sites showing direct and reverse polarizations with very few intermediate values. In none of the rocks examined was it possible to detect any physical or chemical difference between the direct and reversed specimens. In each of these cases the samples were taken from a limited area, and the reversals might conceivably have been caused by a purely local reversal of the earth's field at the time of magnetization. However, since it is very difficult to envisage a mechanism which would change the direction of the earth's field locally through almost exactly 180° without showing a series of intermediate directions, all three authors concluded that if a field reversal did in fact occur it must have been world wide, and have amounted to a rather sudden reversal of the main dipole field.

On the other hand Graham (1953) holds that the hypothesis of repeated reversals of the mainfield is not yet proved, and that some physical or chemical effect of the type envisaged in Néel's four alternative hypotheses (Néel 1949, 1952) may have been the main cause of the adverse magnetization of rocks. Such self reversals have been observed in igneous rocks by Nagata (1951) although the phenomenon appears to be rare and his specimens cannot be considered at all typical.

Returning to our own results it seems evident that if the present magnetization of these Palaeozoic and Mesozoic rocks was acquired by orientation of the magnetic particles in the unconsolidated sediments, the results

can only be interpreted on the postulate of field reversal. If the very convincing argument put forward by Bruckshaw and Robertson, and by Hospers is accepted this would imply at least two and probably several additional reversals of the main dipole field since Devonian times. It is conceivable however that the observed results are not due to reversal of the main field, but to chemical and physical changes which have occurred in the rocks since compaction.

Acknowledgments

We wish to convey our sincere thanks to Professor P. M. S. Blackett under whose general direction this work has been carried out. We are also indebted to numerous colleagues, both physicists and geologists, for much helpful advice and criticism, and in particular to Professor O. T. Jones who furnished information concerning the Triassic sediments. We wish to thank Mr. J. H. Leng and Mr. J. L. Lloyd, whose unpublished results have been quoted in the text, and Mr. A. H. Chapman who gave very considerable assistance in constructing the magnetometer and in preparing and measuring the rock specimens. A substantial part of this research was carried out in the Physical Laboratories of the University of Manchester, and we take this opportunity of expressing our appreciation of the facilities afforded to us. Finally we are grateful to the Department of Scientific and Industrial Research for the award of a grant on which the work was largely financed.

References

Blackett, P. M. S., 1952, *Phil. Trans. Roy. Soc.* A, **897,** 309.

Bruckshaw, J. McG., and Robertson, E. I., 1949, *Mon. Not. Roy. Astr. Soc., Geophys. Suppl.*, **5,** 308.

Bullard, E., 1949, *Proc. Roy. Soc.* A, **197,** 433.

Fisher, R. A., 1953, *Proc. Roy. Soc.* A, **217,** 295.

Graham, J. W., 1953, *J. Geophys. Res.*, **58,** 243.

Hospers, J., 1951, *Nature, Lond.*, **168,** 1111; 1953, *Kon. Ned. Ak. v. Wet.* B, **56,** 468.

Johnson, E. A., Murphy, T., and Torreson, O. W., 1948, *Terr. Mag.*, **53,** 349.

Jones, O. T., private communication.

Kawai, N., 1951, *J. Geophys. Res.*, **56,** 73.

Königsberger, J. G., 1932, *Geol. Beitr. Geophys.*, **35,** 51.

Nagata, T., 1943, *Bull. Earthq. Res. Inst., Tokyo,* **21,** 1; 1951, *Nature, Lond.*, **169,** 704; 1953, *Rock Magnetism* (Tokyo: Maruzen and Co.).

Néel, L., 1949, *Ann. de Geophys.*, **5,** 99; 1952, *Comp. Rend.*, **234,** 1991.

Roche, A., 1950, *Comp. Rend.*, **230,** 1608.

Runcorn, S. K., 1954, *Trans. Amer. Geophys. Union*, in press.

LXVII. *Royal Society Depository for Unpublished Mathematical Tables*

The Editor has received a request from the Mathematical Tables Committee of the Royal Society that a list of the tables accepted up to the end of 1953 into its Depository of Unpublished Tables should be published, together with brief descriptions, in the *Philosophical Magazine*. The Committee of the Society is of the opinion that it would be very valuable, especially from the point of view of users of tables, to have a complete list published in this journal.

Until the changed conditions of recent years forced a revision of policy upon the Editors, the *Philosophical Magazine* throughout its history has afforded facilities for the publication of mathematical tables in its contents. The Editors therefore gladly accede to the Society's request by publishing the following particulars which have been communicated to them by the Assistant Secretary of the Royal Society.

In 1951 the Royal Society established a depository for unpublished mathematical tables. It is hoped to form a valuable collection of unpublished tables that would otherwise be less generally available. The following is a list of the tables accepted up to the end of 1953 together with a brief description of each. The tables may be consulted in the Library of the Royal Society and photocopies may be prepared at the expense of those who desire them.

1. E. M. Ibrahim, *Tables for the plethysm of S-functions.*

This comprises about two dozen large sheets of manuscript. The purpose of these specialized algebraic tables is described by the author in *Quart. J. Math.* (Oxford Series) (2), **3,** 50–55, 1952. They relate to a special type of multiplication connected with symmetric functions and extend to partitions of a total degree of 18.

2. Submarine Signal Division of the Raytheon Manufacturing Company, Transducer Department, Boston, *Sines and Cosines of the Decimal Circle.* 10 lithographed octavo pages of tables.

This table gives $\sin\alpha$ and $\cos\alpha$ for $\alpha/2\pi=0(0{\cdot}001)1$ to 5 decimals when the entry is less than $\frac{1}{6}$ and to 4 decimals otherwise.

3. A. Gloden, (i) *Table de factorisation des nombres* $2N^2+1$ *pour* $0<N\leqslant1000$. (ii) *Table des solutions minima de la congruence,* $2X^2+1\equiv0$ (*mod* p^2) *pour* $p<10^3$. *Factorisation des nombres* $2X^2+1$ *correspondants.*

(i) This gives a table of complete factorizations into prime factors. (14 typed pages.)

(ii) This consists of three typed sheets. The contents are best described by an example; corresponding to, e.g., $p=107$, page 1 gives the value 2316, and on page 2 is given the factorization $2.2316^2+1=107^2.937$. **Here 2316 is the least value of N for which $2N^2+1$ has a factor 107^2.**

The tables cover the 80 primes $<10^3$ for which the representation $2X^2+1$ is possible.

4. M. S. Corrington, *Tables of Fresnel integrals, modified Fresnel integrals, the probability integral, and Dawson's integral.* Radio Corporation of America, R.C.A. Victor Division. 25 quarto pages.

These useful tables give values for $x=\frac{1}{2}\pi u^2=0(0{\cdot}001)0{\cdot}02(0{\cdot}01)2$ of the functions

$$C(u)=\tfrac{1}{2}\int_0^x J_{-\frac{1}{2}}(t)\,dt = \int_0^u \cos(\tfrac{1}{2}\pi t^2)\,dt$$

$$S(u)=\tfrac{1}{2}\int_0^x J_{\frac{1}{2}}(t)\,dt = \int_0^u \sin(\tfrac{1}{2}\pi t^2)\,dt$$

$$Ch(u)=\tfrac{1}{2}\int_0^x I_{-\frac{1}{2}}(t)\,dt = \int_0^u \cosh(\tfrac{1}{2}\pi t^2)\,dt$$

$$Sh(u)=\tfrac{1}{2}\int_0^x I_{\frac{1}{2}}(t)\,dt = \int_0^u \sinh(\tfrac{1}{2}\pi t^2)\,dt$$

$$H(\sqrt{x})=\frac{\sqrt{2}}{\pi}\int_0^x K_{\pm\frac{1}{2}}(t)\,dt = \int_0^x \frac{e^{-t}}{\sqrt{\pi t}}dt=\frac{2}{\sqrt{\pi}}\int_0^{\sqrt{x}} e^{-t^2}\,dt$$

and $$D(\sqrt{x})=\frac{\sqrt{2}}{i\pi}\int_0^{-x} K_{\pm\frac{1}{2}}(t)\,dt=\int_0^x \frac{e^{t}}{\sqrt{\pi t}}dt=\frac{2}{\sqrt{\pi}}\int_0^{\sqrt{x}} e^{t^2}\,dt.$$

Two versions of the tables are given, one to 8 decimals, with an error up to 2 final units, and another to 5 decimals.

5. A. Gloden, *Tables des solutions des congruences* $X^{2^n}+1\equiv 0 \pmod p$, $n=4, 5, 6, \quad p<10^4$. 7 typed pages.

This tabulates all integer solutions not exceeding $\frac{1}{2}p$ of the congruences $x^{16}\equiv -1$, $x^{32}\equiv -1$, $x^{64}\equiv -1 \pmod p$, for primes $p<10^4$ for which such solutions exist.

6. C. Mack and Miss M. Castle, *Tables of* $\int_0^a I_0(a)\,da$ *and* $\int_a^\infty K_0(a)\,da$. 2 pages of tables and 2 pages of description.

The integrals have been tabulated to 9 decimal places for the range of argument $a=0(0{\cdot}02)2(0{\cdot}1)4$. A brief description of the method of computation is given and also of the extent to which the tables are interpolable.

7. C. W. Jones and J. C. P. Miller, and J. F. C. Conn and R. C. Pankhurst, *Tables of Chebyshev Polynomials.* 2 typed double-foolscap sheets.

These tables give exact values of $C_n(x)=2\cos(n\cos^{-1}\frac{1}{2}x)$ for $x=0(0\cdot02)2$ and $n=1(1)10$. For $n=8$, 9, 10 they extend and complete the curtailed values given in the table, with the same title and authorship, in *Proc. Roy. Soc. Edinb.*, **62,** 187–201, 1946 (see R.M.T. 381, *M.T.A.C.*, **2,** 262, 1947).

8. A. Gloden, *Table de factorisation des nombres* N^4+1 *dans l'intervalle* $3000<N\leqslant6000$. 52 typed pages.

This gives complete factorization into prime factors for the majority of the values of N considered. For other values of N, all factors $<600\,000$ are listed.

This table extends a previous table by the author for $N=1001(1)3000$, and a table of Cunningham's for $N=1(1)1000$. See A. J. C. Cunningham, 1923, *Binomial Factorisations*, Vol. 1, pages 113–119.

9. Admiralty Research Laboratory, *Solution of the equation* $(y'')^2=yy'$ *and two other equations.* 3 foolscap manuscript pages of tables and 4 pages of description.

The solution of the equation $(y'')^2=yy'$ for which $y=0$, $y'=1$ when $x=0$, is tabulated to 6 decimals for $x=0(0\cdot05)0\cdot5(0\cdot1)6$ and facilities are provided for interpolation.

The integral

$$F(\beta,\rho)=\frac{2}{\sqrt{\pi}}\frac{e^{-\rho^2}}{\beta^2}\int_0^\beta I_0(2\rho\eta)\,e^{-\eta^2}\,\eta\,d\eta$$

is tabulated to 4 decimals for the range $\beta=0(0\cdot25)4$, $\rho=0(0\cdot25)5$. Interpolation is possible in this table, but no differences are provided.

The root x of the equation $u\sin x-\cos x+e^{-ux}=0$ that lies between π and 2π is tabulated to 4 figures for $u=0\cdot1(0\cdot01)0\cdot3(0\cdot02)2$ and $\sqrt{u}=0(0\cdot02)0\cdot5$. Interpolation is linear.

10. J. Cossar and A. Erdelyi, *Dictionary of Laplace Transforms.*

This valuable work gives pairs of functions $f(t)$, $\phi(p)$ connected by the relation

$$\phi(p)=\int_0^\infty e^{-pt}f(t)\,dt=L\{f(t)\,;\,p\}.$$

$\phi(p)$ is called the Laplace transform of $f(t)$.

There are several parts :

Part 1. 42 pages. Introduction ; notes and abbreviations, general formulae, short table of Laplace transforms, bibliography.

Part 2. 109 pages. Functions $\phi(p)$ classified according to $f(t)$.

Part 3. 74 pages. Functions $f(t)$ classified according to $\phi(p)$.

Part 2A, covers $f(t)$ rational, algebraic, powers with arbitrary index, jump- and step-functions, exponential, logarithmic, trigonometric, hyperbolic and composite elementary functions.

Part 2B, covers $f(t)$ with the following forms : Bessel functions and products, Bessel function and Fresnel integrals ; sine, cosine, exponential and logarithmic integrals ; Legendre, Gegenbauer, Jacobi, Hermite, and Laguerre polynomials ; parabolic cylinder, Bateman k- and Whittaker functions ; Legendre functions, Gauss's series, general hypergeometric series, functions of two or more variables ; theta functions.

Part 3A, covers $\phi(p)$ as for $f(t)$ in Part 2A, and Part 3B covers higher transcendental functions for $\phi(p)$ as Part 2B does for $f(t)$. It gives also a list of corrections and additions to Part 2.

11. D. H. Shinn, *Tables of Fresnel's integrals.* vii+28 foolscap typescript and manuscript pages.

Tables I and II give the functions $C(u)$ and $S(u)$ defined under 4 (Corrington) above to 5 decimals for $x=\frac{1}{2}\pi u^2=0(0{\cdot}01)0{\cdot}2(0{\cdot}02)1(0{\cdot}05)20$ and for $u=\sqrt{2x/\pi}=0(0{\cdot}01)0{\cdot}4$.

Table III gives 5 decimal values of $R(u)$ and $\frac{1}{2}\pi u^2-\theta(u)$ where

$$R(u)=[\{C(u)-\tfrac{1}{2}\}^2+\{S(u)-\tfrac{1}{2}\}^2]^{\frac{1}{2}} \quad \text{and} \quad \theta(u)=\tan^{-1}\frac{C(u)-\frac{1}{2}}{-S(u)+\frac{1}{2}}$$

for $t=1/u=0(0{\cdot}01)0{\cdot}3$.

Table IV gives the second difference correction, extracted with permission from *Interpolation and Allied Tables*, pages 788–789. H.M. Stationery Office, London, 1936.

A 7-page introduction gives definitions, references and notes of the interpolation and construction of the tables.

12. J. K. Skwirzynski, *Tables of the error integral of a complex variable.* 5 typescript foolscap pages + 2 pages of diagrams.

These tables give real and imaginary parts of the function

$$\operatorname{erfc}(z)=\frac{2}{\sqrt{\pi}}\int_z^\infty e^{-t^2}\,dt=\frac{2i}{\sqrt{\pi}}\int_{i\infty}^{iz} e^{t^2}\,dt$$

to 4 decimals, where $z=ae^{ib}$ for $a=0(0{\cdot}05)1{\cdot}3(0{\cdot}1)1{\cdot}5$ and $b=0(5^\circ)45^\circ$. There is also a brief introduction indicating the formulae used for the construction of the tables, and two pages of diagrams exhibiting the results.

13. Published and Withdrawn.

14. National Physical Laboratory, *Tables of the complex Jacobian Zeta function.* 9 foolscap pages.

The Jacobian Zeta function Z_n of modulus $k=\sin\alpha$ can be found from the tabulated function f_1 by the relations

$$Z_n(K\psi_1+iK'\phi,\,k)=f_1(\psi_1,\,\phi,\,\alpha)+if_2(\psi_1,\,\phi,\,\alpha)-\tfrac{1}{2}i\pi\phi/K$$
$$f_2(\psi_1,\,\phi,\,\alpha)=f_1(1-\psi_1,\,1-\phi,\,\tfrac{1}{2}\pi-\alpha)$$

where K, K' are the complete elliptic integrals of modulus k. f_1 to 3 significant figures is given for $\psi_1=0(0{\cdot}1)1$; $\phi=0(0{\cdot}1)1$; $\alpha=5°(5°)85°$. No provision is made for interpolation.

15. National Physical Laboratory, *Tables of Binomial Coefficients.* 20 quarto pages.

The binomial coefficients $C_n=\binom{x}{n}$ are given to six decimal places for $x=0(0{\cdot}001)1$; $n=2(1)8$. These are coefficients in the Newton–Gregory formula for interpolation with forward differences.

16. National Physical Laboratory, *Tables of Multhopp's Influence Functions.* 72 foolscap pages + 3 pages of description.

The following integrals occur in Multhopp's aerodynamic theory of wing loading :

$$i(X, Y)=1+\frac{1}{\pi}\int_0^{\pi}\frac{(1+\cos\phi)(2X-1+\cos\phi)}{\sqrt{(2X-1+\cos\phi)^2+4Y^2}}\,d\phi$$

$$j(X, Y)=\frac{4}{\pi}\int_0^{\pi}\frac{(2\cos^2\phi+\cos\phi-1)(2X-1+\cos\phi)}{\sqrt{(2X-1+\cos\phi)^2+4Y^2}}\,d\phi$$

$$ii(X, Y)=\int_{-\infty}^{X} i(t, Y)\,dt$$

$$jj(X, Y)=\int_{-\infty}^{X} j(t, Y)\,dt.$$

Four-decimal values, within a final unit, are tabulated in the half-plane $Y\geqslant 0$. For convenience of arrangement and economy of space X and Y are replaced by R and ψ, where

$$R^2=(2X-1)^2+4Y^2 \qquad X=\tfrac{1}{2}+\tfrac{1}{2}R\cos\psi$$

$$\tan\psi=2Y/(2X-1) \qquad Y=\tfrac{1}{2}R\sin\psi.$$

Values are given at the pivotal points

$$\psi=0(1°)180°$$

$$R=0{\cdot}2(0{\cdot}05)2 \qquad 1/R=0(0{\cdot}05)0{\cdot}5.$$

The function $ii(X, Y)$ which becomes infinite with R, is replaced near $1/R=0$ by the function $ii(X, Y)-\frac{1}{2}R(1+\cos\psi)$.

Except in certain exceptional regions near $\psi=0$ and $\psi=180°$ where no provision is made for interpolation the table is interpolable using second differences. Most of these are given.

17. National Physical Laboratory, *Integrals of Bessel Functions.* 2 quarto pages.

Ten-decimal values of $\int_0^x J_0(t)\,dt$ and $\int_0^x Y_0(t)\,dt$ for $x=0(0{\cdot}5)50$. No provision is made for interpolation.

18. National Physical Laboratory, *Table of*

$$\int_0^{2\pi} J_1^2\,(2k \sin \tfrac{1}{2}\theta) \cos^2 \tfrac{1}{2}\theta \, d\theta.$$

1 quarto page.

Four-decimal values are given for $0(0{\cdot}1)5(0{\cdot}5)10$. The table is interpolable using second differences, but no differences are given.

19. National Physical Laboratory, *Tables of*

$$\frac{J_0(x)}{H_0^{(2)}(x)} + \sum_{n=1}^{\infty} 2(-1)^n \frac{J_n(x)}{H_n^{(2)}(x)} \cos n\,(\pi - \theta) \text{ and}$$

$$\frac{J_0'(x)}{H_0^{(2)\prime}(x)} + \sum_{n=1}^{\infty} 2(-1)^n \frac{J_n'(x)}{H_n^{(2)\prime}(x)} \cos n(\pi - \theta).$$

10 foolscap pages.

Two-decimal values of the real and imaginary parts are given for $x=0(0{\cdot}2)2(0{\cdot}5)5(1{\cdot}0)10$; $\theta=0(0^\circ{\cdot}5)5^\circ$, $10^\circ(10^\circ)180^\circ$. A second table gives these functions in polar form $re^{i\alpha}$ (r to two decimals, α to $0^\circ{\cdot}1$).

These functions occur in the theory of the reflexion of electromagnetic waves from infinite cylinders.

20. National Physical Laboratory, *Table of an Integral used in calculating profiles of water waves.* 6 quarto pages.

Writing $F=\int_0^{\pi/2} \sec^3\theta\, e^{-\alpha^2 \sec^2\theta} \cos(\beta \sec\theta)\, d\theta$, the four tables give three-decimal values of the functions indicated below. Modified second differences are given.

Table I	$2\alpha^2 F$	$\alpha=0{\cdot}2(0{\cdot}05)1$	$\beta=0{\cdot}0(0{\cdot}1)1{\cdot}5$
Table II	F	$\alpha=0{\cdot}2(0{\cdot}05)1$	$\beta=1{\cdot}5(0{\cdot}1)3{\cdot}0$
Table III	F	$\alpha=0{\cdot}2(0{\cdot}05)1$	$\beta=3{\cdot}0(0{\cdot}1)6{\cdot}0$
Table IV	F	$\alpha=0{\cdot}3(0{\cdot}1)1$	$\beta=6{\cdot}0(0{\cdot}1)60\alpha^2$

This integral is used in calculating wave profiles and the wave resistance due to a ship's motion.

21. A. Young and T. Murphy, *Tables of the Langevin function and its inverse.* 6 foolscap manuscript pages of tables and 3 pages of description.

The Langevin function $\mathscr{L}(x)=\coth x-(1/x)$ appears in the theory of ferromagnetism. The inverse function $\mathscr{L}^{-1}(x)$ is important in the theory of elastomers.

The tables comprise :

(i) five manuscript pages of $\mathscr{L}(x)$, $x=0(0{\cdot}1)7{\cdot}50$, six decimals ;

(ii) one manuscript page of $\mathscr{L}^{-1}(x)$, $x=0(0{\cdot}01)1{\cdot}00$, six decimals, with second differences in both cases.

A table of discrepancies in small tables of $\mathscr{L}(x)$ by Emden and Boll is also given.

22. A. Gloden, *Factorisation de nombres* $2N^4+1$, $N \leqslant 1000$. 17 foolscap pages.

This typescript by Professor A. Gloden forms an incomplete factor table. Further factors have been added by J. C. P. Miller so that now all prime factors not exceeding 10 000 have been entered. Almost all cofactors $<10^9$ have been investigated by application of Fermat's theorem, that is by finding the residue of 2^{N-1} (mod N) and 3^{N-1} (mod N). If the residue is unity in each case the number may be presumed to be prime; if the residue is not unity, the factors have been sought and found.

Proof of primality of numbers satisfying the Fermat test has been completed for $N<2\times10^8$; completion of the proof is still needed for other numbers $<10^9$ and examination of cofactors exceeding 10^9 remains to be done.

In all, 553 numbers have been completely factorized, and 86 others have a remaining cofactor that satisfies Fermat's test but which exceed 2×10^8.

23. A Ferrier, *Factorization of* $N=3n^4-1$, $0<N\leqslant1000$. 1 manuscript sheet 24×18 in.

This table gives factors of $3n^4-1$ for $n\leqslant1000$. All prime factors up to 3000 are given, and many higher ones. Factorization is complete for $n\leqslant100$ and for 216 other values of n.

24. D. F. Ferguson, C. E. Gwyther and J. C. P. Miller, *High-accuracy square- and cube-roots.*

Square Roots, computed by *D. F. Ferguson*, 22 foolscap pages.

$\sqrt{N}$ to 50 decimals $N=1(1)100(10)1000$

25 decimals $N=100(1)1000(10)10000$.

The former are marked "all checked and guaranteed" on the typed sheets. The latter are marked more simply "all checked".

All values should be correct throughout; rounded to nearest final unit. An independent calculation by *J. C. P. Miller* (3 foolscap pages) exists for $N=1(1)100$, also to 50 decimals. Values curtailed without rounding at 50th decimal, but a + indicates >5 units in 51st decimal.

The only discrepancy in the last digit is for $N=22$, where D.F.F. has 4, J.C.P.M. has 3 without a +.

Cube Roots, computed by *C. E. Gwyther*, 5 foolscap pages.

$\sqrt[3]{N}$, $\sqrt[3]{N^2}$ to 21 decimals $N=1(1)100$

to 15 decimals $N=10(10)1000$, $N=100(100)10000$

$\sqrt[3]{N}$, $\sqrt[3]{N^2}$ to 13 decimals $N=101(1)200$.

Gwyther states "$N^{1/3}$ and $N^{2/3}$ have been calculated to 25 decimal places. In no case does $N^{1/3}\times N^{2/3}$ differ from N by more than $\pm1\times10^{-20}$.

$(10N)^{1/3}$, $(100N)^{1/3}$, $(10N^2)^{1/3}$ and $(100N^2)^{1/3}$ have been calculated to 17 or 18 decimal places. In no case does $(10N)^{1/3}\times(100N^2)^{1/3}$ or $(100N)^{1/3}\times(10N^2)^{1/3}$ differ from $10N$ by more than $\pm 1\times 10^{-16}$ ".

Values should therefore be accurate.

25. Admiralty Research Laboratory, *A solution of the equation* $(y'')^2=yy'$. 16 foolscap pages.

The solution y for which $y(0)=0$, $y'(0)=1$ and y'' is negative near the origin, is tabulated to 6D for $x=0(0{\cdot}002)6$ while $\log y$ is given to 6D for $x=6(0{\cdot}01)7{\cdot}5$. Second differences are provided where necessary for interpolation. A brief account of the properties of this function is included in Table 9.

26. Admiralty Research Laboratory, *Table of*

$$F(\beta,\rho)=\frac{2}{\sqrt{\pi}}\frac{e^{-\rho^2}}{\beta^2}\int_0^\beta I_0(2\rho\eta)\,e^{-\eta^2}\,\eta\,d\eta.$$ 10 foolscap pages.

This integral is tabulated to 4D for $\beta=0(0{\cdot}05)2{\cdot}5$, $\rho=0(0{\cdot}05)3$ to $4{\cdot}25$. No differences are provided but interpolation is linear to 3D. This function is also referred to in Table 9.

27. Admiralty Research Laboratory, *Table of*

$$F(x)=2x\sum_{n=0}^{\infty}\{x^2+(2n+1)^2\}^{-3/2}$$ *and of* $x^{-1}F(x)$.

8 foolscap pages.

In each case values are given to 4D for $x=0(0{\cdot}002)1{\cdot}5(0{\cdot}01)5$. Interpolation is linear.

28. Admiralty Research Laboratory, *Table of*

$$G(x)=6x^2\sum_{n=0}^{\infty}\{x^2+(2n+1)^2\}^{-5/2}.$$

5 foolscap pages.

$G(x)$ is given to 4D for $x=0(0{\cdot}002)1{\cdot}5(0{\cdot}01)5$. Interpolation is linear.

29. Admiralty Research Laboratory, *Table of*

$$f(x)=\sum_{n=0}^{\infty}(-1)^n(2n+1)\{x^2+(2n+1)^2\}^{-5/2}$$ *and of* $x\,f(x)$.

4 foolscap pages.

In each case values are given to 4D for $x=0(0{\cdot}005)2(0{\cdot}05)5$. Interpolation is linear.

30. Admiralty Computing Service, *Tables of*

$$f(x, y)=\frac{1}{2\pi}\int_0^{2\pi} \exp\left(-x\cos\theta-y\cos^2\theta\right) d\theta$$

for $x=0(0{\cdot}25)5$, $y=0(0{\cdot}25)5$; 3D *and* 4D. 2 foolscap pages.

The tabular values are unlikely to be in error by more than one unit in the last figure retained. See *M.T.A.C.*, **2,** 291.

31. Admiralty C. S., *Tables of* $Y=\mu\,[f(\theta)-1]$, $S=\mu\int_0^{\theta}\frac{f(u)\,du}{\cos u+\mu\sin^2 u}$, $S-Y$, *where*

$$f(\theta)=\exp\left\{\int_0^{\theta}\frac{\sin u\,du}{\cos u+\mu\sin^2 u}\right\}$$

for $\theta=0°(1°)90°$; $\mu=0{\cdot}05, 0{\cdot}1(0{\cdot}1)0{\cdot}5, 0{\cdot}4(0{\cdot}2)1(0{\cdot}5)7(1)12$.

Y, S are tabulated to 3D ; $S-Y$ to 3D for $0\leqslant\theta\leqslant40°$ and to 4D for $41°\leqslant\theta\leqslant90°$. 10 double foolscap sheets of tables + 2 pages of introduction. See *M.T.A.C.*, **2,** 291.

32. Admiralty C. S., *Tables of* A, B, C, D, *defined by*

$$A(a, x)-iB(a, x)=\int_0^x \mathrm{e}^{-2\pi ir}\,dt$$

$$C(a, x)-iD(a, x)=\int_0^x \mathrm{e}^{-2\pi ir}\,dt/r$$

where $r^2=a^2+t^2$.

A, B, C, D are given to 4D for the ranges $x=0(0{\cdot}05)1{\cdot}5$; $a=0(0{\cdot}1)1{\cdot}5$. $5\frac{1}{2}$ foolscap pages of tables + $1\frac{1}{2}$ pages of introduction.

Although the last figure cannot be guaranteed it is unlikely to be in error by more than 0·7.

No means for interpolation are provided. Generally, third and higher differences can be ignored in interpolating in the x-direction, but must be included when interpolating in the a-direction. See R.M.T. 262, *M.T.A.C.*, **2,** 36.

33. Admiralty C. S., *Tables of the integrals*

$$A_n(x)=\int_0^x \frac{\cos\left(n-\frac{1}{2}\right)\pi t/x}{1+t^2}\,dt$$

$$B_n(x)=\int_0^x \frac{\cos\left(z_n\,t/x\right)}{1+t^2}\,dt$$

$$C_n(x)=\int_0^x \frac{\cosh\left(z_n\,t/x\right)}{1+t^2}\,dt$$

for $n=1, 2, 3$ *where* z_n *is the n-th positive root of the transcendental equation*

$$\tan z+\tanh z=0.$$

The three functions are tabulated to 4D ; in part A for $n=1$ and in part B for $n=2, 3$. In all cases the range is

$$x=0(0{\cdot}01)1 \text{ and } 1/x=0(0{\cdot}01)1.$$

33A, 4 foolscap pages of tables + 2 pages of introduction ; 33B, 8 foolscap pages of tables + 4 pages of introduction.

Information is given as to accuracy, interpolation and the method of computation. See R.M.T. 267, 268, *M.T.A.C.*, **2,** 39, 40.

34. Admiralty C. S., *Values and contours of*

$$\int_0^\infty \frac{e^{-k}\,[J_0\,(kx)\cosh\,(ky)-1]}{\sinh k}\,dk.$$

Values are given to 4D for $x=0(0{\cdot}1)5$, $y=0(0{\cdot}1)1$. 5 foolscap pages of tables + 1 chart + 5 pages of introduction. See R.M.T. 334, *M.T.A.C.*, **2,** 175.

35. Admiralty C. S., *Table of* $f(x)=e^{-x}\int_0^{\pi/2} e^{x\cos\theta}\sin^2\theta\,d\theta$ *to* 5D *for* $x=0(0{\cdot}01)5(0{\cdot}1)20$. An auxiliary function $x^{3/2}f(x)$ is tabulated to 4D for $1/x=0(0{\cdot}01)0{\cdot}2$. 4 foolscap pages of tables + 2 pages of introduction. See R.M.T. 266, *M.T.A.C.*, **2,** 38.

36. Admiralty C. S., *Zeros of the first ten Laguerre polynomials and the corresponding Christoffel numbers.* The zeros $x_i^{(n)}$ are tabulated to 8D, and the corresponding Christoffel numbers λ_i to 8S. 2 foolscap pages of tables + 3 pages of description. See R.M.T. 252, *M.T.A.C.*, **2,** 31.

37. Admiralty C. S., *Tables of the integrals*

$$C(t)=k^{\frac{1}{4}}\int_0^\infty e^{-u}\cos\,(2tk^{\frac{1}{4}}u-ku^2)\,du$$

$$S(t)=k^{\frac{1}{4}}\int_0^\infty e^{-u}\sin\,(2tk^{\frac{1}{4}}u-ku^2)\,du$$

6 foolscap pages of tables + 4 pages of introduction.

The integrals are tabulated for the values of the parameter k equal to $\frac{1}{4}$, $\frac{1}{2}$, 1, 2, 4 and 8, for a range of t to which $\sqrt{(S^2+C^2)}$ is at least ten per cent of its maximum value. Values of S, C and $\sqrt{(S^2+C^2)}$ are given to three decimal places, the last figure being possibly in error by two or three units. See R.M.T. 293, *M.T.A.C.*, **2,** 80.

38. Admiralty C. S., *Tables for the summation of trigonometrical series.* 22 foolscap pages of tables + 2 pages of introduction.

Tables of cos ux and sin ux, for use in the summation of Fourier series, are given for the ranges $u=1(1)10$, $x=0°(1°)180°$, and also for radian argument $x=0(0{\cdot}01)3{\cdot}14$. The number of decimals given is

5D for $n=1, 2, 3, 4$.

4D for $n=5, 6, 7$.

3D for $n=8, 9, 10$.

Since all the entries for n greater than 4 occur in previous columns, 5 decimals can be obtained in individual values if necessary for a special purpose. See R.M.T. 277, *M.T.A.C.*, **2,** 70.

39. Admiralty C. S., *Tables of the incomplete Airy integral.* 5 foolscap pages of tables + 12 pages of introduction.

Values of $F(x, y)=\frac{1}{\pi}\int_0^\pi \cos(xt-yt^3)dt$ are given to 4D for the ranges $x=-2{\cdot}5(0{\cdot}1)+4{\cdot}5$; $y=0{\cdot}10(0{\cdot}02)1$ and zero.

The error in the last figure does not exceed one unit. Interpolation in the x-direction requires second differences, in the y-direction fourth differences, if full tabular accuracy is to be preserved. If higher differences than the second are neglected in interpolation in the y-direction, a maximum error of two units will be incurred. See *M.T.A.C.*, **2,** 296.

40. Admiralty C. S., *Tables of the functions associated with the Airy integral for complex arguments.* 9 pages of introduction + five parts totalling 11 double foolscap + 12 foolscap pages of tables + 5 pages of introduction.

These functions are referred to in a paper by C. Domb and M. H. L. Pryce entitled " The calculation of field strengths over a spherical earth ". *J. Instn. Elect. Engrs*, **94,** 325 (1947). See R.M.T. 260, *M.T.A.C.*, **2,** 35.

41. Admiralty C. S., *Tables of the function* $C(m, \mu\ ;\ x)$.

The hypergeometric function $C(m, \mu\ ;\ x)=F(1, m-\mu\ ;\ m, x)$ is tabulated to 4D for $4m=40(1)44$, $80(1)84$; $4\mu=4(1)20$; $x=0{\cdot}8(0{\cdot}02)0{\cdot}9(0{\cdot}01)1$. This function is useful in the summation of slowly convergent series. There are no facilities for interpolation. 16 foolscap pages of tables + 2 pages of introduction.

LXVIII. *The Surface Energy of Colloidal Metals in Ionic Lattices*

By Allen B. Scott*
H. H. Wills Physical Laboratory, University of Bristol†

[Received January 28, 1954]

Abstract

The energy of the interface between small particles of alkali metal and an alkali halide lattice has been calculated. The energy is sufficient to account for the observed heat of dissociation of the colloidal particles to form F-centres. An estimate of the size of the particles is provided.

§ 1. Introduction

Recent experiments upon alkali halides coloured by excess alkali metal by Scott and Smith (1951) and Scott, Smith and Thompson (1953) have provided values for the heat absorbed in the formation of F-centres from colloidal metal imbedded in the crystal lattice. Seitz (1954) has pointed out that these observed heats are much lower than those which are calculated for the formation of F-centres from metal outside the crystal; he discussed possible reasons for the difference, but was unable to account in a quantitative way for the low cohesive energy of the colloidal metal on the basis of either surface energy or compression of the metal. However, Seitz considered only the surface energy of the metal itself, rather than the energy of the lattice-metal interface. It is the purpose of this paper to describe a more detailed calculation of the energy at the interface for colloidal potassium in KCl and sodium in NaCl, which is found to be quite sufficient to account for the low cohesive energy of the metal.

For the process: colloid→F-centre, the observed heat, ΔH, is 0·35 ev per atom for additively coloured KCl at 350°. The heat of vaporization of liquid potassium at 350°, calculated from the value at the boiling point and C_p of the liquid and vapour, is 0·92 ev per atom. Rögener (1937) found that the heat evolved in the formation of an F-centre from the vapour is 0·10 ev from measurements made between 500° and 700°c. We will assume it to be about the same at 350°. Thus the heat required to form an F-centre from the liquid metal outside the crystal is 0·82 ev, so that the colloidal metal in the lattice exhibits a cohesive energy lower than the normal value by 0·47 ev per atom.

For Na in NaCl, at 490°, the heat of dissociation of the colloid is 0·39 ev, the heat of vaporization of liquid sodium is 1·15 ev, and the

* Communicated by the Author.

† Now at Department of Chemistry, Oregon State College, Corvallis, Oregon, U.S.A.

heat of formation of an F-centre from the vapour is about zero, according to the data of Mollwo (1933). The cohesive energy of the colloidal metal is thus 0·76 ev per atom lower than that of the bulk metal.

The energy of the lattice-metal interface is the sum of energies arising from the following sources :

(*a*) Coulombic forces due to lattice ions acting on ions in and near the lattice surface surrounding the metal particle.

(*b*) Van der Waals and repulsive forces due to lattice ions acting on ions in and near the lattice surface surrounding the metal particle.

(*c*) Surface energy of the liquid metal.

(*d*) Interaction between the lattice ions and the conduction electrons of the metal, represented by the formation of image charges in the metal.

(*e*) Van der Waals and repulsive forces acting between the lattice ions and the atom cores of the metal.

Of these only (*c*) can be obtained by direct experiment. The energy arising from (*e*) may be neglected, since Wigner and Seitz (1934) have shown that interactions of the Van der Waals and repulsive types between alkali metal atom cores contribute very little to the cohesive energy, and the internuclear distance between the lattice ions and the atom cores of the metal can hardly be much less than between the metal atoms themselves.

The energy arising from (*a*), which we will call the Coulombic surface energy of the lattice, can be found by evaluating the energy necessary to remove a small block of ions from the lattice to produce the surface of a cavity. This will give a more precise result than would be obtained by using the Coulombic energy for a plane lattice surface, since the corners and edges of the cavity will contribute significantly to the energy. That arising from (*b*) may be obtained satisfactorily from the part of the plane-surface energy due to Van der Waals and repulsive forces, by treating the cavity as a cube, as corner and edge effects are much less important for the shorter range forces. Shuttleworth (1949) has calculated the contribution of these forces to the plane-surface energy for several alkali halides. The energy due to (*d*) may be estimated following the choice of a suitable model for the lattice-metal interface.

Energies due to (*a*), (*b*), (*c*), and (*d*) above have been calculated for metal particles occupying cubical cavities from 3 to 8 ions on the edge in KCl and NaCl. As well as supplying an adequate reason for the observed heat of dissociation of the colloidal metal, some insight into the forces operative at the interface is gained.

For all sizes of particle, the metal has been considered to possess the structure of the perfect alkali metal lattice ; the justification for this assumption is the fact that the colloidal metal particles have been found to have very nearly the optical and photoemissive properties of the metal in bulk (Scott, Smith and Thompson 1953). While the structure of the liquid metal will not have the regularity of that of the solid, the quantity which is important in the present calculation, namely the average closeness of packing, may be obtained from the lattice constants of the solid with appropriate density corrections.

It must be emphasized, however, that the smaller particles may possess a structure intermediate between that of the bulk metal and that of an aggregate of negative-ion vacancies with their associated electrons. Unfortunately, there is not yet sufficient information about the existence or properties of such intermediate structures to allow them to be taken into account in a calculation of this kind.

§ 2. The Coulombic Surface Energy

The energies we require are the total surface energies or surface enthalpies, which are the free surface energies at 0°K. We expect that the surface of the cavity enclosing the metal would assume the shape of a regular polyhedron to minimize the energy. Shuttleworth's results show that the energy of the (100) face of the NaCl lattice is much lower than that of the (110) face and it is presumed that the (100) face has much the lowest energy of any of the faces. A cube has very nearly the lowest surface energy of any solid bounded only by (100) planes ; thus, to simplify calculations, it will be assumed that the colloidal particle consists of a cubical cavity cut in the lattice and filled just to capacity with liquid metal. The difference in surface energy of a cube of metal compared with a sphere of equal volume is much less than the energy saved by using only (100) planes.

The Coulombic total surface energy of the cavity, V_c, is half the energy required to cut the small cube out of the lattice at 0°K and remove it to infinity, since the cavity surface is half the total new surface produced. The work required is

$$W=2\left(\frac{ne^2}{2r_0}\,\alpha_{\mathrm{M}}-\frac{ne^2}{2r_0}\,\alpha'_{\mathrm{M}}\right)$$

where n is the number of ions in the cube removed, r_0 is the lattice constant at 0°K, α_{M} is the Madelung constant for the infinite lattice, and α'_{M} is a number analogous to the Madelung constant, but applicable to the finite lattice when separated from the rest. The first term in brackets gives the energy of the ions of the cube when it is inside the infinite lattice ; the second term gives the energy of the same ions in the cube when cut out of the lattice and removed to infinity. The factor 2 enters because the ions surrounding the cube undergo an equal increase in energy as the cube is removed. Then

$$V_c=\frac{ne^2}{2r_0}(\alpha_{\mathrm{M}}-\alpha'_{\mathrm{M}}).$$

α'_{M} may be found for the finite cube by direct summation of all the electrostatic potential energy terms due to interaction between pairs of ions. This is quite feasible for cubes having less than 10 or 12 ions on the edge ; for larger cubes V_c may be found easily by more approximate methods if desired.

Emersleben (1952 a) has evaluated $(n/2)\alpha'_{\mathrm{M}}$ for several small cubes of even n. We have calculated α'_{M} for cubes of 3, 5, and 7 ions on the

edge and at the same time have confirmed Emersleben's results for cubes 2, 4, and 6 ions on the edge. α'_M and V_c for cubes from 2 to 8 ions on the edge are given in table 1. r_0 for KCl was taken as 3·10 A and for NaCl, 2·75 A.

Table 1

$\sqrt[3]{n}$	α'_M	V_c (ev)	Image effect (ev)	$V_{v,r}$ (ev)	Metal surface energy (ev)	Total	Metal atoms	Energy per atom (ev)
				KCl				
2	1·4560	5·41		— 1·25			2	
3	1·5665	11·34		— 2·83			4	
4	1·6287	17·6	— 3·3	— 5·0	5·8	15·1	13	1·16
5	1·6561	26·5	— 5·6	— 7·9	9·1	22·1	31	0·71
6	1·6736	37·1	— 8·2	—11·3	13·0	30·6	53	0·58
7	1·6850	49·8	—11·5	—15·4	17·7	40·6	100	0·41
8	1·6939	63·7	—15·3	—20·1	23·1	51·4	154	0·33
				NaCl				
2	1·4560	6·12		— 1·78			2	
3	1·5665	12·82	— 2·44	— 4·01	5·26	11·63	6	1·94
4	1·6287	19·9	— 3·8	— 7·1	9·4	18·4	23	0·80
5	1·6561	30·0	— 5·7	—11·1	14·6	27·8	47	0·59
6	1·6736	42·0	— 8·0	—16·0	21·0	39·0	94	0·41
7	1·6850	56·3	—10·7	—21·8	28·6	52·4	145	0·36
8	1·6939	72·1	—13·7	—28·5	37·4	67·3	232	0·29

Alternatively, the Coulombic surface energy may be found by the use of Emersleben's (1952 b) relations for the energies of faces, edges, and corners of finite NaCl lattices. Agreement with that calculated from α'_M is within a few tenths of a per cent for cubes of 64 ions and larger. For the smaller cubes, the edge and corner corrections are influenced by the proximity of the opposite edges and corners ; also for odd n, the lack of neutrality of the lattice introduces an error if n is small.

The quantity V_c calculated above is based upon the assumption that the surface ions remain on ideal sites and are themselves unpolarized, which is not strictly true. Verwey (1946), in collaboration with J. E. Asscher, treated the problem of surface polarization of the alkali halides, and concluded that the plane of the surface cations should lie closer to the next underlying plane of ions in the crystal than does the plane of surface anions. Also the surface anions will be considerably polarized by the non-symmetrical crystalline field, while the cations will be only slightly polarized being much smaller. These effects serve to lower the

Coulombic surface energy, but the extent of the energy decrease is very sensitive to the choice of the function used to represent the repulsive forces between the ions, so that it can hardly be evaluated with confidence. Verwey computed that the Coulombic surface energy of NaBr, calculated on the basis of no polarization, would be reduced from 122 to 90 erg/cm² by these effects.

There is no justification of using this result either as a fixed or proportional correction to V_c in NaCl or KCl, as the polarizability of Cl^- is markedly lower than that of Br^-; also, the repulsive forces would not be represented by the same equations. We would expect that the reduction of surface energy would be less for the chlorides, and we see later that the influence of the metal is to diminish further the effects of surface polarization, so that a correction for it may be neglected without introducing serious error.

§ 3. Van der Waals and Repulsive Forces

Shuttleworth gives as the contribution of Van der Waals and repulsive forces to the plane-surface energy −87 and −157 erg/cm² for (100) faces of KCl and NaCl respectively. The negative sign is used to indicate that these energies are to be subtracted from the Coulombic energy. $V_{v,r}$ the effect of these forces on the surface energy of finite cubical cavities, calculated simply from the plane-surface values and the surface area of the cavities, is given in table 1.

§ 4. Surface Energy of the Metal

The surface area of the metal was taken to be that of the cavity, and its surface energy found from the experimental surface energies of the alkali metals. Some error is involved in considering the metal to join the lattice continuously in the edges and corners, as the radius of curvature of the metal surface cannot be less than the atomic radius; however, the small error is compensated to a large extent by neglecting the increase in energy due to the sharp curvature at the corners and edges.

The most reliable results for the surface energy of liquid sodium appear to be those of Poindexter and Kernaghan (1929), who found it to be 206 erg/cm² at 103°, with a very slight decrease with temperature. Extrapolation to 0°K is hardly justified, but would have the effect of increasing the final surface energy somewhat. Unfortunately, there is no correspondingly reliable information for liquid potassium. Quarterman and Primak (1950) recalculated the previously accepted drop-weight value of Quincke (1868) and found it to be greater than 500 erg/cm² at the melting point. Using the capillary rise, they found it to lie between 86 and 95 erg/cm², the uncertainty arising from the lack of knowledge of the contact angle, which was, however, not greater than 26°. Empirical curves for the surface energy of liquid metals as a function of other properties such as atomic volume, heat of fusion, and heat of vaporization, as given by Skapski (1948), Atterton and Hoare (1951), and Mukherjee

(1951), indicate that if potassium is normal in this respect, its surface tension is about half that of sodium, or somewhat higher. The value of 100 erg/cm^2 was used as a suitable compromise.

The metal surface energies given in table 1 are of course subject to the uncertainty arising from the choice of the bulk metal structure to represent the actual structure of the colloidal particles.

§ 5. Lattice–Metal Interaction Energy

We have seen that the only significant interaction between the lattice ions and the metal is that due to formation in the metal of image charges corresponding to each ion. It will be assumed that the potential energy of an ion a distance x from the metal surface, due to its image, is $-e^2/4x$, although this is only strictly true for an infinite grounded metal surface and for x large compared to atomic dimensions. We can thus consider a plane of ions adjacent to the metal as having another plane of charges in the metal at a distance $2x$, and compare the potential due to the plane of images with that due to an actual plane of ions at the distance r_0. Since most of V_c arises from the separation of adjacent planes, this comparison will afford a reasonable estimate of the reduction to be

Fig. 1

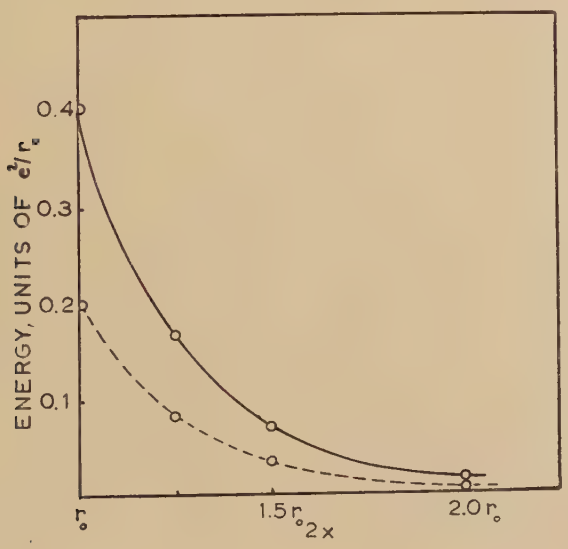

expected in V_c as a result of the image potentials. In view of the rather arbitrary assumptions which must be made in order to select an appropriate value for x, it was not considered worthwhile to attempt a more detailed solution of this problem by taking into account the finite size and shape of the particle and the interactions of ions more remote than the first layer; as it is, the image potentials, based on the approximate treatment, reduce the value of V_c by less than 25%.

The potential energy of two square 36-ion planes of the NaCl lattice, as a function of their separation, $2x$, is shown in fig. 1. The broken curve, just half the height of the full curve, gives the energy for a plane of ions and its image plane in the metal. To assign x, we must inquire into the details of the interface between the metal and the lattice.

In the first place, it must be noted that, if the metal is considered to have a truly plane surface, x may be taken equal to the Cl^- radius for all ions on the sides of the cavity whether anions or cations (fig. 2 (*a*)). If the metal be considered as composed of rigid spheres, with the metal surface represented by the actual surface of the spheres, x is greater than r_{Cl^-} for some ions and less for others (fig. 2 (*b*)). In either case, x may be satisfactorily taken as equal to r_{Cl^-}. It must be pointed out, however, that the electron charge distribution of the metal almost certainly extends beyond what is usually called its ' geometrical surface ' and will penetrate the lattice ions to some extent, so that the actual surface of the metal cannot be precisely described by any geometrical surface.

Fig. 2

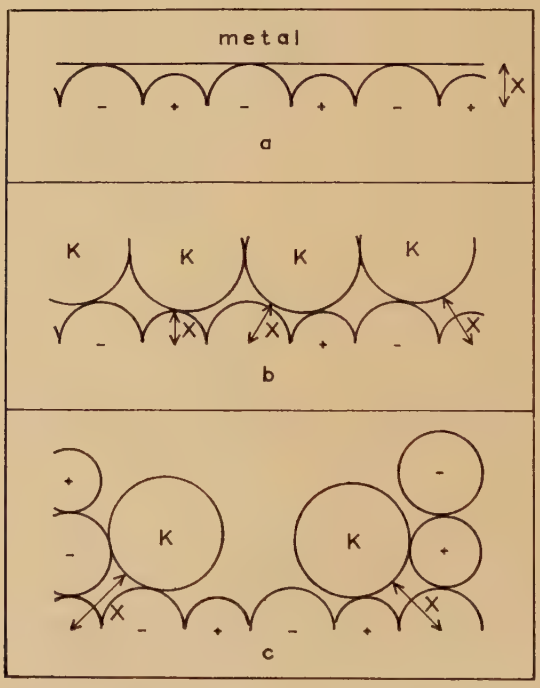

We further observe (fig. 2 (*c*)), that due to the limit imposed on the radius of curvature of the metal surface by the finite atomic radius, x will be greater than r_{Cl^-} for all ions located along the edges and in the corners of the cavity, and will in fact average about r_0, in the case of KCl.

The numerical calculation of the effect of image potentials is best illustrated by using an example. In the case of KCl having a cavity formed by removing a cube 6 ions on edge, there are 294 ions on the

surface of the cavity, of which 84 are on the edges and corners. The image energy for a plane of ions at the distance of the edge ions ($x=r_0$) is about 0·03, and for the other ions at the distance $x=r_{Cl^-}=0{\cdot}58\,r_0$ about 0·30 of the interplanar energy at the normal separation r_0. The average for the entire surface can then be taken as $0{\cdot}22\,V_c$. The ratio of the image potential energy to V_c changes with the size of the cavity for KCl, since the ratio of edge ions to total ions on the surface changes, but lies between 0·19 and 0·24 for the cases included in table 1.

The atomic radius of Na and the ionic radius of Cl^- are nearly equal, so that Na atoms may be more closely packed into the corners of a cavity in NaCl. Thus x may be taken as r_{Cl^-}, or $0{\cdot}64\,r_0$, for all ions, and the image potential energy is $0{\cdot}19\,V_c$.

The effect of surface polarization of the crystal lattice on the metal–lattice interaction must be considered. The displacement of the surface anions toward the metal would increase the average value of x for all the ions of the lattice, and the presence of the image charges would decrease the polarization of the surface anions. Both effects would serve to cancel the effect of polarization on V_c.

§ 6. Surface Energy per Atom

The four contributions to the energy of the interface are summed for the several sizes of lattice cavity in table 1. To obtain the number of metal atoms in each of the cavities, it is not sufficient merely to divide the volume by the usual atomic volume, since a high proportion of the atoms are on the surface and occupy a volume roughly twice the volume of an atom in the interior. By assuming that the liquid metal will utilize b.c.c. packing, and has the structure of the metal in the bulk, it is not difficult to obtain the number of atoms which will fit without compression in a given cubical space, assigning the usual volume to atoms in the interior, and a surface volume to those on the surface. Room-temperature lattice constants for K and Na were corrected to 350° and 490°, respectively, by the use of densities, and used for the liquids for this purpose ; the edge of the unit cube is : K, 5·55 A ; Na, 4·40 A.

Only 2 or 3 atoms will fit in the cavities of 2 and 3 ions on edge in KCl, so that the surface energy of the metal could not even be approximated. For the same reason, no final value was calculated for the smallest particle of Na in NaCl.

The total interfacial energy per atom in the metal particle is plotted in fig. 3. It may be seen that a particle of 80 atoms of K, and 30 atoms of Na, would possess the required additional energy to account for the observed heat of dissociation. These sizes are within the range estimated by Scott, Smith and Thompson (1953) on the basis of other considerations, and it may be concluded that surface effects alone are responsible for the decrease in cohesive energy. The actual mean value of the particle size may differ considerably of course from that obtained by this simplified calculation, and the range of size within a given crystal is undoubtedly quite wide.

The experimental evidence indicates that the surface energy for K particles in KBr must be about 0·17 ev per atom. The plane-surface energy of KBr given by Shuttleworth is a little less than that of KCl, and the surface polarization is certainly much greater, so that the mean particle size is not necessarily larger than for K in KCl.

Fig. 3

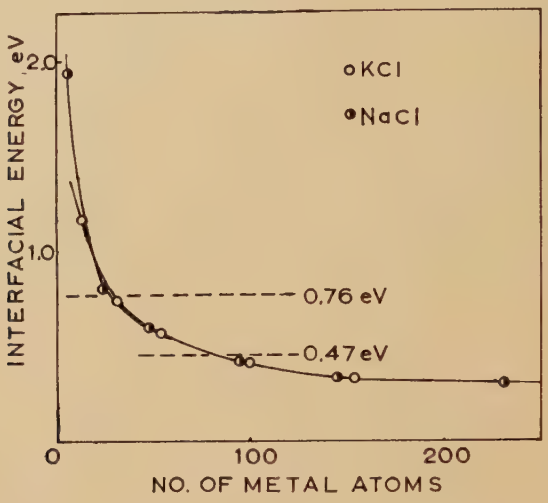

It must next be considered whether additional metal will enter the particle, under compression, in order to lower the surface energy per atom. From the discussion of Seitz (1954) it would appear that considerable compression might occur at the expense of a relatively small loss of surface energy per atom. However, his calculation was based on a process of coagulation carried out at constant volume, whereas the processes of interest here take place at constant pressure, since the temperature at which equilibrium is established is in the usual case high enough for ionic diffusion to take place quite readily. The increase in Gibbs free energy upon compressing metallic potassium to 0·9 its volume, for example, by adding 6 more atoms to the 53-atom particle without increasing its volume, is 0·18 ev per atom, while the surface energy per atom would be decreased by only 0·001 ev. Thus, compression of the metal certainly would not occur.

§ 7. Further Growth of Particles

It would be expected that after an initial apparent equilibrium between F-centres and colloid is established a slow growth of the more stable large particles would occur, accompanied by the ' dissolving ' of the smaller ones. We can obtain some fairly quantitative ideas regarding precipitation times and growth rates if we assume that F-centres migrate from site to site at the same rate as do negative ion vacancies. Seitz (1946) gives the jump frequency of a vacancy as

$$\nu = \nu_0 \exp(-\epsilon''_0/kT),$$

where ν_0 is the reststrahlen frequency of about 10^{13} sec^{-1}, and ν for negative ion vacancies in KCl is about 10^{-5} sec^{-1} at room temperature. We then find ϵ''_0 to be 1·1 ev and ν at 350° to be about 10^4 sec^{-1}. At each jump the vacancy moves to the nearest equivalent site, a distance of $\sqrt{(2)}\times 3{\cdot}1\times 10^{-8}$ cm, so that it will wander by random jumps a total of about 4×10^{-4} cm/sec. Now if a KCl crystal contains 10^{17} alkali metal atoms/cm^3, distributed as 100-atom particles, the average length of zig-zag path travelled by an F-centre between collisions with metal particles is about 0·03 cm. For this calculation, the mean cross sectional area of the particles was computed from the atomic volume to be 5×10^{-14} cm^2 and the F-centre was considered as a point. The probability of collision in a path of length l is the ratio of the total cross section of particles within a sphere of radius l to the surface area of the sphere, and, for l equal to the mean free path, is 0·5. Then

$$0{\cdot}5=\frac{(4/3)\pi l^3(10^{15})(5\times 10^{-14})}{4\pi l^2}$$

and $l=0{\cdot}03$ cm. This result holds whether the path travelled between collisions is straight or zig-zag, and gives in either case the total distance travelled. It may be seen that the mean time between collisions is $0{\cdot}03/4\times 10^{-4}$, or about 10^2 sec.

After attainment of the initial equilibrium between F-centres and small particles, alkali metal must be transferred from the smallest particles to larger ones in such a way that the equilibrium F-centre concentration is not exceeded, i.e. for every F-centre detached from one particle one must collide with and join another particle ; thus an average of about 10^2 seconds is required for the transfer of an F-centre from one particle to another. If all particles were identical, the time for the growth of large particles would be infinite, as all particles would lose F-centres and gain them back with equal probability. On the other hand, if there were two sets of particles, equal in number but with one set having cross sections negligible compared with those of the other set, an F-centre escaping from a small particle would have unit probability of colliding with a large particle instead of with another small particle, and the time required to add n atoms to each large particle would be $n\times 10^2$ sec. The actual time would be greater than this, due to a spread of particle sizes through a wide range, so that we may expect the time required, for example, to build up particles containing 10^4 atoms from those containing 100 atoms to be considerably more than 10^6 sec after attainment of initial equilibrium at 350°.

On the other hand, initial coagulation from an excess concentration of F-centres (e.g. 10^{17}/cm^3 at 350°) would be much more rapid. If the trapping diameter of the initial nucleus is assumed to be twice the potassium atom diameter, the mean total path an F-centre would travel before colliding with a nucleus is 0·15 cm, provided there are 10^{15} nuclei/cm^3 so that the initial equilibrium size of particles would be 100 atoms each. The mean coagulation time is thus $0{\cdot}15/4\times 10^{-4}$,

or 400 sec, in rough agreement with the observation of Theisen and Scott (1952).

It is seen that the rate of growth after establishment of the initial equilibrium is determined by the collision time of F-centres with particles, which depends on the particle concentration but not on that of the F-centres, while the time of initial coagulation of the particles depends on the F-centre concentration as well as that of the nuclei. The concentration and size of particles present at the attainment of the initial equilibrium is governed by the concentration of nuclei present, and the excess F-centre concentration.

Seitz (1954), in a comment upon this calculation, has pointed out that in order for the number of metal atoms in a particle to be much less than the number of ion pairs removed in producing the lattice cavity, pairs of vacancies of opposite sign must condense along with the F-centres. Since such ion pairs are believed to migrate much more rapidly than single vacancies, and presumably therefore more rapidly than F-centres, the condensation of pairs would not alter the coagulation and growth times which have been estimated here.

Prolonged heating at fairly high temperatures, where the jump frequency of F-centres would be greatly increased, should result in the growth of the larger particles, as observed by Mollwo (1932) in additively coloured NaCl. The heat of dissociation of such particles should approach much more nearly the heat of formation of F-centres from liquid metal outside the crystal.

Acknowledgments

The author wishes to thank Professor N. F. Mott for his generous interest and assistance, and Professor F. Seitz and Dr. F. C. Frank for valuable discussions of this problem. The assistance afforded the author by a Fulbright Award and a fellowship of the Guggenheim Memorial Foundation is gratefully acknowledged.

References

Atterton, D. V., and Hoare, T. P., 1951, *Nature, Lond.*, **167,** 602.
Emersleben, O., 1952 a, *Z. Phys. Chem.*, **199,** 170; 1952 b, *Z. Elektrochem.*, **56,** 305.
Mollwo, E., 1932, *Nachr. Ges. Wiss. Göttingen II*, 254; 1933, *Z. f. Phys.*, **85,** 56.
Mukherjee, N. R., 1951, *J. Appl. Phys.*, **22,** 1215.
Poindexter, F. E., and Kernaghan, M., 1929, *Phys. Rev.*, **33,** 837.
Quarterman, L. A., and Primak, W. L., 1950, *J. Am. Chem. Soc.*, **72,** 3035.
Quincke, G., 1868, *Ann. Phys. (Pogg.)*, **135,** 621.
Rögener, H., 1937, *Ann. d. Phys.*, **29,** 386.
Scott, A. B., and Smith, W. A., 1951, *Phys. Rev.*, **83,** 982.
Scott, A. B., Smith, W. A., and Thompson, M., 1953, *J. Phys. Chem.*, **57,** 757.
Seitz, F., 1946, *Rev. Mod. Phys.*, **18,** 384; 1954, *Ibid.* (in press).
Shuttleworth, R., 1949, *Proc. Phys. Soc.* A, **62,** 167.
Skapski, A. S., 1948, *J. Chem. Phys.*, **16,** 389.
Theisen, F., and Scott, A. B., 1952, *J. Chem. Phys.*, **20,** 529.
Verwey, E. J. W., 1946, *Rec. Trav. Chim. Pay-Bas*, **65,** 521.
Wigner, E., and Seitz, F., 1934, *Phys. Rev.*, **46,** 509.

LXIX. *Electromagnetic Separation of Spallation Products*

By Göran Andersson
The Gustaf Werner Institute for Nuclear Chemistry,
University of Uppsala, Uppsala, Sweden*

[Received March 22, 1954]

Summary

An electromagnetic isotope separator has been applied to the separation of radioactive spallation products of Vanadium. The decay curves for the different mass numbers provided data for a determination of relative formation cross sections. A fair agreement with earlier results, obtained with chemical methods, was found. In some cases, where such methods have failed, complementary information was gained. The investigation also confirmed the mass assignments of ^{43}K and ^{44}K. A 34 minute activity on mass number 45 could not be identified.

§ 1. Introduction

Ordinary radiochemical techniques used in spallation yield measurements (e.g. Batzel *et al.* 1951) fail to differentiate between isotopes with similar radiation characteristics. A further difficulty is that separation and purification procedures are often rather time-consuming. The present investigation was undertaken in order to test the possibility of using a small electromagnetic isotope separator, recently put into operation at this institute, as a complement to the chemical methods.

Electromagnetic separation offers several advantages. Mass determined, carrier-free and extremely thin samples are obtainable. The time needed is comparatively short. In yield measurements, however, the different ionization probabilities of the elements imposes a restriction. Any kind of calibration of the ion source is complicated by the unknown chemical status of the radionuclides formed in spallation. There is also the difficulty of reproducing the ion source conditions exactly on different occasions. Thus, by this method it will be possible to determine only relative formation cross sections for isotopes of the same element.

§ 2. Apparatus

The isotope separator is of the parallel beam type (Koch and Bendt-Nielsen 1944, Bergström *et al.* 1949). Pending a more detailed technical description, a few features, essential for the actual kind of investigation described here, will be mentioned.

The ion source (of the oscillating electron type) is provided with an internal furnace for temperatures up to about 2000°C. By means of a vacuum gate, the furnace can be loaded without breaking the main vacuum in the apparatus. This is necessary for work with short-lived activities.

* Communicated by Professor T. Svedberg.

In order to ensure optimal focusing for all mass numbers collected simultaneously, care was taken to place the collector device in the focal plane. The mass difference covered is about 20%.

§ 3. Experimental Procedure

The Uppsala synchro-cyclotron was used to bombard Vanadium with 187 Mev protons. Immediately after irradiation the target was transferred to the ion source furnace of the isotope separator. During a 15 minute run the separated ion beams corresponding to mass numbers 41–48 were collected on Al plates, suitable for β-counting. To fix the mass scale, the position of ^{40}A from inactive argon gas, let into the ion source, was continuously observed on a fluorescent screen. Thirty minutes after the end of the bombardment the activity counting was started.

§ 4. Results

Table 1

Mass number	Half lives	Identification
41	1·80 h	^{41}A
42	12·5 h	^{42}K
43	22·4 h 3·84 h	^{43}K ^{43}Sc
44	2·46 d 3·90 h 20 m	^{44}Sc^{m} ^{44}Sc ^{44}K
45	3·0 h 34 m	^{45}Ti ?
46	—	—
47	3·3 d 33 m	^{47}Sc ^{47}V
48	1·83 d	^{48}Sc

The analysis of the decay curves gave the result shown in table 1. In some cases, notably ^{43}K and ^{44}K, proposed but low classified mass assignments (Hollander *et al.* 1953) were confirmed. The 34 minute activity on mass number 45 could not be identified. It was found, however, in three separate runs. The yield obtained seems to indicate the possibility of a new potassium isotope. This will be the subject of continued investigations. Of course, the presence of a molecular ion with mass 45 can not be excluded.

In table 2 the measured cross sections (column 2) are compared with some results obtained by Rudstam (1953) under identical irradiation

conditions (column 3). From his more extensive investigations, based on chemical separation methods, he concluded that the cross section distribution for spallation with high energy protons shows certain regularities. For the actual case (187 MEV protons and Vanadium) his results were found to fit approximately the formula

$$\sigma(M, Z)=\exp\,[0{\cdot}358M-12{\cdot}82-1{\cdot}80\,(Z-0{\cdot}466M)^2],$$

where σ is the cross section in mb and M and Z are mass number and atomic number respectively. This formula has been used to calculate the values given in column 4.

Table 2

Nuclide	Cross sections relative to ^{42}K resp. ^{47}Sc		
	Present inv.	Rudstam 1953	Calculated
^{43}K	0·33	0·64	0·36
^{44}K	0·058	not measured	0·064
^{43}Sc	0·36	0·40*	0·20
^{44}Sc+^{44}Sc^{m}	1·47	1·7 *	0·95
^{48}Sc	0·38	0·48	0·21

* Calculated from measurements of ^{44}Sc^{m} and ^{43}Sc+^{44}Sc.

It may be worth mentioning, that to the cross section of ^{44}Sc+^{44}Sc^{m} the two isomers were found to contribute very nearly equally.

§ 5. Discussion

The results are seen to support the general ideas suggested by Rudstam (1953) concerning the spallation yield distribution. Too far-reaching conclusions as to the quantitative agreement should not be drawn from this preliminary investigation. The usability of the electromagnetic separation technique in spallation studies is, however, rather well demonstrated. It may be pointed out that this should hold good also in fission yield investigations.

Acknowledgments

The author wishes to thank Professor T. Svedberg for his stimulating interest in this work, Mr. G. Rudstam for valuable information and many discussions, Mr. B. Smith for technical assistance and the cyclotron crew for cooperation.

References

Batzel, R. E., Miller, D. R., and Seaborg, G. T., 1951, *Phys. Rev.*, **84,** 671.
Bergström, I., Thulin, S., Svartholm, N., and Siegbahn, K., 1949, *Arkiv Fysik*, **1,** 281.
Hollander, J. M., Perlman, J., and Seaborg, G. T., 1953, *Rev. Mod. Phys.*, **25,** 469.
Koch, J., and Bendt-Nielsen, B., 1944, *Kgl. Danske Vid. Selsk. Mat. Fys. Medd.*, **21,** No. 8.
Rudstam, G., 1953, *Phil. Mag.*, **44,** 1131.

LXX. *The Markings in the Cleavage Surfaces of Zinc Single Crystals*

By A. Deruyttere
Institute de Métallurgie, Université de Louvain*
and
G. B. Greenough
Department of Metallurgy, University of Sheffield†

[Received March 15, 1954]

Summary

Zinc single crystals of various orientations were broken by applied tensile stresses at −196°c. The two faces of the cleavage fracture were examined and compared; in general they differed markedly. It was noted that the cleavage crack tends to propagate along the active slip direction, and that the distribution of the twins and kink bands is related to the region of the origin of the fracture and to the direction of crack propagation. The majority of the observations on the twins are entirely in accord with the theory of Bilby and Bullough (1954), although more experimental work is necessary to clarify some points where there are discrepancies. In the case of the kink bands, however, there is little agreement between the observations and the theoretical results.

§ 1. Introduction

In the course of an experimental investigation of the cleavage fracture of zinc single crystals of various orientations caused by applied tensile stresses (Deruyttere and Greenough 1953), some attention was paid to the appearance of the cleavage faces. One of the observations concerned the probable direction of propagation of the crack across the cleavage plane, and the identification of this enabled a detailed application to be made of the theory of the twin formation by a moving crack. This theory is described in an accompanying paper (Bilby and Bullough 1954), and is later referred to simply as BB. We re-examined our observations in the light of this theory, and studied certain aspects of the cleavage surfaces further. It was felt that the publication of the theory justified the immediate presentation of a summary of the available experimental data, although it is clear that additional experimental evidence is still necessary on certain aspects.

It has been known for a long time that cleavage fractures in metals are very often associated with the formation of twins in the crystal near the cleavage face. Whether these twins appeared first and initiated the cleavage fracture (Bruckner 1951), or whether the process of fracture

* Formerly Department of Metallurgy, University of Sheffield
† Communicated by the Authors.

itself caused stresses high enough to produce the twinning (Tipper and Sullivan 1951), has been a subject of controversy and one of the aims of the experimental work was to investigate this point. Initially it was proposed to examine both cleavage faces produced by each fracture and to attempt to correlate the twins appearing on each side. It was thought that any twins visible in one face only probably developed after the crack had passed, while those common to both faces might have been either present before fracture started or produced by the propagating fracture in the region ahead of the crack.

There has been much work reported on the examination of cleavage faces, not only in metals and minerals in both the monocrystalline and polycrystalline states, but also in amorphous materials like glass. Generally, the appearance of the faces is very complicated and many types of markings are visible, some clearly associated with the crystallography of the substance and others not. Of the crystallographic type the most prominent are twins, usually with associated accommodation kinks, other kink bands, and steps in the surface caused by the fracture jumping from one cleavage plane to another. The surface topography associated with the twins and kink bands has been extensively studied recently (Pratt and Pugh 1952, Pratt 1953). Markings of a non-crystallographic type are less easy to interpret. One of the few generally accepted observations is that there is frequently visible on cleavage faces a 'river' pattern of striations which are parallel to the direction of propagation of the advancing cleavage, i.e. perpendicular to the edge of the advancing crack (Tipper and Hall 1953, Pratt 1953). The direction of propagation of the cleavage crack, and its probable starting point, is a matter of particular importance for the application of the BB theory and these markings are discussed here. In addition to these striations there are other less regular markings of different appearance which are cliffs connecting neighbouring cleavage planes, but no suggestions are available concerning their significance.

§ 2. Experimental Observations

In our experimental work, Tadanac Electrolytic zinc was employed (impurities 0·002% Pb, 0·0015% Cd, 0·0015% Fe and 0·001% Cu). Cylindrical single crystals 6 mm diameter and 18 cm long were grown using a vertical travelling furnace in precision-bore glass tubing internally coated with graphite. Care was taken throughout to avoid accidental strains before the tensile tests, which were made at −196°c. Most of the crystals extended plastically by slip before fracture occurred, the amount of glide strain increasing as the angle between the applied tensile stress and the cleavage plane, χ, decreased from 90°. The maximum glide strain observed was about 40%. Crystals in which $\chi < 12°$ were observed to twin on a macroscopic scale before fracture, and the cleavage face in those crystals alternated between the basal plane of the twin and that of the original crystal. The detailed observations on the cleavage

faces were confined to the remaining crystals of which some 35 have been examined. A second series of crystals were tested at −77°c and examined, the observations made on this series were very similar to those described here.

The observations on the faces are conveniently summarized in the form of general principles, but it should be emphasized that none of these principles are rigorously obeyed, some exceptions were found to all.

A. *Striations*

They cover most of the cleavage face and appear to run out from a particular region in it. Near this region the lines follow no particular crystallographic direction, but at larger distances *the lines tend to be parallel to the active slip direction.* Figure 1 (Plate 19) illustrates the striations coming from a well defined region, marked as ' Source '. Near to the edge of the cleavage face, or to a particularly high step on the cleavage face, the striations often leave this preferred direction, e.g. see both figs. 1 and 2 (fig. 2, Plate 20). Near the edge the marks usually become perpendicular to it (Tipper and Hall 1953, have also noted this), and occasional cases have been observed in this work where the striations follow a latent slip direction when this is nearly perpendicular to the edge. Examination at high magnifications (up to $\times 1000$) of regions in which curved striations appeared, showed no departure from smooth curves on a microscopic scale, and the striations were therefore considered to be non-crystallographic in character.

For the detailed application of the BB theory it is necessary to establish as certainly as possible the direction in which the crack propagates. Striations similar to these discussed here were observed by Tipper and Hall (1953), and by Pratt (1953), under conditions where the direction of propagation of the crack was known. In both cases the striations were parallel to the direction of propagation. To confirm this, we fractured a few zinc crystals in which the crack was initiated at a known point by a narrow groove etched in the crystals. Here the striations ran parallel to the known direction of propagation of the cleavage. This interpretation fits the appearance of the cleavage faces most naturally, and it is not easy to envisage any other interpretation.

B. *Twins*

In general, the amount of twinning observed in the cleavage faces decreased with increasing χ, being prolific in crystals when $\chi \sim 20^\circ$ and rare when $\chi > 50^\circ$. This dependance of the number of twins with χ requires further investigation, particularly in view of the BB point that the applied stress is not in the correct direction to cause the growth of twins formed by the moving crack in crystals with $\chi \gtrsim 40^\circ$. At the moment, the results suggest that twins are only seen on crystals with high χ if there is some other possible disturbing feature such as a particularly high jump from one cleavage plane to another.

In all the crystals, the vast majority of the twin traces were at 60° *to the active slip direction* (i.e. to the preferred direction of propagation of the cleavage). This is in excellent agreement with BB. Of these two twin traces, the most prominent was that most nearly parallel to the minor axis of the elliptical cleavage surface, i.e. the trace of the twin plane for which the applied macroscopic twinning stress was largest.

Twin traces in the third possible direction, parallel to the active slip direction, were only seen in a few crystals (fig. 2 (*a*) shows one of the largest seen). A close examination showed that in each case the striation in the region of the rare twin were not parallel to the active slip direction. In no case was a twin trace found parallel to the striations. Thus these rare twins do not constitute an exception to the BB theory, the details of which are calculated assuming a crack propagation direction parallel to that of the active slip, and are sensitive to errors in this assumption. It should be remembered that the macroscopic applied stress is not of the right orientation to cause this third twin trace in the majority of crystals examined (BB). Only in two crystals, each with $\chi \simeq 18°$ and $\lambda \simeq 31°$, was the applied stress such as to produce twin traces parallel to the active slip direction and in both these no such trace was found, while there were many twins giving traces at 60°.

In no case in all the crystals examined were twins found in both faces in matching positions. In some cases twins in one face corresponded to well-defined lines in the opposite face, e.g. compare the upper half of fig. 1 (*a*) and (*b*), which were at first taken to be matching twins. In these cases the lines were examined particularly carefully by using polarized light, by etching the original cylindrical surface for signs of twins running into the metal from the line on the cleavage face, and by examining the topography of the surface. It was clear that the lines were steps in the surface. It is interesting to note that they may, in fact, represent true prismatic (or pyramidal) cleavage in zinc. It should also be noted that in the face containing the matching twin there must also be a step to fit the step on the untwinned face.

In the figures, the most obvious difference between the twins and the steps is that the accommodation kinks associated with the twins are usually visible, while the steps have no associated kinks. The steps matched the twins accurately in a lateral direction, but were usually not as long. These matching twins and steps were only observed in crystals with $\chi < 40°$. In all crystals, twins could be found in one face without any corresponding mark in the second, e.g. compare the lower part of fig. 1 (*a*) and (*b*). The coincidence of steps and twins is anticipated in the BB theory. More detailed evidence of topography of the surface near these matching twins and steps is required.

In all crystals, the twins were at one side of the source of the fracture, that being the side on which the cleavage plane makes an acute angle with the crystal surface (see fig. 3). Very few exceptions to this principle were found, and this is precisely the rule deduced in the BB theory.

C. *Kinks*

Apart from the accommodation kinks, well marked kink bands could be seen in many of the cleavage faces. Figure 2 (*b*) shows a well-developed series. *These kink bands were confined to the opposite side of the source to that occupied by the twins* (see fig. 3) and were normal to the active slip direction. There were never any matching marks on the opposite face. Kink bands were usually confined to cleavage faces in crystals where $\chi < 30°$.

Fig. 3

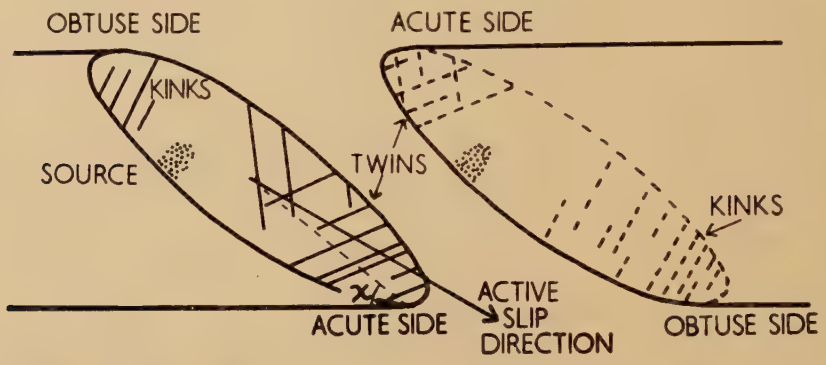

Diagram illustrating the distribution of twins and kinks relative to the position of the source of the cleavage crack in a zinc single crystal.

The observations on kink bands are not in accordance with BB, whose results indicate that kinks should form with equal facility on both sides of the source and in both faces.

D. *Non-Crystallographic Markings*

These vary in definition from the rather faint striations discussed in A to the heavily marked steps discussed in B. Two samples are shown in fig. 2. They usually run in the same general direction as the striations, although they wander more and are rarely strictly parallel to the striations. They are cliffs connecting cleavage on neighbouring planes and, as would be expected, they correspond exactly on the opposite faces.

The only feature noted which appeared to have any significance was that matching steps and twins were associated with large changes in direction in the marks, or even their complete stoppage. Twins with no matching step, however, had little effect on the direction or intensity of the markings. In fig. 2 (*a*) the twin to the right of the indicated ' non-crystallographic markings ' has not affected the markings, while the twin to the left has. In this connection, the regular deviations caused by matching twins and steps on the striations should be noted, e.g. see fig. 1.

Although in this paper a distinction is made between ' striations ' and ' non-crystallographic markings ', it might be that there is no fundamental difference between them. Here, again, more experimental work is required to discover their precise significance.

§ 3. Discussion

The main reason for publishing this brief paper now was to demonstrate how closely the experimental results and the theory of Bilby and Bullough (1954) are in agreement.

Their most important results are that the moving crack can initiate twins giving traces at 60° to the direction of propagation and that the distribution of twins over the cleavage faces takes a particular form, viz. on both sides of the cleavage they are confined to the part of the face between the source and the acute intersection of the face with the cylindrical surface of the crystal (see fig. 3). If the applied stress caused the formation of twins directly they would not be confined to particular regions of the face and, in a few crystals (e.g. $\chi \simeq 18°$, $\lambda \simeq 30°$), twin traces might be found parallel to the direction of active slip. The experimental results confirm the BB theory completely in this respect. Concerning the variation of the amount of twinning with varying χ, BB point out that while the moving crack can initiate twins whatever the value of χ, it is likely that they will only grow to appreciable size if the applied stress is of the correct orientation. This is so only for crystals in which $\chi \lesssim 40°$. In our experimental work, although twins were much more common in crystals with low χ values, they were observed in crystals for which $\chi \gtrsim 40°$. There is thus some discrepancy between the theory and the observations, but a much more detailed experimental investigation will be necessary on the variation of the twinning with χ to establish all the important features of the relationship.

With regard to the kinks, BB predict that kinks should appear at all points in the cleavage face, and that most kinks should appear on crystals for which $\chi \simeq 45°$. Experimentally the results are in complete contradiction to this, the kinks are observed to appear largely in the regions where twins are absent and also most kinks are found in crystals of low χ. BB point out, however, that if it is easier to cause twinning than kinking, then in regions where the stresses are of the correct sign to initiate twinning this will occur preferentially. Thus kinking would be largely confined to those regions in which twinning was not possible, thus resolving one discrepancy. On the other hand, this postulate does not explain the difference between the theoretical and observed χ values at which kinking is most probable, and it is clear that some further refinement of the theory is necessary.

§ 4. Conclusions

In zinc fractured at −196°C, the cleavage crack tends to propagate in a direction parallel to the active slip direction. Both twins and kink bands appear on the cleavage faces, and neither can be matched with

similar twins and kinks in the opposite face, although some twins are matched by steps. There is a very definite relation between the positions of the twins and kinks and the direction of propagation of the crack (see fig. 3). The distribution and orientation of the twin traces agree completely with the theory of Bilby and Bullough (1954), but there is no agreement in the case of the kinks.

Acknowledgments

It is a great pleasure to acknowledge the frequent discussions we have had with Dr. B. A. Bilby and Mr. R. Bullough, and also the helpful comments of Dr. A. R. Entwisle. One of us, (A. D.), wishes to thank the British Council for a scholarship held during the course of this work.

References

Bilby, B. A., and Bullough, R., 1954, *Phil. Mag.*, **45,** 631.
Bruckner, W. H., 1951, *Welding J.*, **30,** 459 s.
Deruyttere, A., and Greenough, G. B., 1953, *Nature, Lond.*, **172,** 170.
Pratt, P. L., 1953, *Acta Metallurgica*, **1,** 692.
Pratt, P. L., and Pugh, S. F., 1952, *J. Inst. Metals*, **80,** 653.
Tipper, C. F., and Hall, E. O., 1953, *J. Iron Steel Inst.*, **175,** 9.
Tipper, C. F., and Sullivan, A. M., 1951, *Trans. Amer. Soc. Metals*, **43,** 906.

LXXI. *The Formation of Twins by a Moving Crack*

By B. A. Bilby and R. Bullough
Department of Metallurgy, University of Sheffield*

[Received March 15, 1954]

Summary

Expressions are derived for the elastic stresses round a long straight crack of constant form moving in an isotropic elastic medium under a general state of applied stress. These are used to examine the mechanical twinning to be expected on the cleavage surfaces of single crystals, on the assumption that this twinning is initiated by the high local stresses near the propagating fracture crack. It is assumed that the twin formation is controlled by the value of the local shear stress on the twinning plane resolved in the twinning direction. The theory is applied in detail to the twinning and certain other features of the deformation associated with the cleavage fracture of zinc single crystals. It provides a consistent explanation of some experimental observations reported in an accompanying paper by Deruyttere and Greenough. Applications of the analysis to other materials, and to other inhomogeneities causing high local stresses are also discussed.

§ 1. Introduction

When a metal which forms mechanical twins is broken, such twins are frequently to be found on or near the surface of fracture. There has been considerable discussion of the role played by these twins in the fracture process, and particularly about whether they are all formed during the fracture, or whether some form before fracture starts and help to initiate it. The present paper is one of a series on the role of inhomogeneities of stress in initiating mechanical twinning (Bilby and Entwisle 1954), and in it we examine the nature of the twinning to be expected if it is initiated by the high local stresses set up near the propagating fracture crack. It is assumed that twin formation is determined by the value of the local shear stress on the twinning plane resolved in the twinning direction. In § 2 expressions are derived for the stresses round a crack moving under a general state of applied stress P_{ij}. The results are applied to the cleavage fracture of zinc in § 3. A preliminary comparison with experiment of the detailed predictions there made is given in an accompanying paper by Deruyttere and Greenough (1954),† who have made a recent study of cleavage fracture in this metal. Some limitations of the analysis and further applications are discussed in § 4.

* Communicated by the Authors.
† Referred to as D.G. in the sequel.

§ 2. The Stress Field of a Moving Crack

Let x, y, z be a Cartesian coordinate system and let P_{ij} be the applied stress tensor. We calculate the stresses round a long straight crack lying along the z axis and moving with uniform velocity c in the x direction (fig. 1). Our primary interest is in the distribution of the stresses near the head of the crack. As will appear, this is not affected by the length of the crack in the x direction; accordingly, the crack is assumed to remain of *constant* length $2a$ along the x axis. The shape of the crack in the xy plane is taken to be a straight slit, so that the only internal surfaces free from traction are normal to the y axis. If the constant applied stress P_{ij} is removed, the boundary conditions on the stresses p_{ij} are at ∞,

$$p_{ij}=0, \quad \ldots \quad (1)$$

and, when $-a \leqslant x' \leqslant +a$, where $x'=x-ct$,

$$p_{xy}=-P_{xy}=-S_0, \quad \ldots \quad (2)$$

$$p_{yy}=-P_{yy}=-T_0, \quad \ldots \quad (3)$$

$$p_{yz}=-P_{yz}=-S_1. \quad \ldots \quad (4)$$

There are thus no magnified stresses due to the other components P_{xx} and P_{xz} of the applied stress tensor. It is convenient to consider separately the three problems in which $-S_0$, $-T_0$ and $-S_1$ each act alone and then superpose the results. Since all quantities are independent of z, the first two are problems in plane strain and the third is one in anti-plane strain. By considering the symmetry each problem can be reduced to one in the half space $y>0$ defined by boundary conditions on $y=0$. These are:

Problem I

$$p_{xy}=-S_0, \quad -a \leqslant x' \leqslant +a \quad \ldots \quad (5)$$

$$p_{yy}=0, \quad \text{all } x' \quad \ldots \quad (6)$$

$$u=0, \quad |x'|>a \quad \ldots \quad (7)$$

Problem II

$$p_{yy}=-T_0, \quad -a \leqslant x' \leqslant +a \quad \ldots \quad (8)$$

$$p_{xy}=0, \quad \text{all } x' \quad \ldots \quad (9)$$

$$v=0, \quad |x'|>a \quad \ldots \quad (10)$$

Problem III

$$p_{yz}=-S_1, \quad -a \leqslant x' \leqslant +a \quad \ldots \quad (11)$$

$$w=0, \quad |x'|>a. \quad \ldots \quad (12)$$

Here u, v, w are the displacements in the x, y, z directions respectively. Problem II has been solved by Yoffe (1951); we treat the other two in a similar way, except that we obtain immediately from known results the solutions of the dual integral equations which appear (eqns. (17) and (18) below).

For Problem I we choose the following displacements from the general expressions for Rayleigh waves given by Love (1934):

$$u_1(x', y)=A\left[\exp(-\gamma sy)-\left(\frac{1+\beta^2}{2}\right)\exp(-\beta sy)\right]\cos sx', \quad (13)$$

$$v_1(x', y)=A\left[-\gamma\exp(-\gamma sy)+\left(\frac{1+\beta^2}{2\beta}\right)\exp(-\beta sy)\right]\sin sx', \quad (14)$$

where A and s are constants and $\gamma^2=1-c^2/{c_1}^2$, $\beta^2=1-c^2/{c_2}^2$; $c_1=\{(\lambda+2\mu)/\rho\}^{1/2}$ and $c_2=(\mu/\rho)^{1/2}$ are the velocities of dilatational and shear waves in an isotropic elastic medium of density ρ and elastic constants λ, μ. These displacements satisfy the condition (6) and have the required symmetry. General displacements may now be written down as Fourier integrals

$$u(x', y)=\int_0^\infty A(s)(u_1/A)\,ds, \quad (15)$$

$$v(x', y)=\int_0^\infty A(s)(v_1/A)\,ds. \quad (16)$$

Calculating the stress p_{xy} and using (5) and (7) we obtain dual integral equations for $A(s)$

$$\int_0^\infty A(s)\cos sx'\,ds=0, \qquad x'>a \quad (17)$$

$$\int_0^\infty sA(s)\cos sx'\,ds=-\frac{S_0}{H}, \qquad 0\leqslant x'\leqslant a \quad (18)$$

where $H=\mu[-2\gamma+(1+\beta^2)^2/2\beta]$. Equations of this form were obtained by Yoffe, when discussing Problem II, but were not solved directly. They may be transformed by the substitutions $s=\xi/a$, $x'=\eta a$, $A(\xi/a)=\xi^{-1/2}f(\xi)$ and the result

$$\cos(\xi\eta)=(\pi\xi\eta/2)^{1/2}J_{-1/2}(\xi\eta),$$

into a standard form (Titchmarsh 1937, see also Tranter 1952). The solution is:

$$A(s)=-\frac{aS_0J_1(sa)}{Hs}. \quad (19)$$

We can now evaluate the displacements and stresses by (15) and (16). After some reduction and addition of the constant stress $P_{xy}=+S_0$, we obtain for the crack moving under the stress S_0 alone, the stresses

$$Hp_{xx}/S_0=\gamma^2m_1\mathscr{I}f(z_1)+\mu\chi\mathscr{I}f(z_2), \quad (20)$$

$$Hp_{yy}/S_0=\gamma^2m_2\mathscr{I}f(z_1)-\mu\chi\mathscr{I}f(z_2), \quad (21)$$

$$Hp_{xy}/S_0=-2\mu\gamma\mathscr{R}f(z_1)+\left(\frac{\mu\chi^2}{2\beta}\right)\mathscr{R}f(z_2), \quad (22)$$

where

$$f(z)=z/(z^2-a^2)^{1/2}, \quad . \quad . \quad . \quad . \quad . \quad . \quad . \quad . \quad (23)$$

$$\left.\begin{aligned} z_1&=x'+i\gamma y, & m_1&=\lambda-(\lambda+2\mu)/\gamma^2,\\ z_2&=x'+i\beta y, & m_2&=(\lambda+2\mu)-\lambda/\gamma^2,\\ & \chi=1+\beta^2, \end{aligned}\right\} \quad . \quad . \quad . \quad . \quad (24)$$

and $\mathscr{R}f(z)$ and $\mathscr{I}f(z)$ denote the real and imaginary parts of $f(z)$ respectively.

For Problem III we choose the general displacement

$$w(x', y)=\int_0^\infty B(s)\exp(-\beta sy)\cos sx'\,ds. \quad . \quad . \quad . \quad (25)$$

Evaluating the stresses and inserting the boundary conditions (11) and (12), dual integral equations for $B(s)$ are obtained. These are of the same form as (17) and (18), but with $-S_0/H$ replaced by $S_1/\mu\beta$. On superposing the constant stress $P_{yz}=+S_1$, the expressions for the stresses round a crack moving under S_1 alone are

$$p_{zy}/S_1=\mathscr{R}f(z_2), \quad . \quad . \quad . \quad . \quad . \quad . \quad . \quad (26)$$

$$\beta p_{zx}/S_1=\mathscr{I}f(z_2), \quad . \quad . \quad . \quad . \quad . \quad . \quad . \quad (27)$$

where z_2 and $f(z)$ are defined by (23) and (24). For convenience, the solutions obtained by Yoffe of the crack moving under $P_{yy}=T_0$ alone are given below in a similar notation :

$$Np_{xy}/T_0=2\mu[-\mathscr{I}f(z_1)+\mathscr{I}f(z_2)], \quad . \quad . \quad . \quad . \quad . \quad . \quad . \quad (28)$$

$$Np_{yy}/T_0=-\gamma m_2\mathscr{R}f(z_1)+\left(\frac{4\mu\beta}{\chi}\right)\mathscr{R}f(z_2), \quad . \quad . \quad . \quad . \quad . \quad (29)$$

$$Np_{xx}/T_0=\gamma m_1\mathscr{R}[1-f(z_1)]+\left(\frac{4\mu\beta}{\chi}\right)\mathscr{R}[1-f(z_2)], \quad . \quad . \quad (30)$$

where f and χ are given by (23) and (24) and

$$N=-\gamma m_2+\frac{4\mu\beta}{\chi}. \quad . \quad . \quad . \quad . \quad . \quad . \quad . \quad . \quad (31)$$

The complete solution for the crack moving under the general stress tensor P_{ij} is given by the sum of (20)–(22), (26)–(27) and (28)–(30) together with the components P_{xz} and P_{xx} of the applied stress. Solutions for the corresponding static problems can be obtained, for example, by the method outlined for Problem I in the Appendix and it is readily verified that, when $c\to 0$, the stresses in the dynamic problems reduce to these.

Approximate expressions may be obtained for the stresses in the neighbourhood of $x'=a$, $y=0$ by using the coordinates (r, θ) where $x'-a=r\cos\theta$, $y=r\sin\theta$ and calculating the stresses as a function of θ for small constant r. Using a notation similar to that of Yoffe (1951), let

$$z_0=a+r\exp(i\theta)=a[1+k_0\exp(i\theta_0)],$$

$$z_1=a[1+k_1\exp(i\theta_1)], \qquad z_2=a[1+k_2\exp(i\theta_2)],$$

where

$$\left.\begin{aligned} k_1&=k_0[1-(c^2/c_1^2)\sin^2\theta]^{1/2},\\ k_2&=k_0[1-(c^2/c_2^2)\sin^2\theta]^{1/2},\\ \tan\theta_1&=\gamma\tan\theta, \qquad \tan\theta_2=\beta\tan\theta. \end{aligned}\right\} \quad . \; . \; . \; . \; . \; . \quad (32)$$

Then, when $(r/a)\ll 1$ we have

$$f(z_n)\simeq g(\theta_n, k_n),$$

$$g(\theta_n, k_n)=\frac{\exp(-i\theta_n/2)}{\sqrt{(2k_n)}}=R_n+iI_n, \quad . \; . \; . \; . \; . \quad (33)$$

where $n=0, 1, 2$. The approximate expressions for the stresses are now obtained by substituting R_n for $\mathscr{R}f(z_n)$ and I_n for $\mathscr{I}f(z_n)$ in (20)–(22), (26)–(29). In (30) we also use $R_1, R_2 \gg 1$. For $c=0$, the approximations in this region are

$$\left.\begin{aligned} p_{xx}&=T_0(R_0-A_0B_0)+S_0(2I_0-A_0C_0),\\ p_{yy}&=T_0(R_0+A_0B_0)+S_0(A_0C_0),\\ p_{xy}&=T_0(A_0C_0)+S_0(R_0-A_0B_0),\\ p_{yz}&=S_1(R_0),\\ p_{zx}&=S_1(I_0), \end{aligned}\right\} \quad . \; . \; . \quad (34)$$

where $A_0=(\sin\theta_0)/2$ and $C_0+iB_0=\exp(3i\theta_0/2)/\sqrt{(2k_0)}$.

The half length a of the crack, appears in all these approximate stresses only in the external factor $1/\sqrt{(2k_0)}$. Thus it affects the absolute magnitude of the stresses, but not their relative magnitude or distribution. Our use of a moving crack of constant form is therefore justifiable (Yoffe 1951). To represent in this model the stresses near the ends of a crack expanding from the origin along the $+x$ and $-x$ directions, however, we require not only the stresses near $x'=+a$, $y=0$ for a crack moving with $c=+c_0$, but also those near $x'=-a$, $y=0$ for a crack moving with $c=-c_0$. The latter are readily found from the former by considering the symmetry. Let $z_0'=-a-r\exp(i\phi)$, $\phi=\pi-\theta$. Then for the crack moving under T_0 and S_1 the stresses round z_0 with $c=+c_0$ are the same as those round z_0' with $c=-c_0$ when $\theta=+\phi$, while for the crack moving under S_0, this is true when $\theta=-\phi$.

§ 3. Twins Appearing in Cleaved Zinc Crystals

We now use the results of § 2 to discuss the fracture of zinc single crystals broken under simple tension. When χ_1, the angle (at fracture) between the axis of tension and the (0001) plane, is greater than about 12° the fracture takes place by simple cleavage on this plane (D.G.).

Our results for $(r/a)\ll 1$ derived for a long straight crack will approximate locally to the stresses near the edge of a curved crack spreading normally to its line, provided the curvature is not too large, and the appropriate

local direction of propagation is taken. This direction of propagation is suggested by examination of striations on the cleavage surfaces. These usually radiate from some area on the surfaces, and it is inferred that fracture begins here, and that the striations are normal to the spreading edge of the crack. Now it has been found (D.G.) that when χ_1 is not too large, these striations are often straight and parallel to the active slip direction over a large area of the cleavage surface. Accordingly we examine first the stresses round a long straight crack moving in the basal plane normal to itself in that $\langle 11\bar{2}0\rangle$ direction making (at fracture) the least angle λ_1, with the applied tension axis. Then the x and y axes of § 2 lie along the active slip direction and normal to the basal plane respectively. Of course, to apply the analysis to any region where the crack is assumed to move in a different direction, a different choice of x axis would be necessary. We shall later examine the twinning predicted if a long straight crack moves in a direction perpendicular to the active slip direction and find that it does not agree with that observed over most of the surfaces.

In the coordinate system x, y, z the direction cosines of the axis of applied tension T are $(\cos\lambda_1,\ \sin\chi_1,\ \delta)$ where $\delta=(\sin^2\lambda_1-\sin^2\chi_1)^{1/2}$. Thus

$$P_{ij}=T\begin{pmatrix}\cos^2\lambda_1, & \sin\chi_1\cos\lambda_1, & \delta\cos\lambda_1\\ \sin\chi_1\cos\lambda_1, & \sin^2\chi_1, & \delta\sin\chi_1\\ \delta\cos\lambda_1, & \delta\sin\chi_1, & \delta^2\end{pmatrix} \quad . \quad . \quad (35)$$

In practice the angles χ_1 and λ_1 are very nearly equal, and we may set $\chi_1=\lambda_1$ so that $\delta=0$. We then have the crack moving in the x direction with

$$\left.\begin{aligned} T_0&=T\sin^2\chi_1,\\ S_0&=T\sin\chi_1\cos\chi_1.\end{aligned}\right\} \quad . \quad . \quad . \quad . \quad . \quad . \quad . \quad (36)$$

P_{xx} does not contribute to the magnified stresses. Let new axes x', y', z' be chosen for each twinning plane so that z' is the normal to the twinning plane and x' is the twinning direction. Then the shear stress on the twinning plane resolved in the twinning direction, p'_{xz}, is of the form

$$p'_{xz}=f_0p_{xx}+g_0p_{yy}+h_0p_{xy}. \quad . \quad . \quad . \quad . \quad . \quad . \quad . \quad (37)$$

Expressions for f_0, g_0 and h_0 for the different twinning planes are given by Bilby and Entwisle (1954). In their work x' and z' were so chosen that if the stress p'_{xz} is positive it assists twinning when the axial ratio is greater than $\sqrt{3}$. To identify the twinning planes, the conventional axes of reference for a hexagonal crystal X_0, Y_0, U_0, Z_0 are taken so that Y_0 coincides with x, and Z_0 with y. It is convenient to denote the complementary pairs of twinning planes by TX, TX', TY, TY' and TU, TU' to indicate the basal slip direction which they contain (here we have omitted the zero subscript, since there is no danger of confusion with other axes). Thus $TY(\bar{1}012)$ and $TY'(10\bar{1}2)$ are those containing the active slip direction.

Using the approximations of § 2 the values of p'_{xz} in the neighbourhood of the ends P and N of the crack moving as shown in fig. 1 were calculated

for various velocities of propagation. The results are shown in figs. 2–5 where p'_{xz} is shown as a function of χ_1 and θ, $0 \leqslant \chi_1 \leqslant \pi/2$, $-\pi \leqslant \theta \leqslant +\pi$ by contour maps. Values for the N region, $-\pi \leqslant \phi \leqslant +\pi$ and for other

Fig. 1

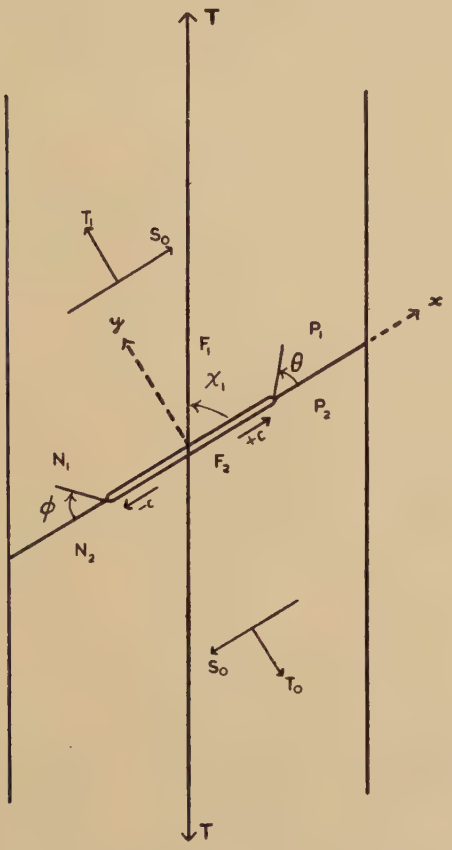

Cross section of a zinc single crystal under axial tension T. A crack has nucleated on the cleavage plane (0001) and is spreading along this plane in the $+x$ and $-x$ directions with velocity $+c$ and $-c$ respectively. Twinning is expected in the regions P_2 and N_1 of the cleavage faces F_2 and F_1 respectively.

χ_1 ranges follow from the symmetry. None of the qualitative conclusions given below was altered by varying Poisson's Ratio from $\nu=0$ to $\nu=0{\cdot}4$ and the stresses are therefore shown for $\lambda=\mu$ or $\nu=0{\cdot}25$. Since the planes TX' and TU are nearly perpendicular to TX and TU' respectively, we always have $p'_{xz}(TX) \simeq p'_{xz}(TX')$ and $p'_{xz}(TU) \simeq p'_{xz}(TU')$. Moreover, when

$$\chi_1=\lambda_1, \quad p'_{xz}(TX)=p'_{xz}(TU'), \quad p'_{xz}(TX')=p'_{xz}(TU)$$

and

$$p'_{xz}(TY)=p'_{xz}(TY').$$

Accordingly, we show only $p'_{xz}(TX, TU')$ for velocities $c=0$ (fig. 2), $c=0{\cdot}7c_2$ (fig. 3) and $c=0{\cdot}89c_2$ (fig. 4). The shape of the contours of $p'_{xz}(TX, TU')$ for $c=0{\cdot}5c_2$ is similar to that for $c=0$, except that the positive tongue at $\theta\sim-30°$ extends up to $\chi_1=90°$, $-5°<\theta<+10°$ first crossing $\theta=0$ at $\chi_1\sim65°$. There is also little difference in the magnitudes of the stresses at these two velocities. The contours of $p'_{xz}(TY, TY')$ are of the same general shape as those of $p'_{xz}(TX, TU')$ *at the same velocity*, but the TY, TY' stresses are much smaller. Figure 5 shows $p'_{xz}(TY, TY')$ for $c=0{\cdot}5c_2$.

Fig. 2

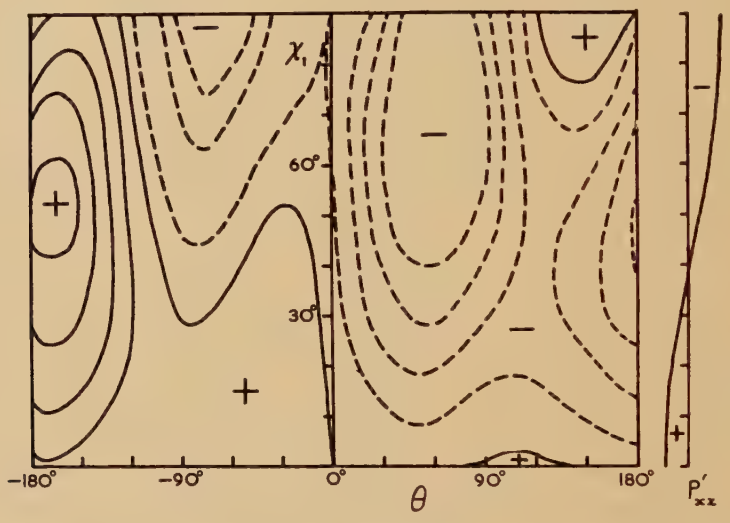

A contour map of the stress p'_{xz} on the twinning planes TX, TU' due to the magnified stresses near the tip of a stationary crack. The contours shown are for equal intervals of 2·5 in units of $Tm^2/\sqrt{(2k_0)}$ where $m^2=1/[4(3+s^2)]$, and s is the axial ratio. The positive and zero contours are shown by full lines and the negative contours by broken lines and this convention is also adopted in figs. 3–6. On the right is a plot showing the variation of the macroscopic stress P'_{xz} with χ_1.

The large stresses near the ends of the moving crack may be expected to produce not only twinning, but also other forms of plastic deformation. Thus we show in fig. 6 the stress p_{xy} for $c=0{\cdot}5c_2$; this stress tends to cause slip (which would not be readily visible) and also the formation of first order kink bands (Z-bands) lying perpendicular to the slip plane and slip direction. (These Z-bands are to be distinguished from accommodation kinks associated with twins.) Large numbers of Z-bands have been observed on the cleavage surfaces (D.G.).

Since the stresses round the crack fall off rapidly, while the twinning (and presumably the kinking also) extends to a large distance from the fracture surface, it is clear that the primary role of the crack stresses is

Fig. 3

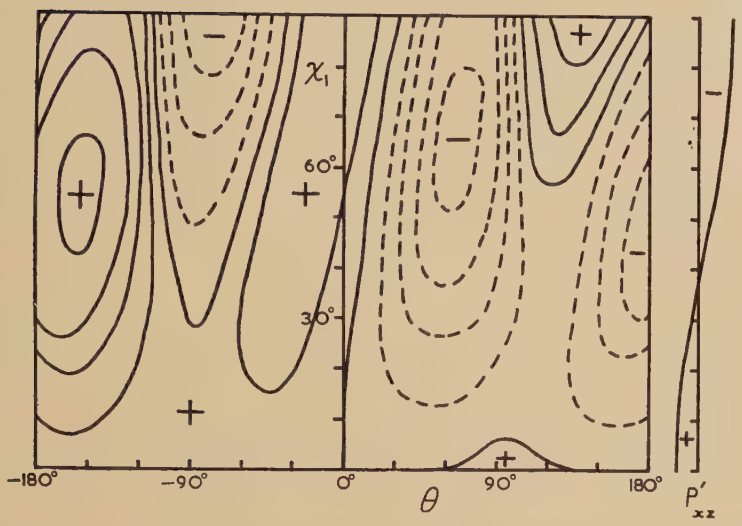

A contour map of the stress p'_{xz} on the twinning planes TX, TU' due to the magnified stresses near the tip of a crack propagating with velocity $c=0{\cdot}7c_2$. The contours shown are for equal intervals of 4·0 in units of $Tm^2/\sqrt{(2k_0)}$: on the right is a plot showing the variation of the macroscopic stress P'_{xz} with χ_1.

Fig. 4

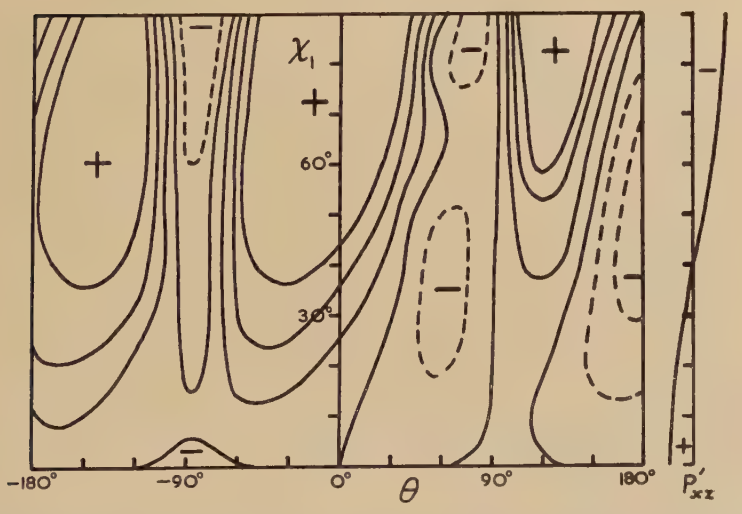

The stress p'_{xz} (TX, TU') for a velocity of propagation $c=0{\cdot}89c_2$. The contours shown are for equal intervals of 20·0 in units of $Tm^2/\sqrt{(2k_0)}$.

Fig. 5

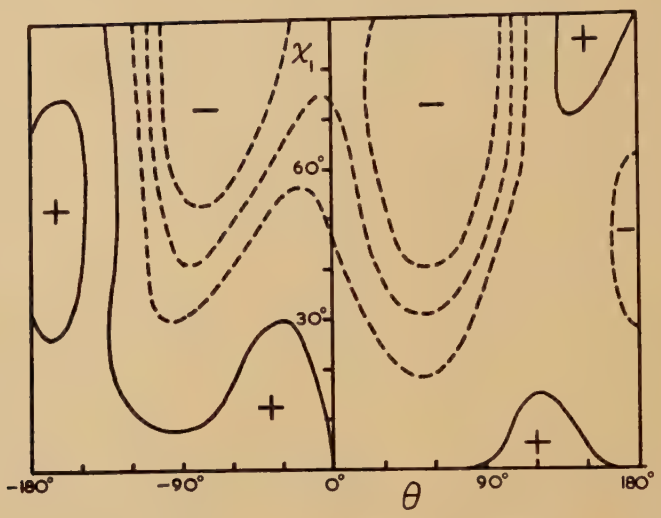

A contour map of the stress p'_{xz} on the twinning planes TY, TY' due to the magnified stresses near the tip of a crack propagating with velocity $c=0{\cdot}5c_2$. The contours shown are for equal intervals of 2·0 in units of $Tm^2/\sqrt{(2k_0)}$. For the TY, TY' planes P'_{xz} is always negative when $\chi_1=\lambda_1$.

Fig. 6

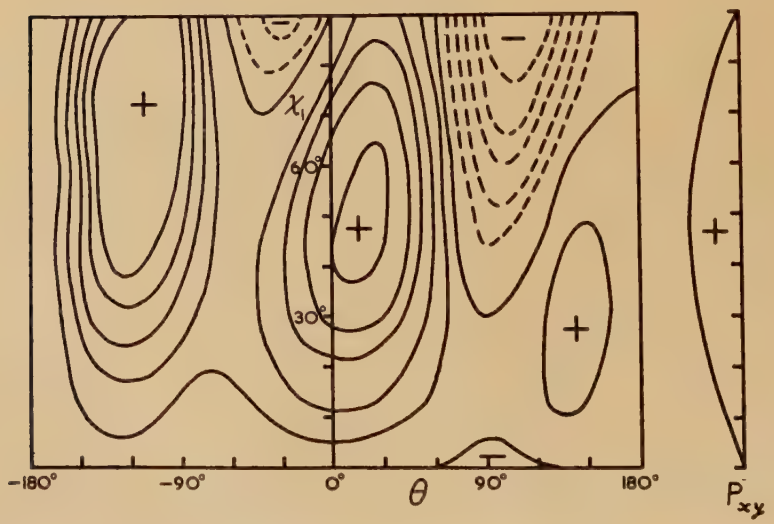

A contour map of the magnified shear stress p_{xy} near the tip of a crack propagating with velocity $c=0{\cdot}5c_2$. The contours shown are for equal intervals of 1·0 in units of $Tm^2/\sqrt{(2k_0)}$: on the right is a plot showing the variation of the stress P_{xy} with χ_1.

to initiate the twins and Z-bands. A brief discussion of this initiation in the static case has already been given (Frank and Stroh 1952); the twins and Z-bands present similar problems, and in the following, to avoid repetition, we refer to the twins only. The stress field of a twin and of a crack under tangential stress are of the same general kind. Thus if a crack is long enough to enable a small twin to form near its tip, the twin can extend. We may say that the crack extends temporarily as a twin. When the twin reaches a critical length, it can grow under the macroscopic stress alone if this is favourable. This critical length has been estimated for a Z-band (first order kink band) to be about 10^{-3} cm under a stress of $10^{-3}\mu$ (Frank and Stroh 1952). In discussing the appearance of the much larger twins and Z-bands visible on the fracture surfaces it is thus pertinent to consider the appropriate macroscopic shear stress as well as the magnified stresses due to the crack. Accordingly these macroscopic stresses are also shown (in arbitrary units) as a function of χ_1 (assuming $\chi_1=\lambda_1$) in small diagrams to the right of the contour maps in figs. 2–6. The macroscopic stresses are denoted by capital letters, thus $P'_{xz}(TX, TU')$.

We can now make certain predictions about the twinning to be expected on the cleaved surfaces in the regions P_1, N_1 and P_2, N_2 on the assumption that this is governed by the magnitude and sign of p'_{xz}. The regions P_1 and N_2 are distinguishable from P_2 and N_1; the former are those lying between the area where the crack was initiated and that part of the edge of the cleavage face where the latter makes an obtuse angle with a generator of the broken portion of the cylindrical crystal. For P_2 and N_1 the corresponding angle is acute.

(1) As we have remarked above, the TY, TY' stresses are much smaller than those on TX, TU'. In fact there are a few regions where $p'_{xz}(TY, TY')$ is positive and greater than $p'_{xz}(TX, TU')$ but it is always small compared with other $p'_{xz}(TX, TU')$ values at the same χ_1. Twins on TY, TY' should therefore be much rarer than those on TX, TU' and TX', TU. Consideration of $P'_{xz}(TY, TY')$ merely reinforces this conclusion, since, as this is always negative for $\chi_1=\lambda_1$ it will actually oppose the growth of any TY, TY' twins nucleated by the crack.

(2) For $c=0$ and $c=0{\cdot}5c_2$, $p'_{xz}(TX, TU')$ is always negative for positive θ except in small regions at $\chi_1 \sim 0°$ and $\chi_1 \sim 90°$ when it takes small positive values. This asymmetry of sign persists at $c=0{\cdot}7c_2$, although there are now small positive stresses ahead of the crack ($\theta \sim 0°$) for $\chi_1>15°$ (fig. 3). At $c=0{\cdot}89c_2$, although asymmetry of magnitude persists, especially for $\chi_1<30°$, there are large positive twinning stresses for $\theta>0°$ and $\theta<0°$ for all χ_1, and when $\chi_1>20°$, also just ahead of the crack ($\theta \sim 0°$). The complete absence of matched twins, and the marked asymmetry of twinning observed (in agreement with (3) below) suggest that the positive twinning stresses are small for $\theta \sim 0°$, and very different in magnitude for $\theta>0°$ and $\theta<0°$. We infer that the crack velocity is probably less than $0{\cdot}89c_2$. The predictions which follow are

however, not very sensitive to crack velocity, although for $c \leqslant 0{\cdot}7c_2$, they are suggested by the asymmetry of sign of the appropriate stresses.

(3) Twinning is to be expected in the regions P_2 and N_1 but not in P_1 and N_2, since here p'_{xz} is usually not even of the right sign. Note that this conclusion would be exactly reversed for a metal such as magnesium in which $(c/a) < \sqrt{3}$. We cannot of course distinguish these regions by considering the macroscopic stress alone.

(4) The largest twinning stresses due to the crack occur when χ_1 is about 45°, while the macroscopic stress $P'_{xz}(TX, TU')$ changes sign at $\chi_1 = 38° 57'$, and takes increasing positive values when χ_1 is less than this. Thus twins nucleated above $\chi_1 \sim 40°$ will have their growth opposed by the applied stress. Accordingly we may expect a general increase in the number and size of twins as χ_1 falls below 40°. The formation of twins which appear when $\chi_1 > 43°$ must be due to the crack stresses and not to the macroscopic stresses which oppose their growth.

The above predictions about the distribution of twinning are in general agreement with the experimental observations (D.G.). The confirmation of (3) in particular, is strong evidence that the twinning is indeed controlled by the magnified stresses near the crack. A further point of interest is that the experimental observations (D.G.) suggest that the twins form, or at least break through the surfaces, after the latter have parted. It may then be significant that the largest twinning stresses occur in the region behind the head of the crack.

(5) The macroscopic stress for Z-band formation,

$$P_{xy} = S_0 = T \sin \chi_1 \cos \chi_1,$$

is always positive (fig. 6) when $0 \leqslant \chi_1 \leqslant \pi/2$. Thus, although the kinking movement is the same in either sense, the growth of Z-bands with a positive shear is favoured, and of those with a negative shear opposed. by the macroscopic stress. From fig. 6, which shows also the contours of the magnified p_{xy} stress at $c = 0{\cdot}5c_2$, therefore, we should expect Z-bands to appear in all four regions P_1, P_2, N_1, N_2. The observation is that such bands appear frequently in regions P_1 and N_2 (where twins are absent) but only very rarely in P_2 and N_1 (D.G.). This suggests that the material deforms by twinning rather than by kinking if the stress system permits. Since P_{xy} and p_{xy} both have their largest values where $\chi_1 \sim 45°$, we might expect the amount of Z-band formation to be greatest in this region, but this however, is not observed (D.G.).

We have also calculated the $p_{\theta\theta}$ stress and the normal stress on the prismatic planes $\{10\bar{1}0\}$ in the regions P and N. The $p_{\theta\theta}$ stress is very large all round the head of the crack for $c = 0{\cdot}89c_2$ and $\chi_1 = 90°$ as shown by Yoffe (1951). For smaller χ_1, however, there is asymmetry of magnitude and sign at all velocities and the largest positive stresses occur for $\theta < 0°$. It follows that the crack should tend to branch in this direction. This conclusion may be readily demonstrated for $c = 0$ (Mott 1953) by pulling a sheet of paper with a slit in it inclined to the axis of tension. In the zinc crystal because of preferred crystallographic

weakness, the branching will probably occur by side-stepping on prismatic planes. The sense of a step due to this cause should thus be up from P_1 towards P_2 on the F_1 surface, and up from N_2 towards N_1 on the F_2 surface. Steps parallel to twin traces have been observed on the fracture surfaces (D.G.), but detailed information about their sense is not yet available. It has been noted, however, that associated with these steps there appears always to be a corresponding twin on the opposite cleavage face. A possible explanation of this phenomenon is that the crack is temporarily arrested (or slowed down) as it side steps, and that this increases the probability of twin formation, since there is little change in the magnitude of the twinning stresses except at the highest velocities.

Finally, we have examined the magnified twinning stresses when the crack is assumed to move in a direction perpendicular to the active slip direction. The stresses on TY, TY' are then usually considerably greater than those on the other twinning planes, so that we should expect that twins on the latter would be much rarer than those on the former. This is contrary to experience over most of the fracture surface, and we thus have some justification for our choice of the active slip direction as the direction of propagation of the crack.

§ 4. Discussion

Although the stresses $p'_{xz}(TX, TU')$ and $p'_{xz}(TX', TU)$ are never very different when $\chi_1=\lambda_1$, the latter is nearly always a little greater when both stresses are positive. Also, as χ_1 decreases from 90° the macroscopic stress $P'_{xz}(TX, TU')$ first becomes positive at $\chi_1=42°\,52'$ and remains always greater than $P'_{xz}(TX, TU')$ as χ_1 decreases to zero. It would be interesting if further study revealed that the TX', TU twins predominated. These twins can be distinguished from TX, TU' by determining their surface tilts, for example, by interferometric methods. Further detailed study of the surface topography of crystals cleaved under *controlled* conditions, to determine the sense of steps and Z-bands, and to identify the twins uniquely, would permit a more searching test of the theory.

In this analysis we have assumed that $\chi_1=\lambda_1$. Actually we have $\cos\lambda_1=\cos\chi_1\cos\eta$ where η is the angle measured in the basal plane from $[\bar{1}2\bar{1}0]$ towards $[01\bar{1}0]$ ($\eta=30°$). Although most of the crystals studied have $\chi_1\sim\lambda_1$ (D.G.) it is legitimate to enquire if this additional variable will make any difference to the general predictions of the theory. The expressions for both the macroscopic and magnified twinning stresses no longer group in pairs, but are different for each twinning plane. We now have $S_0=T\sin\chi_1\cos\chi_1(\cos\eta)$ and the additional stresses p_{yz}, p_{zx} in (26), (27) and (34) due to the term

$$P_{yz}=S_1=T\sin\chi_1\cos\chi_1(\sin\eta)$$

of (35). A detailed analysis of the variation of the p'_{xz} stresses for all the twinning planes as a function of χ_1, η and θ would involve much labour, and does not seem worthwhile using stresses based on isotropic

elastic theory. A rough survey shows, however, that the main conclusion (3) of § 3 about the asymmetry of twinning will not be affected, and that the discrepancy in the χ_1 dependence of the Z-band formation mentioned in § 3 (5) remains. In the region $\theta<0°$ where the twinning stresses are positive, the $p'_{xz}(TX)$ and $p'_{xz}(TX')$ stresses become greater than $p'_{xz}(TU')$ and $p'_{xz}(TU)$ as η increases from zero. There is a similar behaviour of the macroscopic stresses. $P'_{xz}(TX')\gtrsim P'_{xz}(TX)$ are the largest twinning stresses throughout the sector $0<\eta<30°$,* while $P'_{xz}(TU)$ and $P'_{xz}(TU')$ decrease, until at $\eta=30°$, we have

$$P'_{xz}(TU)=P'_{xz}(TY), \quad P'_{xz}(TU')=P'_{xz}(TY').$$

There is now a region at small χ_1 where $P'_{xz}(TY)$ and $P'_{xz}(TY')$ are positive. When η is large we might thus expect a preponderance of TX, TX' twins, while it is no longer true that the growth of any TY, TY' twins is always opposed by the macroscopic stress.

As mentioned above (§ 3) although we have used isotropic elastic theory, the main conclusions are not affected by varying Poisson's ratio between wide limits. We do not expect these conclusions to be modified by allowing for elastic anisotropy, but it is possible that some of the detailed predictions about the χ_1 variation would be changed. This may be the explanation of the discrepancy in § 3 (5).

The analysis does not allow for any change in the loading conditions during the fracture, or for local disturbance of the stresses due to inhomogeneities in the path of the cleavage. A special discussion of the latter would, of course, be necessary for each case observed. The former may lead to asymmetry in the stresses in the following way. If the fracture reaches one surface of the crystal much sooner than the other (as for instance, if it starts near one surface), the boundary conditions are altered, since large bending stresses are applied. At low χ_1 these are asymmetrical and greatest just in those regions P_1 and N_2 where most Z-bands appear. This then may afford one explanation of the asymmetry of Z-band formation without invoking any hypothesis about the relative ease of twinning and kinking. We have, however, assumed that $(r/a)\ll 1$ in our results, and it is therefore possible that even if allowance is made for the stress-free surface, there will be little change in the stresses near the head of the crack. There will be changes in the stresses at larger distances where this approximation is not legitimate, but a detailed discussion must await the solution of the appropriate elastic problem. We have also not considered the possibility of the nucleation of one twin by the stresses due to another. This is probably an important factor in regions where complicated interlacing patterns of twins occur. The present method could be used to analyse such patterns by treating the stress field of the initiating twin as approximately that of a crack under the appropriate shear stress.

The method used in this paper can, of course, be applied to analyse the deformation accompanying cleavage fracture in other materials. This has

* We are indebted to Mr. E. Smith for an analytical proof of this result.

not been done here, since the necessary detailed experimental data are not available. For such an analysis, a knowledge of the orientation of the applied stress system with respect to the cleavage surface is required. Thus, data on single crystals, or, if we can ignore constraining effects, on grains of known orientation, are necessary. Moreover the markings on cleavage surfaces are frequently much more complicated and confused than those occurring with zinc, and this is unfortunately true especially in the important example of α-iron. The analysis has, however, been applied to some results on silicon ferrite crystals (Tipper and Sullivan 1950). It is possible to show that large shear stresses due to the fracture crack exist for the observed Neumann lamellae (and also for some that occur rarely). On these, however, the macroscopic shear stress is also large, and the confused surface markings preclude a detailed discussion like that given for zinc. A satisfactory interpretation must await the production of cleavage surfaces with simpler markings.

Finally, we discuss the application of these results to other inhomogeneities which might initiate mechanical twinning. The stresses round many inhomogeneities are approximately the same as those round a crack under shear. Our treatment of the static crack yields elastic stresses identical with those round a bounded slip band in Leibfried's approximation (Leibfried 1951, Nabarro 1952) and we show in the Appendix how his general integral equation follows from our boundary conditions. Thus we can confirm the conclusion that in a hexagonal metal the stress p'_{xz} on TY and TY' due to a group of edge dislocations with Burgers vectors along the Y axis is less than that on all other twinning planes nearly everywhere (Bilby and Entwisle 1954). In addition to cracks under tangential stress and bounded slip bands, the analysis also applies approximately to plates of deformation twin, martensite product and to kink bands. The possible role of any of these inhomogeneities in generating the others has already been emphasized (Frank and Stroh 1952).

Acknowledgments

We are very pleased to acknowledge the stimulating discussions held during the work with Mr. A. E. Deruyttere and Dr. G. B. Greenough and also with Dr. A. R. Entwisle. Financial support for one of us (R.B.) has been provided by the award of the C. G. Carlisle Scholarship. The work was carried out during the tenure of the Royal Society Sorby Research Fellowship by the other author (B.A.B.).

APPENDIX

By considering the symmetry the problem of the static crack under the shear S_0 can be reduced to one in the half-plane $y>0$, defined by the boundary conditions on $y=0$

$$p_{xy}=0, \quad -a\leqslant x\leqslant +a \quad \ldots\ldots \quad (A.1)$$

$$p_{yy}=0, \quad \text{all } x \quad \ldots\ldots \quad (A.2)$$

$$u=0, \quad |x|>a, \quad \ldots\ldots \quad (A.3)$$

together with the condition that $p_{ij} \to S_0$ when $y \to +\infty$. The problem is then readily solved by removing the external stress and obtaining dual integral equations by generalizing the displacements

$$u = A \exp(-sy)[2(1-\nu)-sy] \cos sx,$$

$$v = A \exp(-sy)[sy+(1-2\nu)] \sin sx.$$

Now the tangential traction required to maintain the displacement $u(x, 0)$ is (Nabarro 1947)

$$p_{xy}(x, 0) = -\frac{\mu}{\pi(1-\nu)} \int_{-\infty}^{+\infty} \frac{1}{x'-x} \frac{du}{dx'} dx'. \quad . \quad . \quad . \quad \text{(A.4)}$$

For the crack under shear, u is antisymmetric in y, so that in terms of the relative displacement ϕ of the two surfaces $y = \pm 0$,

$$p_{xy}(x, 0) = -\frac{\mu}{2\pi(1-\nu)} \int_{-a}^{+a} \frac{1}{x'-x} \frac{d\phi}{dx'} dx', \quad . \quad . \quad . \quad \text{(A.5)}$$

where the limits have been changed in view of (A.3). Hence (A.1) requires that

$$S_0 = \frac{\mu}{2\pi(1-\nu)} \int_{-a}^{+a} \frac{1}{x'-x} \frac{d\phi}{dx'} dx'. \quad . \quad . \quad . \quad . \quad . \quad \text{(A.6)}$$

Since, however, for a linear distribution $D(x)$ of edge dislocations of strength b we have

$$bD(x) = -\frac{d\phi}{dx},$$

eqn. (A.6) is precisely Leibfried's integral equation for a distribution of edge dislocations along $-a \leqslant x \leqslant +a$ under an external shear stress S_0. The required solution $D(x)$ is odd in x (since ϕ is even), and is given by Leibfried :

$$D(x) = -\frac{S_0}{\pi A} \frac{x}{\sqrt{(a^2-x^2)}}.$$

It corresponds to a group of positive edge dislocations, $x > 0$ and a group of negative ones, $x < 0$.

References

Bilby, B. A., and Entwisle, A. R., 1954, *Acta Met.*, **2,** 15.

Deruyttere, A. E., and Greenough, G. B., 1953, *Nature, Lond.*, **172,** 170 ; 1954, *Phil. Mag.*, **45,** 624.

Frank, F. C., 1953, *Bristol Summer School.*

Frank, F. C., and Stroh, A. N., 1952, *Proc. Phys. Soc.* B, **65,** 295.

Leibfried, G., 1951, *Zeit. Phys.*, **130,** 214.

Love, A. E. H., 1934, *The Mathematical Theory of Elasticity* (Cambridge, London).

Mott, N. F., 1953, *Bristol Summer School.*

Nabarro, F. R. N., 1947, *Proc. Phys. Soc.*, **59,** 256 ; 1952, *Advances in Physics*, **1,** 269.

Tipper, C. F., and Sullivan, A. M., 1950, *Trans. Amer. Soc. Metals*, **43,** 906.

Titchmarsh, E. C., 1937, *Introduction to the Theory of Fourier Integrals* (Oxford, London).

Tranter, C. J., 1952, *Phil. Mag.*, **43,** 125.

Yoffe, E. H., 1951, *Phil. Mag.*, **42,** 739.

LXXII. CORRESPONDENCE

The Magnetic Properties of Alloys of Cobalt and Nickel with Palladium and Platinum

By E. P. Wohlfarth
Department of Mathematics, Imperial College, London

[Received April 6, 1954]

In a recent paper Simpson and Tredgold (1954) describe results of measurements of, *inter alia*, the Curie temperatures of four Co–Pt alloys with atomic concentrations between 13% and 25% Co. In a tentative discussion of their results, as well as those of Kussmann and Nitka (1938) on Ni–Pt, it was suggested that the ferromagnetism of the Pt rich Co–Pt alloys may arise as a result of strong intra-atomic exchange forces in the

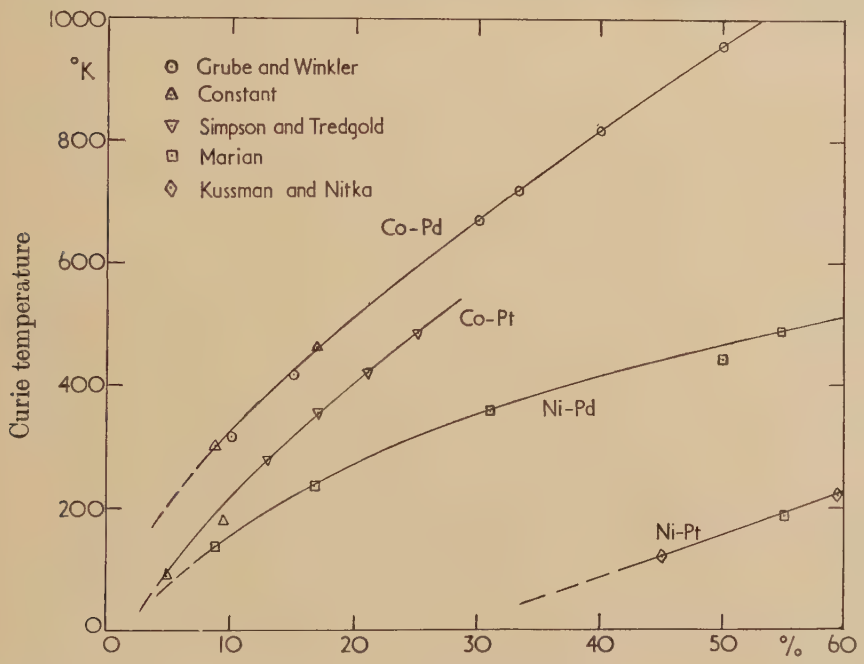

Co atoms, or, alternatively, that there is some exchange interaction between Co and Pt atoms. To interpret the difference between the properties of Co–Pt and Ni–Pt it was suggested that the intra-atomic exchange forces in Ni may be much less pronounced than in Co, in agreement with the fact that the Curie temperature of Ni is lower. The present note aims at a slightly more detailed discussion, considering also the magnetic properties of the analogous Pd alloys.

The figure shows the variation with Co, Ni atomic concentration of the Curie temperatures, the measurements being due to Constant (1930), Grube and Winkler (1935), Marian (1937), Kussmann and Nitka (1938) and Simpson and Tredgold (1954 ; disordered alloys). The curves show a markedly regular decrease of the Curie temperatures from those of Co–Pd down to those of Ni–Pt. For the Pd alloys the Curie temperatures extrapolate to zero at very low Co, Ni concentrations, in contrast to Ni–Pt but as for Co–Pt.

The results may be interpreted on the basis of three of the ideas underlying the collective electron treatment of magnetism (see, for example, Stoner 1951, Wohlfarth 1953), as applied to the present discussion : (1) In all four alloy systems it seems reasonable to assume that the magnetic properties are due to the holes in an energy band (' d band ') containing electrons contributed by both Co, Ni and by Pd, Pt atoms ; let the number of holes per atom in this common band be q. (2) The Curie temperatures of the alloys are determined by the characteristic parameter θ', giving a measure of the exchange and correlation forces between these holes ; on the assumption that these forces have primarily an interatomic origin a simple theory (Wohlfarth 1953), supported by other experimental evidence, shows that $\theta'=\alpha(R)q$, where α is a complicated function of the interatomic distance, R. (3) Unless θ', though still positive, is large enough, the Curie temperature is zero, i.e. the metal or alloy is paramagnetic ; as seen below, quite small changes of θ' may be sufficient to suppress the Curie point completely.

The following approximate values of q may be derived from other experimental results : Pt, 0·25 ; Pd, 0·60 ; Ni, 0·60 ; cubic Co, 1·80 (Wohlfarth 1949 a, b, Hoare and Matthews 1952). On the assumption, necessary in the absence of more detailed experimental results, that the variation of q with atomic concentration is linear, the following values for q are found for alloys with, for example, 30% of Co or Ni in Pd or Pt : Co–Pd, 0·96 ; Co–Pt, 0·72 ; Ni–Pd, 0·60 ; Ni–Pt, 0·35. On the basis of hypothesis (2) above the parameter θ', and hence the Curie temperature, should thus decrease regularly from Co–Pd to Ni–Pt, as observed. For Ni–Pt q and hence θ' seems to be too small for the Curie temperatures to differ from zero for Ni concentrations less than about 30% (see figure). The effect of variations of the interatomic distance may, however, also be important, particularly in Ni–Pd where q remains approximately constant over the whole concentration range, so that such variations are the only effective ones. Here, as discussed previously (Wohlfarth 1949 a, 1953) a slight variation of θ' by only about 20% over the whole range may be attributed to a variation of $\alpha(R)$, consequent on a change of the interatomic distance R from 2·49 A.U. for Ni to 2·75 A.U. for Pd. This slight decrease of θ' is here sufficient to reduce the Curie temperature to zero. An analogous situation occurs on comparing Ni–Cu alloys, for example, with pure Pt. An alloy containing about 40% Cu has the same value of q as Pt but is ferromagnetic, though with a Curie temperature of only about

200°K (Wohlfarth 1949 c). The interatomic distance of this alloy is 2·51 A.U., of pure Pt 2·77 A.U.

In discussing the relative values of the Curie temperatures of Ni and Co and their alloys it was shown earlier (Wohlfarth 1949 b) that here changes are again mainly governed by the relative q values. There thus seems to be no need to invoke such matters as the relative importance of intra-atomic exchange forces in these substances.

References

Constant, F. W., 1930, *Phys. Rev.*, **36,** 1654.
Grube, G., and Winkler, O., 1935, *Z. Elektrochem.*, **41,** 52.
Hoare, F. E., and Matthews, J. C., 1952, *Proc. Roy. Soc.* A, **212,** 137.
Kussmann, A., and Nitka, H., 1938, *Phys. Z.*, **39,** 373.
Marian, V., 1937, *Ann. Phys., Paris,* **7,** 459.
Simpson, A. W., and Tredgold, R. H., 1954, *Proc. Phys. Soc.* B, **67,** 38.
Stoner, E. C., 1951, *J. Phys. Radium,* **12,** 372.
Wohlfarth, E. P., 1949 a, *Proc. Leeds Phil. Soc.*, **5,** 89 ; 1949 b, *Phil. Mag.*, **40,**, 1095 ; 1949 c, *Proc. Roy. Soc.* A, **195,** 434 ; 1953, *Rev. Mod. Phys.*, **25,** 211.

The Specific Heat of Lithium Fluoride at Low Temperatures

By G. O. Jones and D. L. Martin
Department of Physics, Queen Mary College, University of London

[Received May 4, 1954]

The specific heat of lithium fluoride at low temperatures is of particular interest because it shows the greatest variation of Θ_D with temperature over the Debye T^3 region so far observed for any substance. Also, the relatively high value of Θ_D means that it is possible to work at effectively lower temperatures with this salt. According to the results of Clusius and co-workers (Clusius 1946, Clusius, Goldmann and Perlick 1949), who measured the specific heat down to 18·8°K, Θ_D falls slowly from 646° at 272°K to a minimum value of 607° at about 80°K, and then rises steeply at lower temperatures, reaching 750° at 18·8°K. This value for Θ_D is of the same order as that estimated from the elastic data at absolute zero, and it is therefore of special interest to know whether the rise in Θ_D is continued to still lower temperatures and at what temperature the true T^3 region begins.

We have extended measurements of the specific heat of lithium fluoride down to 2°K, using a crystal of mass 200 g and a very light copper calorimeter to which the crystal could be stuck with silicone grease. (This procedure differed from that used by Clusius, who lacquered heater and thermometer wires directly to a much smaller crystal.) Between 30° and

20°K our results are in good agreement with those of Clusius. Below this temperature the rise in Θ_D appears to be arrested, and Θ_D remains constant at 736°K—indicating that the true T^3 region has been reached—within the probable deviation ($\pm 8°$) of our estimate, down to the lowest temperatures employed.

The calculation of Θ_D from elastic data is subject to uncertainty because of disagreement between the results of the various workers (Bergmann 1938, Huntingdon 1947, Sundara Rao 1949, Seshagiri Rao 1949, Hoerni and Wooster 1952) who have studied lithium fluoride. Also, Ballard, Combes and McCarthy (1951) have shown that there are quite large variations in behaviour from one specimen to another. Selecting the results of Huntingdon and making a small extrapolation to absolute zero by comparison with certain results of Durand (1936) to allow for the fact that the measurements were carried out at room temperature, we have the values 10·0, 4·0 and $5{\cdot}6\times 10^{11}$ dyne/cm^2 for c_{11}, c_{12}, and c_{44} respectively. The method of Quimby and Sutton (1953) and a simple formula proposed by Blackman (1951) then both lead to an estimate of 714°K for Θ_D. (The value of 686°K mentioned by Clusius is obtained by the use of a formula due to Blackman (1942) valid only for temperatures of the order Θ_D.) However, values of the elastic constants given by the other authors referred to above lead to values of Θ_D lying between 670° and 770°K. There is thus no evidence of a discrepancy between the values of Θ_D estimated from thermal and elastic data greater than the existing uncertainty in the experimental results.

The experimental method, and the results obtained for lithium fluoride and for other salts, will be discussed in detail in a later publication.

We are grateful to Dr. D. A. Jones and Dr. D. M. Finlayson of the University of Aberdeen for supplying the crystal of lithium fluoride, to Dr. M. Blackman and Dr. R. O. Davies for helpful discussions, and to the Central Research Fund of the University of London for the loan of apparatus.

References

Ballard, S. S., Combes, L. S., and McCarthy, K. A., 1951, *J. Opt. Soc. Amer.*, **41,** 772.
Bergmann, L., 1938, *Ultrasonics* (London: Bell).
Blackman, M., 1942, *Proc. Roy. Soc.* A, **181,** 58; 1951, *Phil. Mag.*, **42,** 1441.
Clusius, K., 1946, *Z. Naturforschg.*, **1,** 79.
Clusius, K., Goldmann, J., and Perlick, A., 1949, *Z. Naturforschg.*, **4***a*, 424.
Durand, M. A., 1936, *Phys. Rev.*, **50,** 449.
Hoerni, J., and Wooster, W. A., 1952, *Acta Crystallogr.*, **5,** 386.
Huntingdon, H. B., 1947, *Phys. Rev.*, **72,** 321.
Quimby, S. L., and Sutton, P. M., 1953, *Phys. Rev.*, **91,** 1122.
Seshagiri Rao, T., 1949, *Curr. Sci.*, **18,** 436.
Sundara Rao, R. V. G., 1949, *Curr. Sci.*, **18,** 336.

The Pile Irradiation of Quartz Crystal Oscillators

By F. B. Johnson* and R. S. Pease†
* Signals Research and Development Establishment, Christchurch.
† Atomic Energy Research Establishment, Harwell.

[Received April 30, 1954]

The natural frequencies of quartz crystal oscillators are changed when the crystals are exposed to x-rays (Frondel 1945). We have found that somewhat similar changes are produced by exposure to pile irradiation, but that the changes are much larger, and demonstrate that two types of effect occur : those due to displacements of atoms ; and those due to ionization.

Fig. 1

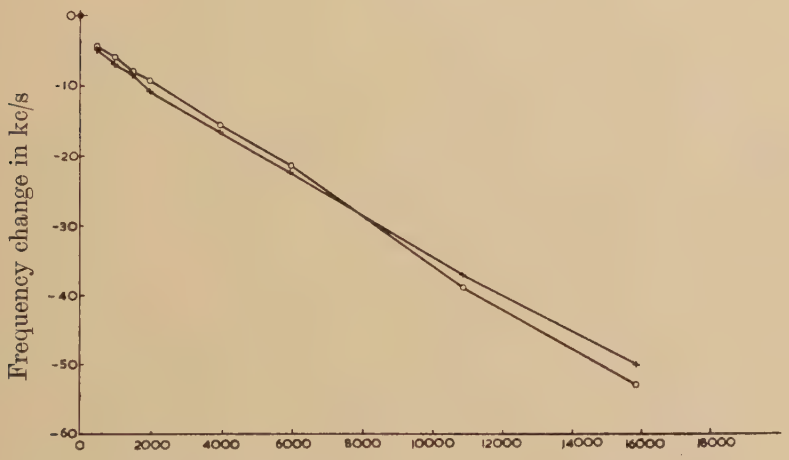

Megawatt-hours of irradiation in BEPO.

Figure 1 shows the frequency changes produced when 7 Mc/s BT cut quartz crystal oscillators were irradiated in the centre of BEPO (the larger of the two Harwell piles). The changes produced at low doses are illustrated by the results shown in fig. 2. There is a relatively rapid initial change of frequency with dose, which merges into a relatively slow linear decrease, illustrated in fig. 1, at doses of between 100 and 150 MWh. The maximum decrease we have observed is 100 kc/s, this maximum being set by the fact that the crystals cease to oscillate at very high doses.

Colour changes also take place. The unirradiated crystals, all of which were obtained from a piece of high grade Brazilian quartz, were uncoloured. In the pile, they darkened rapidly with increasing dose up to a dose of about 100 MWh ; thereafter a slight but steady bleaching took place, and at doses in excess of about 5 000 MWh the crystals were quite transparent and clear again.

The effect of x-rays on crystals from the same source has been investigated, and a decrease of frequency with dose has been found, which ceases after a frequency change of 2·5 kc/s, with variations of ±0·5 kc/s from one crystal to another. These changes are very similar to those produced by pile irradiation at low doses, and by extrapolating the linear portion of curves such as those of fig. 1 back to zero dose, a value of 2·6 kc/s with variation from one crystal to another of ±0·6 kc/s is obtained for the decrease produced by the initial effects of pile irradiation. Pile irradiation produces a darkening of the crystals which is very similar, both in intensity and in its characteristic banding, to that produced by x-ray irradiation (Frondel 1945). The doses absorbed by the crystal for pile and x-ray irradiation have been put on an absolute basis, and it is found that the dose required to produce a frequency change of half the x-ray saturation value is 3×10^{20} and 9×10^{20} ev/gram for pile irradiation at 95°c

Fig. 2

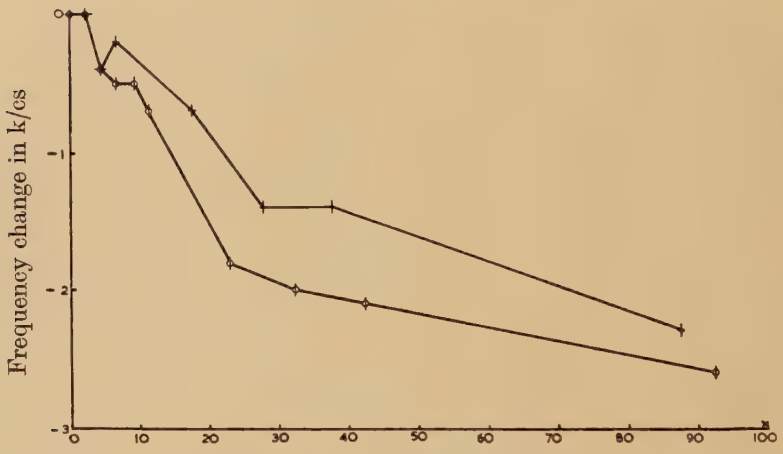

Megawatt-hours of irradiation in BEPO.

and x-ray irradiation at 20°c respectively. The conversion of the dose scales could only be carried out roughly, but serves to show that the order of magnitude of the doses is the same in the two cases. Both the x-ray induced changes and the initial changes produced by pile irradiation are annealed out by similar heat treatment, for instance by heating at 400°c for about 15 minutes.

It is thus evident that the initial effects of pile irradiation are the same as those produced by x-ray irradiation, and that these must be due to ionization since the x-rays used are of insufficient energy to displace atoms. Because of the wide variation of the magnitude of the effects in crystals from different sources, it would appear that the changes are produced by defects, probably impurities, present in the unirradiated crystals, which trap electrons displaced by the ionization (Rutherford, Chadwick and Ellis 1930).

The further changes produced by prolonged pile irradiation must be due to the creation of further defects. The obvious mechanism for this is the displacement of atoms by fast neutron bombardment, some effects of which are already known in quartz (Berman 1951, Wittels 1953, Wittels and Sherrill 1954). At a dose of 10 000 MWh in BEPO, the integrated fast neutron flux is estimated to be 6×10^{18} neutrons/cm^2. From this figure, the scattering cross sections of Si and O, and the application of the expressions due to Seitz (1949) for the number of atoms displaced by energetic ions, we obtain about 2×10^{-4} for the proportion of atoms displaced from lattice sites at this dose. Such a proportion should have observable effects on the unit cell dimensions, and these were therefore measured by means of x-ray powder photographs. The following results were obtained, at 35°c, taking the wavelength of $CuK\alpha_1$ radiation to be 1·54051 Å :—

$$\left.\begin{aligned} a_0 &= 4{\cdot}9136(5)\pm0{\cdot}00015\ \text{Å} \\ c_0 &= 5{\cdot}4048(5)\pm0{\cdot}00015\ \text{Å} \end{aligned}\right\}\ \text{unirradiated quartz,}$$

$$\left.\begin{aligned} a_0 &= 4{\cdot}9186(0)\pm0{\cdot}00015\ \text{Å} \\ c_0 &= 5{\cdot}4067(5)\pm0{\cdot}00015\ \text{Å} \end{aligned}\right\}\ \begin{array}{l}\text{irradiated quartz,}\\ \text{dose}=16\ 000\ \text{MWh in BEPO.}\end{array}$$

Thus the a-dimension expands by 0·10% and the c-dimension by 0·03(5)%. The results of Wittels (1953) with approximately six times the dose, showed the same anisotropy, but, of course, larger expansions. Changes of this order of magnitude can hardly be due to anything but the displacement of atoms.

The annealing of the high-dose damage was observed to take place at higher temperatures than does the annealing of the ionization damage. For instance : heating for 30 min at 800°c was required to eliminate 98% of the damage. From the results of annealing at different temperatures and for different times, the activation energy for the recovery process was estimated to be 0·7 ev.

The defects formed by the displaced atoms do not function as electron traps in the same way as those present in the unirradiated material. The most obvious feature is that they do not increase the darkening of the quartz, but reduce it. A crystal irradiated in the pile for 16 000 MWh, and therefore quite transparent, was irradiated with x-rays : only a barely perceptible colour change was produced, and an *increase* in oscillation frequency. Crystals in which the displacements had been eliminated by annealing showed the same characteristics under x-ray irradiation as the original unirradiated crystals. Thus the bleaching of the ionization effects by prolonged pile irradiation is not due to the elimination of the defects present in the unirradiated material, but to some more subtle mechanism which reduces their effectiveness as electron traps.

Acknowledgments

Thanks are due to the Chief Scientist, Ministry of Supply, and to the Director, A.E.R.E., for permission to publish this letter.

References

Berman, R., 1951, *Proc. Roy. Soc.* A, **208,** 90.
Frondel, C., 1945, *Amer. Mineral.*, **30,** 432.
Rutherford, E., Chadwick, J., and Ellis, C. D., 1930, *Radiations from Radioactive Substances*, p. 187.
Seitz, F., 1949, *Discussions Faraday Soc.*, No. 5, 271.
Wittels, M., 1953, *Phys. Rev.*, **89,** 657.
Wittels, M., and Sherrill, F. A., 1954, *Phys. Rev.*, **93,** 1117.

The Velocity of Elastic Waves in the Solidified Inert Gases

By T. H. K. Barron* and C. Domb†
* Clarendon Laboratory, Oxford
† Royal Society Mond Laboratory, Cambridge

[Received April 1, 1954]

In a recent letter Barker, Dobbs and Jones (1953) reported that they had succeeded in measuring the velocity of propagation of longitudinal elastic waves in solid argon. In attempting to compare their results with theory, the above authors gave an empirical estimate of Poisson's ratio, and were hence able to deduce the compressibility of solid argon. Two independent theoretical estimates were quoted which differed by a wide factor, and the experimental results lay between these two estimates.

We believe that some recent calculations which we have performed on the lattice dynamics of the face centred cubic lattice at low temperatures enable a more direct comparison to be made with theory. The primary purpose of the calculations was to compare accurately the thermodynamic functions of the cubic and hexagonal close packed lattices at low temperatures, but incidentally we were furnished with numerical values of the velocities of propagation of elastic waves in different directions in the crystal.

To make use of the above results we must first pass from a single crystal to polycrystalline material, and various suggestions have been made for averaging the elastic constants in some manner over all orientations (Hill 1952). It seems to us, however, that in the present problem the experimental technique naturally suggests an alternative method. The total time taken for the wave to travel through the crystal is the sum of the individual times taken through the randomly oriented microcrystals. It is apparent therefore that we should average $1/v_l$ over all directions for longitudinal waves to obtain an estimate of $1/\bar{v}_l$, $\bar{v}_l$ being the velocity of propagation of longitudinal waves in the macro-crystal; a similar procedure should be followed for transverse waves.

Our calculations are based on the assumption that the effects both of zero point energy and of forces other than those between nearest neighbours are negligible. For intermolecular forces of the Lennard-Jones

type a preliminary investigation suggests that this should involve an error of about 10%, our estimates being low by this amount. A great simplification is achieved by this approximation, since the results can be expressed in terms of a single force constant, that between nearest neighbours. Results at different temperatures can be derived by modifying the force constant to take account of the thermal expansion of the lattice : this of course neglects effects due directly to the change of temperature rather than to the accompanying expansion (Born 1952). By the force constant we mean $\phi''(r)$, where $\phi(r)$ is the potential energy of two atoms at a distance r apart, and where ϕ' is small compared with $r\phi''$.

Our results for polycrystalline material are as follows :—

$\bar{v}_l$ (velocity of propagation of longitudinal waves)$=1{\cdot}098(a^2\alpha/m)^{1/2}$

$\bar{v}_t$ (velocity of propagation of transverse waves) $=0{\cdot}616(a^2\alpha/m)^{1/2}$

Young's modulus$=1{\cdot}36\alpha/a$

Poisson's ratio $=0{\cdot}27$

Compressibility $=1{\cdot}01a/\alpha$

(α=force constant, m=molecular mass, a=intermolecular distance). A check on the consistency of the assumptions can be made experimentally by determining the ratio $\bar{v}_t/\bar{v}_l$ and comparing with the theoretical value of 0·56. This is independent of the force constant.

Using this model and a Lennard-Jones 6–12 interatomic potential for argon (Fowler and Guggenheim 1952) we estimate the value of $\bar{v}_l$ at the absolute zero as 1470 m sec^{-1} and the compressibility as $0{\cdot}38\times10^{-10}$ cm^2 dyne^{-1}. The velocity is rather low compared with the experimental values given by Barker, Dobbs and Jones, 1300 m sec^{-1} at 78°K and 1600 m sec^{-1} at 60°K, but as mentioned previously we expect the theoretical estimates to be increased by about 10% when distant neighbour interactions and zero point energy are taken into account.

References

Barker, J. R., Dobbs, E. R., and Jones, G. O., 1953, *Phil. Mag.*, **44**, 1182.

Born, M., 1952, *Proceedings of the International Conference on Phase Transitions, Paris*, p. 334.

Fowler, R. H., and Guggenheim, E. A., 1952, *Statistical Thermodynamics*, (Cambridge : University Press), p. 285.

Hill, R., 1952, *Proc. Phys. Soc.* A, **65**, 349.

The Diffusion of Nitrogen in Alpha Iron

By W. R. Thomas and G. M. Leak
The British Iron and Steel Research Association

[Received April 28, 1954]

A study is being made in these laboratories of the effect of nitrogen, carbon and boron on the strain ageing properties of mild steel. In the course of the investigation it was found desirable to measure the diffusion coefficients of these interstitial solutes in α-iron in the range 0–100°c, where most of the experimental work is being done. Apart from Snoek's (1941) earlier work there are only two published determinations (Wert 1950, Fast 1954) of the diffusion coefficient of nitrogen within this particular temperature range.

Only the results for the diffusion of nitrogen in α-iron are reported here. The measurements of diffusion coefficients of the other interstitial solutes will be published later.

All measurements were made by observing the change in internal friction caused by nitrogen in solution in α-iron. The theoretical aspects of the method and the form of the apparatus have been adequately discussed by Polder (1945), Dijkstra (1947) and Zener (1948).

The diffusion coefficient of an interstitial solute atom in a b.c.c. lattice can be related to the mean time of stay in an interstitial site by the expression

$$D=\frac{a^2}{24\tau'}, \qquad \ldots\ldots\ldots \quad (1)$$

where $a=2{\cdot}86\times10^{-8}$ cm for α-iron.

The mean time of stay τ' is related to the relaxation time τ by the expression

$$\tau'=\frac{3}{2}\tau. \qquad \ldots\ldots\ldots \quad (2)$$

The logarithmic decrement, δ, for this type of measurement is given by

$$\frac{\delta}{\pi}=\Delta\frac{\omega\tau}{1+\omega^2\tau^2}, \qquad \ldots\ldots\ldots \quad (3)$$

where ω is the angular frequency of oscillation, and Δ is the relaxation strength of this anelastic effect.

An expression for $\omega\tau$ can be obtained by considering the maximum value reached by the δ-temperature curve. Neglecting variation of Δ with temperature, T, then this maximum value is given by

$$\omega\tau=1. \qquad \ldots\ldots\ldots \quad (4)$$

Taking into account the slow variation of Δ with T^{-1} then the maximum value occurs for

$$\frac{Q}{RT} = \frac{\omega^2\tau^2+1}{\omega^2\tau^2-1}, \qquad \ldots\ldots\ldots \quad (5)$$

where Q is the activation energy for the diffusion process. The diffusion coefficient estimated from eqn. (5) gives values about $3\frac{1}{2}\%$ smaller than those calculated assuming $\omega\tau=1$, within the temperature range considered in this note. The correction has only a slight effect on the activation energy, but mostly affects experimental values for D_0 in the equation $D=D_0 \exp[-Q/RT]$. Since D_0 is subject to an experimental error greater than $3\frac{1}{2}\%$ this correction has been ignored.

In order to calculate the diffusion coefficients, therefore, it is only necessary to know the temperature at which the maximum internal friction due to the solute is observed together with the frequency of mechanical oscillation.

Experimental

High purity iron prepared in collaboration with the N.P.L. (B.I.S.R.A. Reference AHM 12) and of the initial composition given in table 1, was used in this investigation in the form of wire 0·080 in. in diameter.

Table 1

	Wt. %
C	0·0038
Si	0·001
Mn	0·005
Al	0·0027
Cr	0·0013
Ni	0·0014

Table 2

Temp. °C	Frequency of oscillation sec^{-1}	Diffusion coefficient $\times 10^{16}$ cm^2 sec^{-1}
18·5	0·625	0·89
23	1·13	1·62
33·5	2·5	3·57
42·5	6·15	8·78
47·0	8·83	12·62
48·5	9·3	13·28
51·6	10·4	14·88
55·8	12·3	17·68
58·5	18	25·73

An anneal of 5 days at 700°C in flowing wet hydrogen reduced the nitrogen and carbon contents to amounts that were below the limits of

chemical analysis or internal friction measurements. Nitrogen was introduced into the wire by heating it at 1300°C for 24 h in a gas stream containing 99% N_2 and 1% H_2. This treatment ensured homogeneity of the specimen and the absorption of only a small quantity of nitrogen $\sim$0·02%. The wire was quenched in water from 580°C to retain the nitrogen in solution.

The temperature of the internal friction peaks was measured for various frequencies of oscillation. The diffusion coefficients were calculated from eqns. (1), (2) and (4). These results are given in table 2.

Fig. 1

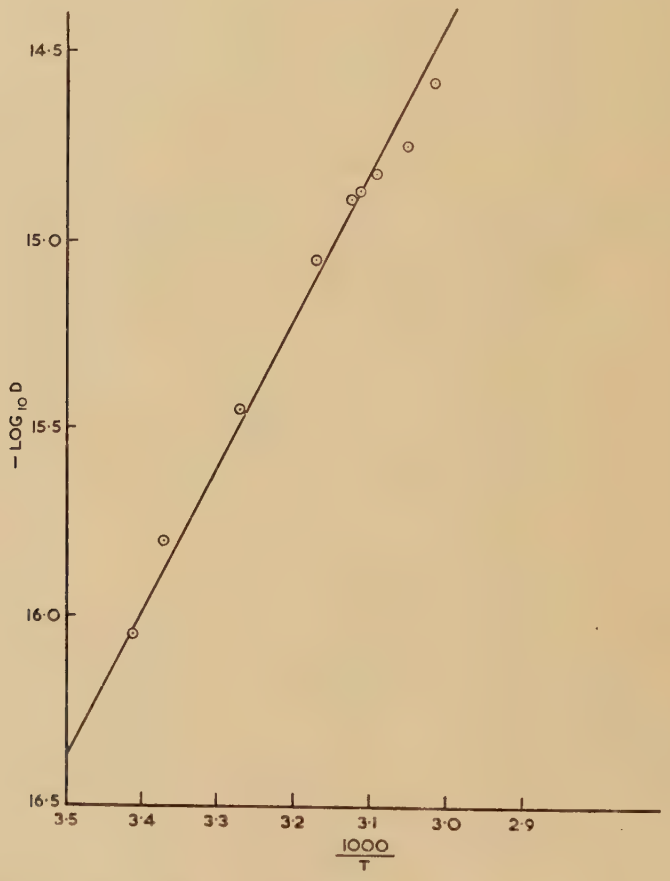

The results are plotted in fig. 1 as $-\log D$ *vs.* $1000/T$, so that the activation energy of the diffusion process is given directly by the slope of the line as $Q = 18\,000$ cal. If the results are plotted on a smaller scale as in fig. 2 together with the values obtained by Wert and Fast, it can be seen that the straight line agrees better with the results obtained by Wert giving a D_0 of $3{\cdot}1 \times 10^{-3}$ cm²/sec compared with a D_0 of $6{\cdot}6 \times 10^{-3}$ cm²/sec given by Fast and 3×10^{-3} cm²/sec by Wert.

Fig. 2

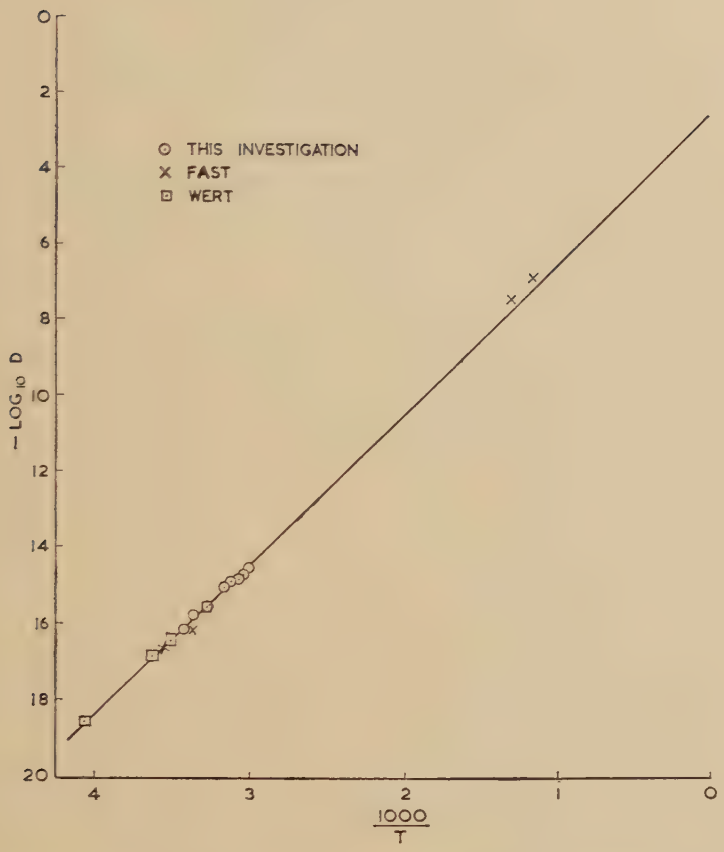

Note added in proof.—The curves in figs. 1 and 2 have been drawn with the same slope. Adjustment of the curve to include Fast's high temperature points, fig. 2, would give undue weight to these points by comparison with the weight of the low temperature points of fig. 1.

References

Dijkstra, L. J., 1947, *Philips Res. Rep.*, **2**, 357.
Fast, J. D., and Verrijp, M. B., 1954, *J. Iron and Steel Instn.*, **176**, 24.
Polder, D., 1945, *Philips Res. Rep.*, **1**, 5.
Snoek, J. L., 1941, *Physica*, **8**, 734.
Wert, C. A., 1950, *Phys. Rev.*, **79**, 601.
Zener, C., 1948, *Elasticity and Anelasticity of Metals* (Chicago: University Press).

LXXIII. *Notices of New Books and Periodicals received*

Atomic Energy: A Survey. Edited by J. Rotblat. [Pp. viii+72.] (London: For the Atomic Scientists' Association by Taylor and Francis Ltd., 1954.) Price 6*s.* 6*d.* bound copies; 4*s.* 6*d.* paper cover.

This book gives the text of seven lectures given under the auspices of the Atomic Scientists' Association last January and February. The Association is to be congratulated on their early appearance in print, especially at a moment when public interest in the subject is so great. The lectures are addressed to an audience not mainly scientific; but none the less most readers of *The Philosophical Magazine* will find in them much that they did not know, that they ought to know and that their friends will expect them to know. Sir John Cockcroft writes about the work of Harwell and its relation to reactor design; Professor Frisch gives a summary of some facts about atomic weapons; Professor Simon reviews the possibilities of power from nuclear reactions, seen against the availability of other sources of power, together with some wise remarks on secrecy and spy hysteria; Dr. Loutit writes on radiation hazards, contrasting them with the medical history of the coal mining industry; Dr. Pochin writes on the rapidly growing medical applications of radioactive isotopes, and Professor Kathleen Lonsdale and Sir George Thomson on the moral issues. N. F. M.

High Voltage Laboratory Technique. By J. D. Craggs and J. M. Meek (Butterworths, 1954.) [Pp. 404.] Price 65*s.*

This book collates the information derived from a very wide range of published papers, and it provides a comprehensive review of the equipments and associated apparatus for producing and measuring high voltages.

The descriptions cover the generation and stabilization of high direct voltages by means of valve and metal rectifier circuits and by electro-static generators. Power frequency cascaded transformers, resonant and higher frequency transformers are discussed, and then there is an analysis of the design and operation of high voltage impulse generators. Equipment is described for generating and measuring high current impulses, and also rectangular pulses of high voltage. Methods are described for the measurement of high direct and alternating voltages and these include, among others, a range of calibrated spark-gaps, resistance or capacitance types of voltmeters and voltage transformers. Spark-gap, oscillographic and other recording methods applicable for measuring impulse and pulse voltages are then included, and followed by an analysis of potential dividers and a description of various oscillographic techniques.

The authors have summarized the salient points from a large number of published papers, and in this manner a book of moderate size is able to indicate the design features, the performance and limitations of many individual items. Any reader with a deeper interest in particular items is referred to the very extensive and well selected bibliography, which includes some 700 references.

The book was primarily intended by the authors for the use of engineers and physicists in high voltage research or development laboratories, and it is of particular interest to research workers who are starting in such a laboratory, or those who require to develop new techniques in this field. The authors make no claim to cover all the requirements of industrial testing at high voltages, or to discuss details of high-voltage phenomena of interest to engineers engaged on power generation or transmission, but nevertheless, their requirements concerning laboratory equipment and techniques are well covered. A. S. H.

Dislocations and Plastic Flow in Crystals. By A. H. Cottrell. (The International Series of Monographs on Physics.) [Pp. 223, illustrated, 9×6 in.] (Oxford : Clarendon Press, 1953.) Price 25*s.* net.

This is a masterly piece of work. The author, himself one of the leaders in the newest development of the theory of the plastic flow, discusses its fundamental features in a fascinating way. The treatment is dominated by the physical point of view. The problems are first discussed in a concrete qualitative way. This is most appealing for a reader not yet familiar with the theory. The mathematical treatment, although thorough, remains in the background and so remains an accessory tool of the theory. The arrangement of the book, which proceeds from simpler problems to more difficult ones, is very well chosen.

For the specialist too, it will be very helpful to learn the ideas of the author in a general survey of this kind. Cottrell's opinions on problems which are not yet settled, are of importance. It need hardly be emphasized that the text is based upon the results of the most recent investigations.

A survey of the chapters will give a better insight into the contents of the book. These are : the interpretation of slip in crystals ; elastic properties of dislocations ; dislocations in crystals ; theories of the yield strength ; work-hardening, annealing and creep. G. Masing.

Neutron Optics. By D. J. Hughes. (New York : Interscience Publishers, Inc., 1954.) [Pp. 136 with 34 figs.] Price $2.50, paper covered.

This is the first of a series of tracts published " to provide non-specialists with authoritative and relatively brief and inexpensive accounts of recent advances in the many specialized branches of physics and astronomy ". The author is a member of the staff of the Brookhaven National Laboratories, and is well-known for his researches in neutron optics ; his five chapters form a very readable account of the subject. The first chapter, which discusses the fundamentals of neutron scattering, compares the optics of neutrons and electromagnetic waves, and the second, showing the relation between different types of investigation—transmission, mirror reflection and coherent diffraction studies—are particularly valuable. The third chapter, describing experimental measurement of cross sections, is noteworthy for a simple account of the electrostatic neutron–electron interaction. A description of the applications of neutron diffraction suffers from the limited space available for this rapidly expanding field and is inevitably illustrative rather than comprehensive. The final chapter on magnetic scattering blends the theoretical work of Halpern and Johnson with a description of the author's own experimental work on transmission and reflection by magnetic materials and the earlier diffraction measurements of Shull and his co-workers on ferro- and anti-ferromagnetics.

A few errors have been noted : for example, the inclusion of the Debye–Waller factor within the coherent scattering amplitude a_j in equation 1.46 leads to the then incorrect statement that this amplitude is independent of scattering angle ; and, page 53, in equation 2.8 the detector distance and sample dimension are respectively misplaced and omitted.

The general reader, with no specialized knowledge of either nuclear physics or crystallography, will find the tract easy and profitable to read. G. E. B.

Bessel Functions and Formulae. Compiled by W. G. Bickley. (Cambridge : University Press.) Price 3*s.* 6*d.*

This reprint of pages xxx to xl from the *British Association Mathematical Tables*, Volume X, contains many properties of and formulae related to Bessel functions, as well as a comparison of different notations used by different authors. A very useful pamphlet. D. P.

The Printing of Mathematics. Aids for Authors and Editors and Rules for Compositors and Readers at the University Press, Oxford. By T. W. Chaundy (University Reader in Mathematics), P. R. Barrett (Mathematical Reader at the University Press, Oxford) and Charles Batey (Printer to the University). (Oxford: University Press; London: Geoffrey Cumberlege, 1954.) [Pp. 105+vi.] Price 15*s.*

The editors of the *Philosophical Magazine*, on looking through this excellent little book, wish that its perusal could be compulsory for all authors of scientific papers, as a knowledge of the Highway Code is for those who apply for a driving licence. The book describes what the compositor has to do; it explains the monotype machine, and shows what can be set up on it and what cannot. Authors will note that P_n and P^n are within the capacity of the machine, but that P_n^m must be set up by hand. We commend, too, the chapter entitled "Recommendations to mathematical authors". Such authors who are writing in English are asked not to forget the dignity and traditions of the language, and told that symbols such as q.e.d. are best left behind in the school room. One might ask if they need show their ugly faces even there. Also many rules are given for writing mathematics with elegance. One in particular the editors would like to commend to all authors, and that is the writing of $\frac{1}{2}\pi$ and never $\pi/2$. N. F. M.

The Earth, its Origin, History and Physical Constitution. By H. Jeffreys. Third edition. [Pp. xiv+392.] (Cambridge: University Press, 1952.) Price 70*s.*

The second edition of this book was published in 1929. In the long period since then it has been the standard authority on the physics of the earth and has probably been more frequently quoted than any other book about the earth. During the interval, geophysics has developed in many directions and has come into much closer relations with geology and prospecting. To have brought *The Earth* up-to-date by attempting to incorporate all this material would have completely changed its scope. The author has wisely refrained from attempting to do this. The third edition has the same framework as the second, covers much the same topics and omits the same things. It is concerned essentially with the application of theoretical physics to the elucidation of the observed facts about the earth; the experimental methods by which the facts are obtained are only lightly indicated. Terrestrial magnetism and electricity and everything connected with prospecting are barely mentioned. The restriction of subject matter has enabled the book to retain the unit of method and outlook that were so marked in the earlier editions; it is still a miracle of compression and elegance.

In some places the revision has perhaps not gone far enough. The older European seismological results are frequently used when modern and better data are available, for example, three plates are devoted to records of the Jersey and Hereford earthquakes of 1926.

Naturally, many things in the book are controversial. Jeffreys still supports the contraction theory of mountain building and is opposed to convection in the mantle and to large-scale movement of the continents. This greatly narrows the range of physical explanations that can be applied to the facts of geology, but it also makes for a unified and unambiguous presentation and avoids a mass of conflicting possibilities. Also, it must be admitted that other views have their own difficulties. E. C. Bullard.

[*The Editors do not hold themselves responsible for the views expressed by their correspondents.*]

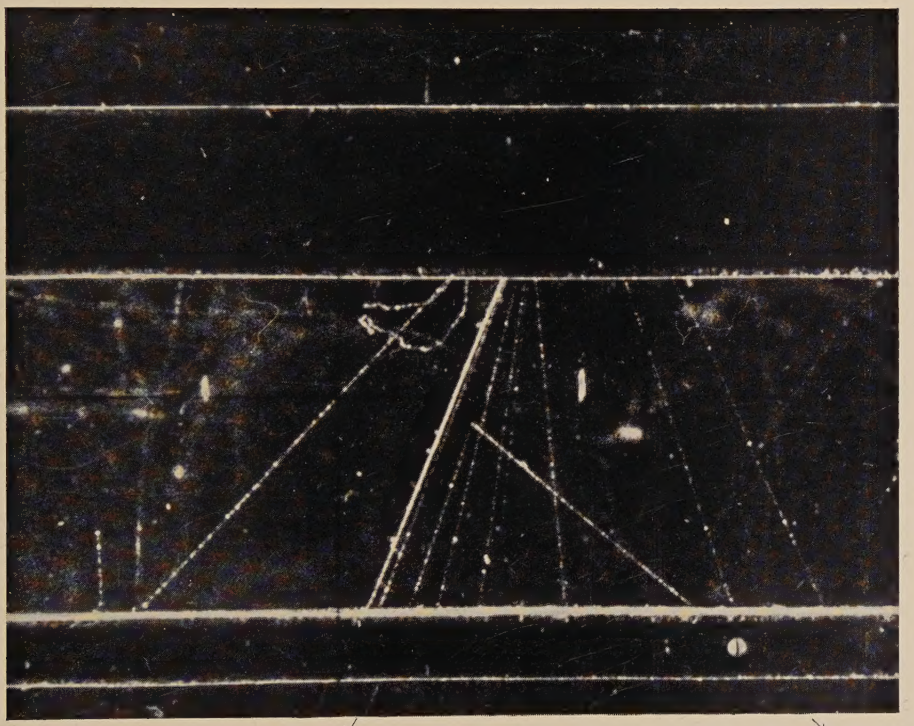

Event D 6379.
Track (1) is that of the proton and track (2) that of the π-meson.

Exposure of sandstones of the Keuper Marl Series on the bank of the river at Radcliffe-on-Trent, near Nottingham (site 8).

Fig. 1

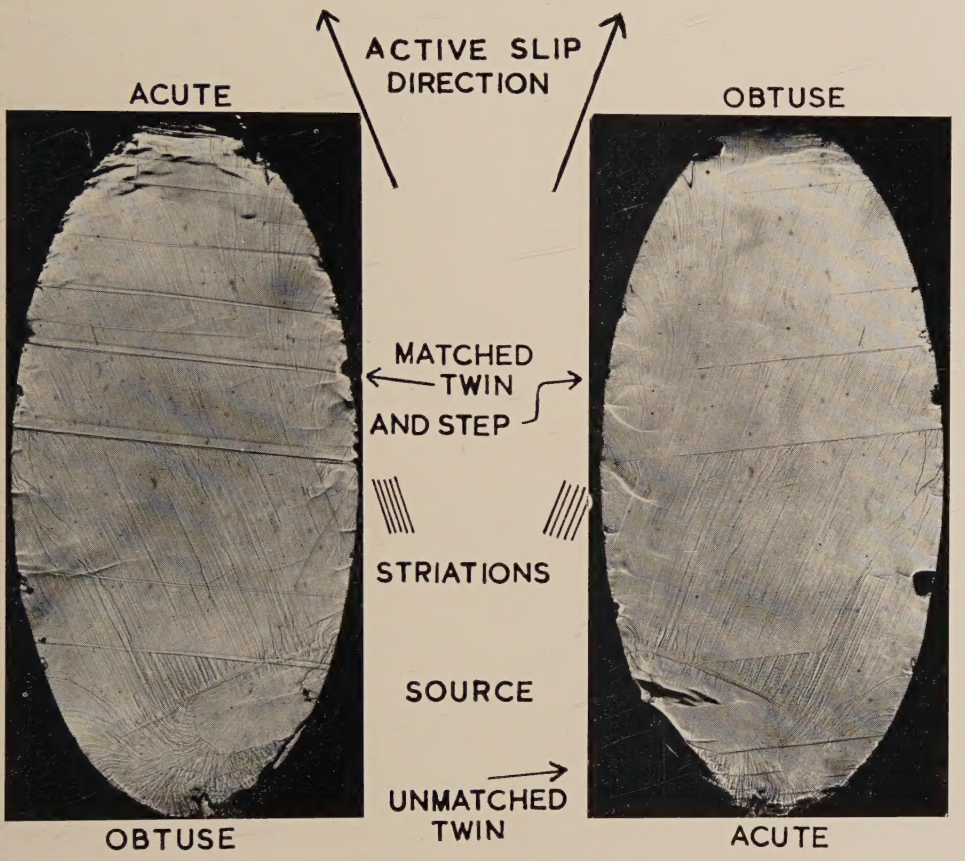

The two cleavage faces of a crystal (χ=25·5°). ×7·5
Note particularly the striations parallel to the active slip direction.

Fig. 2

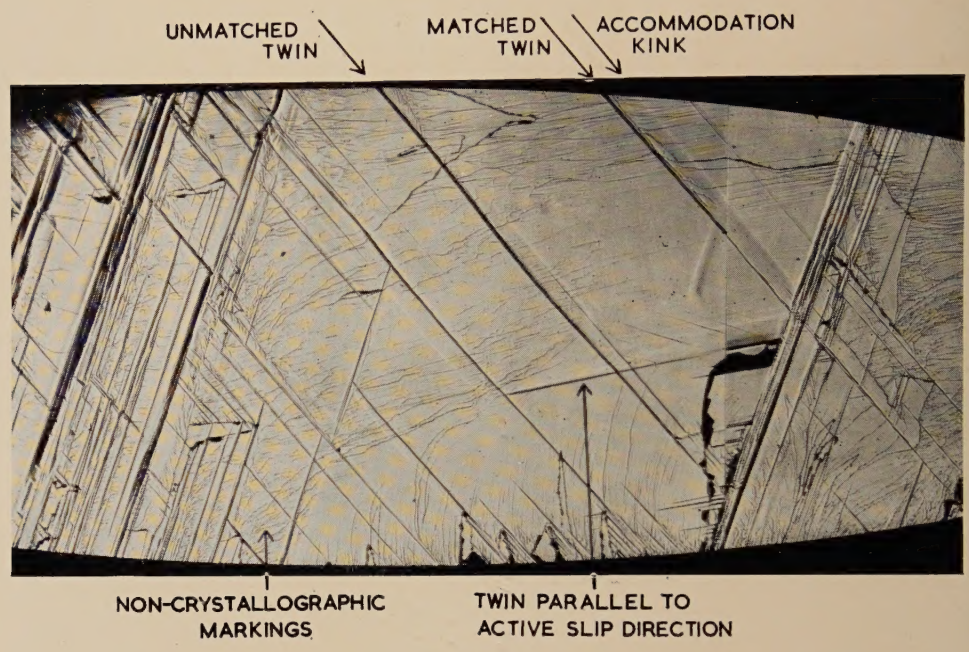

(*a*)

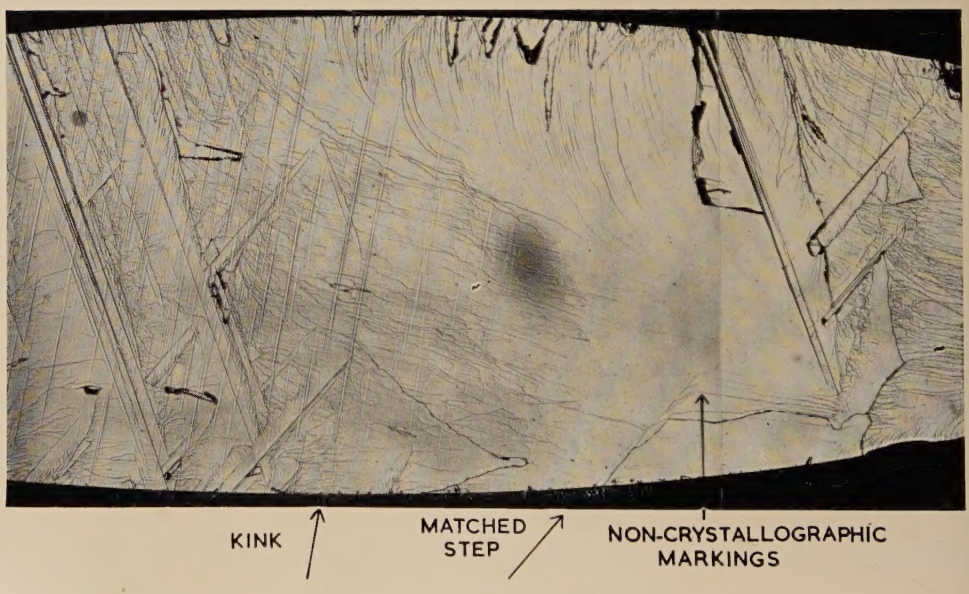

(*b*)

Composite photographs showing parts of the two cleavage faces of a crystal ($\chi=13°$). $\times 10{\cdot}5$

This crystal showed features illustrating all the general principles, and also examples of most of the exceptions. The crack progressed from right to left, the source not being on the photograph. Note twins matched with steps, unmatched twins and kinks. (*a*) is the ' acute ' side of the source.